Using Cyclic Immunofluorescence (CyCIF), Deep-learning, and Human Tumor Microarrays (hTMAs) for Antibody Validation and Creation of an Atlas of Cancers Emphasizing Unique Phenotypes

Using Cyclic Immunofluorescence (CyCIF), Deep-learning, and Human Tumor Microarrays (hTMAs) for Antibody Validation and Creation of an Atlas of Cancers Emphasizing Unique Phenotypes

Connor A. Jacobson

A Thesis in the Field of Biology

for the Degree of Master of Liberal Arts in Extension Studies

Harvard University

March 2023

Abstract

All cancers are different from each other, in their mutation spectrum, primary location of occurrence, and metastases as well as their phenotypic traits and tumor composition. For years, clinicians and pathologists have sought to describe, characterize, and exploit the hallmarks of cancer broadly to identify specific differences between cancer types and subtypes. As medical technology and science advances, so has understanding of the underlying biology of cancer initiation and progression. Further, the ability to identify and visualize subtle differences between types of cancer based on their phenotypic and morphologic presentation aids in the research and design of newer targeted cancer therapies aimed to improve the lives of patients regardless of their original prognosis. Currently, the most widely used method for studying tumor tissue and diagnosis diseases is hematoxylin and eosin staining (H&E) of surgical biopsies with supplemental immunohistochemistry (IHC) or in-situ hybridization (ISH) for molecular biomarkers. These methods are low-plex but highly reliable and have remained the gold standards half a century. IHC typically identifies and quantifies one biomarker of interest at a time and answer specific questions, such as whether or not a particular breast tumor biopsy contains cells that overexpress human epidermal growth factor receptor 2 (HER2) or not. IHC stains require manual interpretation by trained pathologists or histologists based on counting cells (commonly with a binary call as either positive or negative) expressing a particular marker: if there is an abundance of brown-stained HER2+ cells scored on one patient's biopsy slide as compared to a control, then HER2 is scored as

over-expressed. Unfortunately, this is a slow, laborious process that does not take advantage of many advances in computer vision and image analysis. Thus, digital methods that incorporate multiple antibodies have long been sought.

Recently, a modified version of the traditional immunofluorescence assay, called cyclic immunofluorescence (CyCIF), has been used to perform high-throughput, multiplexed imaging of fixed, cultured cells in a multiwell plate format and (Lin et al., 2015) as well as formalin-fixed paraffin-embedded (FFPE) sections of tissue or tumor samples (Lin et al., 2018) on slides in a manner compatible with standard histopathology workflows. As with the IHC assays, the goal is to detect particular cell- or tissue-specific macromolecules with antibodies, but for more analytes to spare tissue and reveal deeper cellular phenotypes. In CyCIF, both unconjugated and conjugated commercially available antibodies, used for indirect IF and direct IF, respectively, can be used, with up to 60 or more different antigens measured on each specimen. This enables a thorough characterization of tissue-intrinsic properties as well as tumor. In doing so, we can provide a more comprehensive and specific understanding of tissue sections and cellular populations as opposed to simply the presence or absence of an antigen or disease. Whole slide imaging (WSI) is performed on tumor biopsies, cycles are registered and stitched together, and a mutli-channel images containing data from numerous antibody stains is then analyzed to define the biological context in which cancer continues to persist.

Here, we used CYCIF to investigate the composition and architecture of human cancers and adjacent normal tissue as a means to describe cellular composition both inside and outside of the tumor and along the tumor boundary, explore cell-to-cell interactions and neighborhood analyses, as well as evaluate the efficacy of commercially

available antibodies. The data we present here, as well as the EMIT dataset on which it is based (Schapiro et al., 2021), defines, characterizes, and highlights noticeable trends of biology in human tissue microarrays (hTMA). I will use the staining of complementary serial sections of TMAs to accomplish our aim of characterizing tumor and benign cell morphology across cancers, uncover patterns across cancer different cancer types, identify morphological distinctions through antibody expression, and evaluate antibody staining across hundreds of reagents through a multi-disciplinary approach. This, beginning with fine-tuned and well-controlled experimentation and the use of deep learning artificial intelligence (AI) and automated post-processing of image-based data. In achieving our aims and showcasing the potential of CyCIF, we hope to translate this current research into an atlas-like resource aimed at addressing many outstanding questions in the fields of histology, pathology, and the newly emerging field of digital histopathology. Though we do not CyCIF does not provide a direct link into clinical care, we show that the results produced through our multifaceted pipeline can, and should, have a direct impact on clinical follow-ups as they pertain to individualized medicine. In detailing a patient's primary tumor biopsy in replicate, with uniquely built-upon CyCIF panels to unearth as much biological and immunological information as possible, we have created an argument as to why high-plex cancer atlases might serve as valuable tools for enhancing our knowledge of disease-specific underlying biology to a never-before-possible standard.

Frontispiece

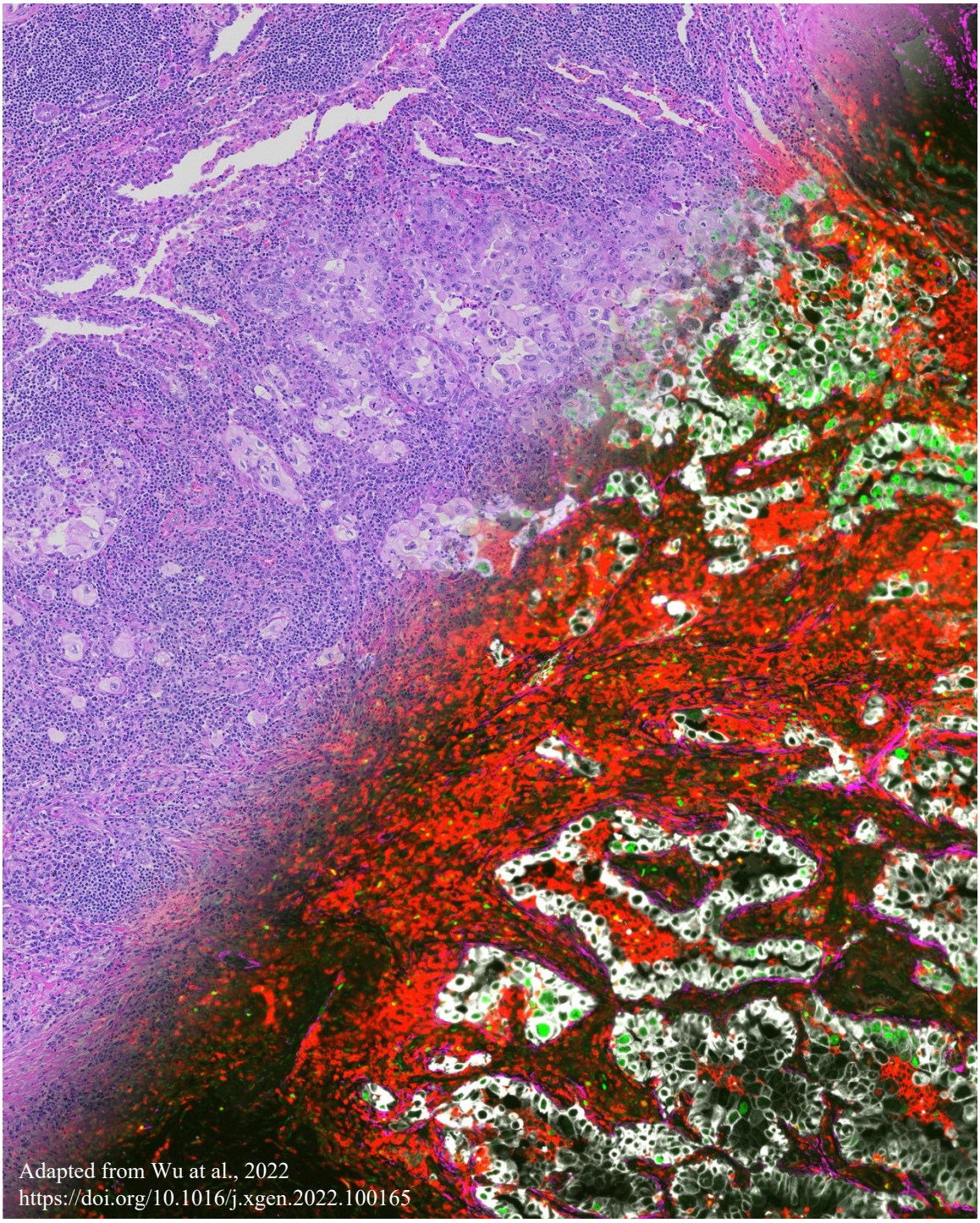

Dedication

This work is dedicated to my family.

To my grandmothers, Oma and Mama, the genesis of my scientific curiosity and my true number one fan.

My parents, for their continuous encouragement, pushing me to be the best that I can be and to continuously challenge myself.

My brother, Jordan, for unwavering support in all the endeavors I choose to undertake. Aja and Caleb, for making my brother happy, a better man, and pushing him to mentor me as only a brother can.

Thank you all so much – I love you.

Acknowledgments

There are many people I would like to acknowledge for their help in this work and for guidance, tutelage, and mentorship throughout my six and a half years spent at Harvard Medical School.

First and foremost, I would like to thank Peter Sorger who took a chance on me Day 1, hiring me as a recent college graduate with limited experience. I spent over six years working in your lab and your constant desire for me to grow as a person and as a scientist has led me to where I am now. Thank you.

Secondly, I would like to thank other members of the LSP and Sorger lab whose advice, support, and friendship has made all of this possible. I would like to thank Zoltan Maliga, Clarence Yapp, Tuulia Vallius, Jeremy Muhlich, Roxanne Pelletier, Laura König, Ajit Johnson, Denis Schapiro, Greg Baker, Sandro Santagata, and all of my esteemed collaborators for giving me the opportunity to perform meaningful work. Hopefully our publications will continue to make an impact.

I would like to identify and acknowledge colleagues for their specific contributions: Editing: PKS, TV, ZM, LK; Experiments: ZM, CY, RP; MCMICRO and UnMICST: CY, DS, JM; Figure preparation: CY, ZM, TV, RP.

Table of Contents

List of Tables

List of Figures

Chapter I.

Introduction

The Current Standing in the Field of Histopathology

Review of sectioned formalin-fixed paraffin-embedded (FFPE) tissue and tumor biopsies stained with the dyes hematoxylin and eosin (H&E) is the primary approach for cancer diagnosis. Staining of negatively (violet: nucleic acids and some proteins) and positively (red: cytoplasmic proteins and connective tissue such as collagens) charged molecules by H&E, respectively, reveal patterns of tissue and sub-cellular architecture to a trained pathologist inspecting the sample at high and low magnification. The patient's clinical information and review of H&E-stained biopsy sections, cell size, and patterns of nuclear and cytoplasmic staining can be used to distinguish tumor, immune and stromal cell types, subtype and grade the cancer. Further, H&E provides a setting in which pathologists can quickly visualize groups of cells their morphologies, which are often distinguishable in the context of cancer, as a result of uncontrolled proliferation. The method has existed for over a century and remains relatively unchanged, yet a staple in the field of histology for its ability to recognize morphologic changes that dictate many contemporary cancer diagnoses (Fischer et al., 2008). Beyond grading the cancer itself, H&E staining can be used as a primary diagnostic tool in differentiating one form of cancer from another through pattern recognition and identification of subtype-specific abnormalities (Chen et al., 2020).

While H&E staining remains a critical component of the histologic workflow that precedes many cancer diagnoses, interpretation requires a high level of human expertise,

meaning the workflow surrounding a single H&E slide requires much effort. While there have been technological advances that allow for H&E staining of many slides at the same time, the interpretation of this data requires one by one pathology review – one of its major limitations. Even in an era of "big data," unassisted pathologist interpretation of H&E results remains the gold standard (Djuric et al., 2017) despite being both burdensome and subject to observer-to-observer variability (Tan et al., 2020). In addition, H&E does not provide detailed molecular information on a cell-to-cell basis and is limited to pattern recognition and qualitative features of tumors. Molecular detail is important in the context of diagnosis to provide quantitative insight into disease state and possible drug response, based on quantification of the presence of a particular protein within a tissue that may be unique to a group of cells or cell states. Not only that, but molecular features reveal mechanisms that can be used to apply existing or develop new treatments and offer insight as to how clinicians can improve a patient's treatment regimen. To reach this next-level of clinical relevance, the method of immunohistochemistry (IHC) is used to detect individual molecules in FFPE biopsy tissue, building upon H&E findings, but with deeper and more specific data on the levels and distribution of a single protein.

Often used to complement the findings seen through H&E staining, and add an additional layer of quantitative value, IHC staining incorporates the use of a clinically relevant (typically monoclonal) antibody as a biomarker in tissue sections. Like H&E, IHC affords the pathologist an easy way to discriminate cell types and cell morphology based on staining patterns. This can make it easier to distinguish benign tissue regions from malignant ones. It is also widely considered to be the gold standard in cancer

assessment and detection of disease-specific molecular changes. In IHC, an antibody is linked to an enzyme, and the antibody itself targets a molecule of interest, such as a mutated receptor or an oncogene. The antibodies are selected by pathologists and clinicians based on the suspected cancer type. For example, in breast cancer, pathologists target specific changes in expression associated with common subtypes such human epidermal growth factor receptor 2 (HER2), estrogen receptor (ER), and progesterone receptor (PR). In clinical practice, at least three slides are subjected to IHC staining (one slide targeting HER2, one targeting ER, and one targeting PR) and pathology review of one marker at a time is used to arrive at diagnostic findings. Based on these findings, antibody or small molecule therapeutics can be provided to target the specific abnormality and improve the patient's clinical outcome. Herein we see the power of IHC in that the detection of a specific gene (protein) and its relative abundance can directly guide clinical intervention.

As compared to H&E, IHC staining introduces a slightly qualitative aspect to the clinical standard. IHC depends on the use of chromogens, such as 3,3′-Diaminobenzidine (Rimm, 2014), commonly referred to as DAB. IHC staining employs the use of a single primary antibody that is linked to DAB. The enzyme, in turn, oxidizes DAB which leaves a brown colored precipitate that is detected through white-light brightfield microscopy, much like H&E. Nonetheless, IHC is frequently used as a diagnostic tool for solid tissue malignancies (Angelo et al., 2014). In the hands of a skilled pathologist, IHC moves beyond the abilities of H&E and can be used to judge relative levels of an antigen, wholly important in grading cancerous specimens, particularly in assessing disease state, to which H&E is relatively naive. Normally, the staining intensity of an antibody in IHC

correlates to its relative expression level or abundance: the darker the stain, the more antigen present (Nguyen, 2013) indicative of a higher burden, such as HER2 overexpression. Though this evaluation is limited to a single antibody, the ability to include a quantitative aspect to histology staining represents another standard in the field and serves as an indispensable tool in assigning tumor type and diagnoses that are heavily dependent on morphological interpretation (Bellizzi, 2020) and expression level. H&E and IHC staining are often the first methods used to detect, classify, and score different malignancies and metastases (Litjens et al., 2018; Rüschoff et al., 2010); thus, their significance in the clinic remains vital. Due to these factors and the capability to detect and appraise cancers, H&E and IHC have a long withstanding presence in the clinic and have remained relatively unvarying for decades.

What remains a limitation of the IHC method is the number of antibodies used. Traditionally, only one antibody is used to target one particular molecule per slide and then multiple batches of slides are used to stain any number of antibodies, such as three slides each stained for HER2, ER, or PR. Recent efforts within the last few decades have improved the capabilities of IHC to incorporate the staining of a second biomarker or antibody, known as double-stain IHC or indirect IHC (Chen et al., 2010). While this may seem a modest improving, it doubles the efficiency of the IHC assay and makes it possible to score co-expression at a single cell level. Even so, it is apparent that the need for additional biomarkers and antibodies screened in IHC remains a key area to investigate further. The use of multiple antibodies simultaneously can vastly improve our understanding of disease and disease status. For example, employing markers such as pan-Cytokeratin (pan-CK), Ki67, Cyclin D1, and PDL1, can be used to better understand

tumor burden, the proliferative nature of cancerous cells, as well as cell death programming that may be occurring within a tumor (Patel & Kurzrock, 2015) – typical hallmarks of cancer. By performing a dual-IHC stain with both pan-CK and Ki67, we can quickly determine not only the presence of tumor, but also how quickly the cells may be proliferating within the tumor and outside of it. These markers provide insight in regards to disease state or progression as opposed to simply the presence or absence of one biomarker – pathologists can see tumor or proliferating cells, but cannot see proliferating cells within the tumor simultaneously by conventional H&E or IHC and their single-marker approaches. Therefore, you need a multi-marker method, a marker to score mitosis (Ki67) and a marker to identify the tumor (pan-CK), to visualize proliferating cells (Ki67+) within the tumorous region (pan-CK+), often signifying a rapidly growing tumor capable of metastasizing (Li et al., 2015).

More than just to detect disease, using additional biomarkers help clinicians and pathologists gauge disease state, severity, and tumor burden. Pathologists also use H&E and IHC staining results to interpret and predict response rate, progression free survival, as well as overall survival (Patel & Kurzrock, 2015), key parameters to consider when considering drug treatments. Taken together, this information can be used to guide or direct drug treatment given the results; the richer and more detailed the results are in regards to mutations, over- and under-expressions, and mutations, the more precise a drug regimen can be provided to a patient. Continuing from the previous example, if there is not a visible HER2 overexpression mutation, there could be another mutation, such as with PR, which would steer drug treatment in an entirely different direction based on the evaluation of IHC slides in a patient-specific manner. That is to say, the ability to

probe and stain for multiple markers simultaneously offers a more well-controlled manner in which we can observe actionable biology. Multiplexing is superior than probing serial sections of the same tumor three with either a HER2, ER, or PR biomarker, which is significantly more time consuming. Overall, there is an unmet need for a histology-related assay to allow for the incorporation of many antibodies simultaneously. Being limited to one or two antibodies per slide does not allow for an in-depth understanding of a patient's tumor, nor does it maximize efficiency in histologic staining.

One of the challenges in interpreting IHC stain results is that there is seldom complementary data, apart from preliminary H&E, limiting the generalized analysis of biomarker data, again a hindrance in the “big data” era. As it currently stands, both H&E and IHC slides are assessed in very large volumes to reach the required sample sizes needed for statistical significance in both the research and clinical hospital-based settings. However, given that there are large numbers and batches of slides that need to be both stained and analyzed, this becomes a long and exhaustive process that requires the time and attention of individuals to perform the staining as well as input from pathologists to evaluate the results. As fresh biopsies are performed in the hundreds each day, a rigorous evaluation, likely performed by multiple pathologists is needed. As mentioned, this manual scoring in the hundreds may actually decrease efficiency as fatigue sets in; it also introduces inter-observer variability among other human error(s). It would involve many trained specialists to assess large cohorts of slides each day to reach the required sample size – exhausting efforts that becomes error prone susceptible to decision fatigue, deferrals, and discrepancies (Wisell and Sams, 2013). By using machine learning, there is the potential to automate review and improve quantification of this process, minimizing

the burdens placed on pathologists while simultaneously increasing both accuracy and throughput. In doing so, we can remove much of the human error introduced once the proper machine learning training sets are prepared. While machine learning may not necessarily improve the speed of analysis, heightened accuracy and precision should not be overlooked.

Adapting to the Evolving Field Using Deep-Learning and Multiplexing

While machine-learning based automation can greatly lessen the burden placed on pathologists in evaluating H&E and IHC slides, the incorporation of multiplexing assays can greatly increase the amount of molecular information we can obtain from a single slide. Therefore, both of these advancements should be highly sought after in terms of moving the field forward in parallel with the technological advances. Recently, there have been developments to train supervised H&E machine learning algorithms to recognize the different morphologies and structures of cells from FFPE slides and guide artificial intelligence (AI) to perform these assessments in the place of actual pathologists. While there has been success in these endeavors, incorporating IHC slides for machine learning supplements the additional layer of quantifiability. Thus, H&E slides need to be integrated with IHC slides for training purposes in targeting specific cellular components and expression levels. While large sample sizes are needed to train deep learning AI, performing one sizable batch of manual annotations, though cumbersome and error-prone (Tellez et al., 2018) is superior to experts redundantly reviewing smaller batches of slides each time which becomes tiresome and burdensome. If a properly curated training set is prepared, then there is no longer a need for manual intervention in individual batch review – the same algorithms can be used each

experiment, likely with frequent improvements. Automation makes these efforts significantly less vexatious.

Previous deep learning processes and automation efforts have proven successful in histopathology (Nadarajan et al., 2019) and can help advance the field if proper controls and supervised training(s) are incorporated. This includes annotating and classifying the different components of a cell, a process known as "labeling" (van der Wal et al., 2021), whereby pathologist-driven manual classification is used to identify particular cell types and structures. Doing so allows for manual interpretation of histology data to remain the ground-truth in assessing H&E and IHC slides, that is to say there is no deviation from the gold standard if it serves as the foundation for machine learning training sets (Aeffner et al., 2017). Labeling efforts include identifying and marking certain cells, such as a B- and T-cells or macrophages, in a way that, when provided with different unmarked field, the machine learning algorithms can use its previously fed information to make the same judgements a pathologist had, but on a much larger scale. This is considered "supervised training" in that pathologists dictate the first-pass as to what a specific immune cell looks like and then the AI then learns from that information to make its own judgements about previously unseen based on cellular morphology and marker expression. Cumulative efforts can translate into increasing the throughput of analysis, quantification, and classification of potentially cancerous cells and tissues on standard pathological slides moving the field forward as a whole.

To target the many components of a cell, a number of different markers must be employed to segregate nucleus, cytoplasm, membrane, and nucleoli etc. Utilizing one or two antibodies for IHC does not accomplish this task and limits the overall efficiency of

the method and its applicability. Moreover, it does not afford researchers the opportunity to incorporate a multiplexed approach – meaning the ability to image-capture multiple distinct fluorescent labels of many markers simultaneously (Taube et al., 2020). However, if a multiplexed IHC assay is performed, in which multiple antibodies or biomarkers can be used and viewed simultaneously, one can target and stain all structures in one pass. Not only are we able to stain the different structures within a cell, we can also employ antibodies that are specific for certain cell types such as CD56 for natural killer (NK) cells, CD66b for granulocytes, and CD146 for endothelial cells, to name a few. In doing so, we can begin to classify cellular structures based on staining localizations and train deep learning algorithms to recognize subtle differences amongst cancer cells between diseases as well as other cell types while being both supervised and confirmed by pathologists – hence supervised machine learning.

The addition of other biomarkers to staining assays vastly improves our knowledge and understanding of relevant biology in a research setting. As we have discussed, H&E and IHC are both strong methodologies in which we can detect and recognize cancers, but by adding other antibodies, research teams can garner a more thorough biological understanding on a tumor-to-tumor basis. Not only can deploying multiple biomarkers highlight the unique components of the cell, other biomarkers can distinguish the same up- and down-regulations seen by IHC, elucidate aberrant signaling, identify cycling cells, and uncover cells undergoing apoptosis among other biological processes as long as the antibodies are available. Further, much like certain markers are specific to particular cell types, an expression profile consisting of multiple markers offers additional insight to the specificity of type and roll of cells, like a CD11c+CD14+

representing a monocyte derived dendritic cell in the early stages of differentiation versus one that is simply CD11c+ (Figueroa et al., 2016), specifically when discussing diverse immune cell populations. Using multiple biomarkers simultaneously provides flexibility and a more efficient approach to the standards. If we can confidently identify and score presence and absence of one antigen at a time, we can do the same with multiple biomarkers so long as they appear in different colors/wavelengths under a microscope (in contrast cannot distinguish two DAB-labeled biomarkers on the same IHC slide). Recent advances have incorporated four labels and two-color imaging within the same IHC-ready tissue (Dixon et al., 2015) conferring many advantages, for example probing for both CD11b and CD11c, traditionally lineage-dependent monocyte markers, here serving as markers specific for separate subtypes of leukemia: acute monoblastic versus microgranular (Gorczyca et al., 2011), another instance whereby subclassification of disease is morphology-driven. We refer to instances in which morphology impacts diagnosis or subtyping with the terms “histologic classification” or “histotype,” the latter borrowed from Lin and colleagues (2022), both of which we will further describe later. Probing for either CD11b or CD11c alone with a single stain cannot distinguish the acute monoblastic histologic classification from microgranular, so a double-stain is necessary for proper diagnosis.

Even with two-to-four-plex capabilities, H&E and IHC evaluation remains limited in its scope and from the amount of molecular information we can ascertain from only a couple of antibodies. Increasing the number of biomarkers and antibodies visualized and quantified beyond two or four can greatly improve the clinical standard as well as elevate overall efficiency because it allows much more precise analysis of cell types and states at

a single cell level. One way to introduce multiplexing capabilities to histopathology is through incorporating immunofluorescence (IF) assays in combination with traditional IHC, known as multiplex immunohistochemistry/immunofluorescence (mIHC/IF). Using this method, Lu et al. found that mIHC/IF had a statistically significant greater diagnostic accuracy than the traditional IHC method in the detection of PD-L1, a key marker of tumor immune escape. They also found that mIHC/IF provided a statically significant higher area under the curve (AUC) for PDL1 sensitivity and specificity as well as positive predictive values and likelihood ratios, standard statistics used to validate findings, as compared to IHC. (Lu et al., 2019). It has also been found that even when using many antibodies, the accuracy and precision for single-cell expression remains high overall (Taube et al., 2020), meaning that multiplexing does not reduce the chief metrics of sensitivity, specificity, and AUC in regards to a breadth of biomarkers. Lu and colleagues suggest several different mIHC/IF modalities that differ in both the number of markers stained and visualized simultaneously as well as the capabilities of many commercially available microscopes necessary to perform these multiplexed scans. In conclusion, Lu insists on the pressing need to employ multiplexed applications to push the field of histopathology towards a more digital trend (digital histopathology) in which traditional H&E and IHC images are collected using digital microscopes for subsequent analysis as opposed to being examined by human experts working at a microscope.

Multiplexed staining and microscopy serve as a pivotal foundation on which we can complement, transform, and advance the ways in which we collect and interpret H&E and IHC data. New commercially available scanners offer a multitude of capabilities to enhance histopathology and make it more digital through multichannel multispectral

imaging. By integrating and visualizing multiple markers, we are not only able to determine that there is dysmorphia in the tumor cells or an overabundance of a particular protein, but we can begin to interpret cellular composition, cellular function, and cell-to-cell interactions, specifically in the tumor microenvironment (TME). Through multiplexed imaging, we can span the anatomical, molecular, and physiological levels to provide a more well-rounded interpretation of antigen expression across tissues and even introduce spatial correlations, heterogeneity across multiple markers, and differences in signaling pathway activation (Andreou et al., 2022). For example, Angelo et al. employed multiplexed ion beam imaging (MIBI) to stain and visualize ten labels simultaneously to provide insight on disease pathogenesis (Angelo et al., 2014). But why stop at ten?

CyCIF Elucidates Underlying Tumor Biology in a Patient-Specific Manner

Newer research has gone above and beyond the capabilities of mIHC/IF and MIBI to further expand upon the traditional IF assay and employ the use of many commercially available antibodies – up to 60 or more markers – on a single FFPE tissue. One such process is known as cyclic immunofluorescence (CyCIF) introduced by Lin and colleagues (2018). In this work, we describe and discuss how CyCIF can be used to complement the traditional workflows currently performed by pathologists in a research setting. It serves a robust assay for balancing throughput with multiplexed abilities allowing for the imaging of up to 80 slides per imaging session and the stain of 60, if not more, antibodies in the same tissue. While we do not claim that CyCIF can be used as a clinically validated tool currently, we do propose that it, and the associated image data, can be used to help interpret, better understand, and confirm H&E and IHC results through its multiplexed nature. In using CyCIF to complement the gold standards, H&E

and IHC data that has been widely accepted as the ground truth, yet hindered by its non-generalizable analysis, can reach statistical significance with large sample sizes, a factor by which it was previously bottle-necked. We hereby suggest that CyCIF is capable of increasing sample through multiplexing antibody staining, but also allowing for a more generalized analysis through the creation of more heterogenous and diverse data.

Not only does CyCIF provide much greater insight into single cell states, which is of immense value, it can also provide data on the context of cell types, cell proportions, and cellular neighborhoods of which mIHC/IF have only begun to scratch the surface. CyCIF also provides a host of down-stream analyses, such as a breakdown of the TME composition, neighborhood clustering, and cell-to-cell interactions through built-in modules that can be run directly after imaging – traditionally incredibly computationally taxing. CyCIF serves as a potent starting point in terms of assessing a high throughput and multiplexed approach to traditional pathology and histology. Beginning with interpretable results from the gold standards, CyCIF can take initial results and propagate them through a fine-tuned pipeline of context-driven antibody staining and down-stream computational methods that can expand our knowledge of a patient's tumor biopsy and disease prognosis. Understanding the biological underpinnings of multiple disease types is an invaluable asset, particularly in the research setting.

As different cancers propose unique challenges to clinicians in treating a patient's tumor with a precise and targeted therapeutic trajectory, it is imperative to determine the cellular composition of the tumor itself, but also the cell populations outside the tumor, along the tumor boundary, and the cell amalgams amongst the tumor-stroma-immune cell interfaces. These cell populations comprise the tumor microenvironment, which has

become an attractive area of research over the last few years as it contributes to tumorigenesis and often dictates disease progression (Arneth, 2019). If we can understand the environment in which the tumor itself resides, the cell-to-cell interactions both inside and outside of the TME as well as the tumor boundary, the tumor composition, and relevant signaling aberrations, we have nearly maximized the amount of biological information extracted. In doing so, we become better able to provide therapeutics, or at least illuminate potential therapeutic targets, for certain cancer types. With the dual-marker approach of IHC, we are not even able to determine TME composition– limiting the degree to which we can understand a patient's tumor. We cannot fully appreciate the biological complexity of these disease states one marker at a time.

For instance, one of the greatest challenges when discussing cancer is understanding how cancer cells evade the immune system and continue to proliferate even in the presence of a high-abundance of both resident and infiltrating immune cells. In theory, the immune cells would kill and clear tumors, but we now have an understanding that cancer cells employ a variety of techniques, such as tumor induced tolerance or anergy (Drake et al., 2006) to evade a normal immune response allowing them to proliferate and replicate uncontrollably. Much of this goes is poorly understood based on conventional histological staining methods, but we can begin to understand some of these evasive techniques through CyCIF using antibodies that stain immune cells, cancer cells, proliferating cells, and mechanistic components that may be dysfunctional in one's tumor.

One of the more telling signs of a specific cancer or cancer subtype in histology is the presence of particular markers or cell types within a tumor as seen through IHC. For example, most breast cancers are hallmarked by an ER, PR, or HER2 hormone receptor over- or under-expression, easily detectable through IHC, an instance whereby unambiguous tumor biomarkers are the staple of diagnoses and dictate therapeutic trajectory (Parise & Caggiano, 2014). While easily detectable through IHC, the underlying biological significance of these over- and/or under-expressions is hardly illuminated through these efforts and additional markers are needed to reveal the context in which these expression irregularities occur. In this work, we aim to perform a deep-dive from many different experimental and analytical angles to further grasp these complex underlying biological processes. We generated an initial dataset comprised of 34 different types of neoplastic tissues and tumors sectioned on human tissue microarrays (hTMA/TMA), we will visualize differences between various cancers through their expression of certain biomarkers and provide a first-pass characterization of a patient's tumor. For instance, the canonical marker for tumor suppression, p53, can be found in varying degrees, depending on tumor status, across many, if not all, malignancies (Duffy et al., 2022), whereas a marker such as ER will be largely specific to breast cancer. Understanding, qualifying, and quantifying various expression levels of tumor markers, as well as immune markers, will reveal similarities and differences across many cancers.

By employing the power of CyCIF, we can further gauge the uniqueness of tumors by their expression of multiple biomarkers. Primarily, we aim to observe phenotypic differences amongst cancer cell types based not only on nuclear and cytoplasmic morphology, as in H&E, but also on patterns of expression of specific

marker proteins. We can further see the phenotypic difference between a cancerous cell and one that is benign based on changes in marker expression levels within a tissue, but also with added information through co-staining of structure-targeting antibodies. Taken together, by incorporating staining with several antibodies that target nuclear or subcellular structures, such as FoxP3, a nuclear marker of T-regulatory cells, or a cytoplasmic marker, such as E-cadherin, we are able to stain the full cytoplasm of cells and make clear distinctions between cell components and between cell types. Using this multiplexed in which we can targets these different aspects of cell biology, we already outperform the standards of histopathology. While there remain many challenges in targeting all of the different cell types, cellular components, and sub-cellular constituents in a given tumor section, we have already extended beyond the capacity of traditional H&E and IHC in identifying dissimilar cell subpopulations. In staining tissue microarrays, we can observe the staining patterns found across many cancer types, neoplastic tissues, and non-cancerous controls to create an atlas-like tool for pathologists and clinicians to reference when reviewing their own histology slides. The nature of a TMA is the perfect setting to perform this type of research and atlas-creation as they are comprised of numerous biopsies on the same slide from different tumor blocks to allow for intra-TMA comparisons of like and unalike cancers. One of the major conveniences of using TMAs for tool creation is that cores can be punched in biological replicate to allow for some confidence to be established within a single slide. We are able to observe and probe for particular biomarkers and antibodies that will allow us to make broad conclusions about specific cancers and particular tumor and tissue biology that will help us understands differences amongst tumors at a deeply phenotypic molecular level. Some

of these resources already exist, but here we plan to extend our findings to a multitude of different malignancies and not just one specific disease. As we will discuss in greater detail, the cores in the TMA are cut in serial section(s), therefore, the biology that we observe in one section, typically five microns thick, may be limited to two dimensions. However, with 25 TMAs stained in succession, we have the ability to sift through the three-dimensional z-sectioning to attain a more complete understanding of some biological processes that may occur in the third dimension, the z-plane, though this remains a limitation of the assay and the imaging capacity of many microscopes.

Using Data to Train Deep-Learning Cell Segmentation Algorithms

Along with understanding the cellular composition of the tumor microenvironment, we need to be able to discriminate between cell types. These TMAs present a dataset through which we can probe and characterize both nuclear and cell surface/membrane morphology amongst cancers and compare them to benign cells. Recent publications propose Multiple Choice MICROscopy (MCMICRO) (Schapiro et al., 2021) and U-Net model for identifying cells and segmenting tissue (UnMICST) (Yapp et al., 2021) as key players in detailing the needs for better cell segmentation, a critical component of multiplexed imaging post-processing and a goal that many research groups share. During cell segmentation, the initial input of a whole, stitched slide is broken down into individual cells, on the order of hundreds of thousands, if not millions, possible through the detection of nuclear Hoechst staining. This way, a whole slide is broken down into individual cells; at a single cell level, segmentation occurs by surrounding individual nuclei with a mask denoting its coordinates for later post-processing. MCMICRO and UnMICST offer alternatives and advancements in cell

segmentation, but require robust training sets to improve. Cell segmentation algorithms and deep learning AI can greatly outperform manual assessment when inspecting cell morphology, especially on a large scale, when fatigue becomes a factor. However, much like with overall H&E and IHC evaluation, there exists a common inner-observed dilemma by experts in the field of image-associated biology whereby there is no ground-truth for the most systematic and automated ways to segment cells; the best way still remains to do so manually on subset of the data.

Manual annotations that we curate for a number of antibodies targeting different aspects of a cell are then used for training deep learning AI algorithms to improve their abilities. This annotation is the aforementioned "labeling," whereby pathologists denote nucleus from cytoplasm and mitochondria from cell membrane. These annotations serve as the supervised training that is then fed to deep learning AI to make the same classifications based on the input(s) it has received. The desire for improvement lingers and is a hotly debated topic while remaining an outstanding limitation in the field – there exists no perfect cell segmentation algorithm. Our data can help guide and improve cell segmentation efforts by producing nuclear and cytoplasmic masks in which contours and cellular components can be human demarcated – the necessary ground-truth (Sadanandan et al., 2017) – used for training supervised deep machine-learning algorithmic AI in large quantities. By being fed first-pass human labeling of the nucleus and cytoplasm, among other cellular components, in one CyCIF image, our AI can interpret these classifications and use them to improve segmentation and call attention to unique cell morphologies and patterns that may suggest one malignancy over another.

Traditionally, in cell segmentation a cell nucleus is located first and then staining intensities are evaluated and categorized as pixels move away from the nuclear centroid. When intensity values fluctuate, algorithms determine that the cytoplasmic edge has been reached and a contoured mask is created encompassing the nucleus, while a secondary mask extends beyond the nucleus to the perimeter of the cytoplasm until the intensity changes once again, either lower to that of background or higher representing a neighboring nucleus. While trained pathologists can discriminate by hand, it becomes an exhaustive and process with the many cells (up to a million) found on a typical whole-slide image. Many goals in the quickly evolving field of histopathology revolve around minimizing the human interface and automating processes wherever possible. Following the trend in imaging, these curations can serve as the foundation for training algorithms to segment vast imaging datasets for us.

Certain cancer types prove to be more difficult to segment due to their intrinsic morphology, such as spindly high-grade serous ovarian cancer (HGSOC) cells, which require meticulous manual annotations of dense clusters of cells or skin-related diseases, such as melanoma, where cells in the hypodermis and subcutaneous tissue are sparse and widespread. A high abundance of fatty adipose tissue (adipocytes) and their resident cell types are notorious for being difficult to segment and analyze in stained sections (Galarraga et al., 2012). The primary goal of analyzing the stains in this dataset is to compare and contrast cellular morphology amongst various cancers while a secondary goal is to evaluate our segmentation tools, check their accuracy, and improve our efforts as well as the efforts in the field through an iterative process.

Another outstanding question in regards to high-throughput microscopy and its role in (digital) histopathology is defining what level of biological relevance antibody staining data can confer and whether or not it can translate into a clinical setting. This ties back to the initial questions about complementing H&E and IHC as the gold standard for pathological biomarker evaluation and tumor delineation (Jager et al., 2016) despite their low plex nature. While no multiplexed imaging assay has been clinically validated, there are efforts to make them so. As the number of clinically relevant antibodies increase, so does the need for a multiplexed staining method. With stains from nearly 600 antibodies, most of which are relevant to the clinic, our work should serve as a first-pass validation resource for a breadth of biomarkers guided and confirmed by pathologists and clinicians. In comparing the required metrics such as AUC, sensitivity, and specificity, we attempt to make a case for CyCIF multiplexing to be equal to, if not greater than, the pathology standards. In doing so, we aim to create a powerful guide for antibody selection. Expert advice will provide insight as to what antibodies should stain particular tumors or tissue, such as Cytokeratin-7 expression in lung cancers, and elevate confidence in choosing the proper antibodies for specific tissues and tumor types in a manner that includes more than just one antibody at a time.

Not surprisingly, there are two camps of thought in regards to the power and relevance of the multiplexed imaging trend towards digital histopathology: for example, Jager and colleagues suggest that any imaging method requiring image registration shall not outcompete the standards of IHC and H&E staining (2016), while others argue that this rapid transition is already occurring and becoming a viable clinical solution (Huss & Coupland, 2020). While we do not posit that CyCIF will revolutionize the field of digital

histopathology and become a mainstay of histopathologic analysis, we do suggest that complementing clinical standards with a multiplexed imaging approach can provide a deeper context and a vastly more information on oncogenic mechanisms. By uncovering more biology, we can further assess clinical samples to help improve precision medicine, targeted therapies, primary patient diagnoses as well as short- or long-term prognoses through a more thorough understandings of tumor on a patient-to-patient basis.

Taken together, this work discusses the benefits and role of multiplexed imaging in the research space, but also its clinical relevance, and addresses some of the primary concerns in the rapidly evolving field. We propose advancements to the standards and alternatives to relatively unchanged processes through three specific aims:

1. Evaluate antibodies through grading proper expression levels, correct cellular- or subcellular localization, true stain versus background (bg) or autofluorescence (af), and qualify staining across tissue types and compare prominent markers to H&E and IHC images – the clinical standards
2. Discriminate between tumor and non-tumor cells through their relative abundance and staining patterns of certain antibodies
3. Investigate cellular morphology, including nuclear, surface, and cytoplasmic staining, across multiple tissue types for comparison. A secondary goal of this aim is to enhance cell segmentation among various cancers through scoring of segmentation masks via antibodies targeting individual cell parts

Through these specific aims we will address and provide support for our hypotheses: if there are expression-level differences amongst malignancies of shared

biomarkers, such as pan-Cytokeratin, as well as cancer-specific ones, such as TTF1, then CyCIF affords us the ability to interpret these expression differences at both a micro and macro level; if there are both cancerous and benign cells intra- and inter-tumor, then they will exhibit morphological differences and each cancer subtype will have its own distinct histotype. If we can stain numerous TMAs and various cancer cores with hundreds of commercially available antibodies, then CyCIF's multiplexed nature will allow for consolidated evaluation and qualification of staining through the presence or absence of on-target expression and allow for comparisons of like antibodies, not possible with lower throughput assays. If we train our supervised machine deep learning AI with manually labeled training data, then we can achieve a higher level of confidence in our AI to improve segmentation in the field, particularly with notoriously difficult cancers, such as ovarian. All of these questions are addressable and provide insight on the current standing of image-related biology. Ultimately, we can push for CyCIF imaging to serve as a key resource in disease diagnosis and provide context for drug therapeutic targets. Here our goals are to consolidate validation resources to make trusted antibody selection more feasible, discern distinct histological classifications amongst many cancers, and improve automation of cell segmentation and other imaging post-processing tasks – all of which can be accomplished through multiplexed CyCIF imaging.

Chapter II.

Methods

CyCIF: A Resource to Find New Molecular Markers

With cancers having many features unique to the individual they afflict, it essential to understand the specific pathology behind a patient's tumor to help clinicians better recognize the underlying causes of tumorigenesis and tumor progression. By identifying and describing these causes, therapies can be suggested in efforts to combat cancer growth, proliferation, and metastases. In this work, we have compiled a dataset that includes biopsies of human tumor from patients with various malignancies and subjected these biopsies to deep cellular phenotyping via cyclic immunofluorescence in efforts to characterize their unique tumors. Using deidentified patient data approved by the Institutional Review Board (IRB), we have created a resource to guide clinicians in their categorization of tumor based on their histological classification as well as expression levels of certain biomarkers on a patient-to-patient basis with the goal of improving precision medicine.

As Peters and colleagues suggest, H&E remains the gold standard of pathology and is needed for evaluating the effectiveness of algorithms or multiplexed staining of antibodies as they relate to histopathology (Peters et al., 2019). Given that H&E has to power and accuracy to both detect and diagnose specific cancers (Cosatto et al., 2013), certain parameters such as sensitivity, specificity, negative predictive value, and AUC (area under the receiver operating characteristic curve) of multiplexed staining must be

compared as they are the critical statistics used for scoring H&E (Yamashita et al., 2021). Therefore, if a multiplexed methodology wants to be clinically implemented and validated, its parameters and statistics must be equal to or better than the manual scoring and assessment provided by experts. Rather than compete against the standard, we propose to expand and complement the findings obtained from H&E data to help further characterize tissues of interest.

While it is easy to see that the progression from H&E staining to IHC offers more insights and specifics than just simple pattern recognition and cell morphology analysis, it also provides a more targeted approach and purpose, honing in on a specific supposed biomarker. Like H&E, the result still remains relatively binary: presence or absence of the biomarker in question despite the added benefit of more quantifiability in the form of positively stained brown cells. While IHC is a more precise method, certain limitations continue to impact both the throughput and the confidence in results, such as the preprocessing of slides (i.e., sectioning, mounting, and fixation), subjective scoring of markers, and uncertain and biased cut-off values (Zhao et al., 2015). Even with a trustworthy technique to extract data from FFPE pathology slides, there still remain challenges that are difficult to bypass. However, with a multiplexed approach we can address some of these limitations and provide a growing improvement to the current practices.

Traditional immunofluorescence assays have enriched our understanding of cellular morphology through the use of antibody staining targeting the unique constituents of a cell. With H&E and IHC staining, we can already discern distinct patterns, morphologies, and antigen presence, but in order to multiplex antibody labeling,

new assays need to be developed. CyCIF, an adaptation of the traditional IF assay, builds upon its strengths, transitioning it to become an iterative, or cyclic process by allowing for staining of three antibodies per cycle (which we will further detail later) for as many cycles as the tissue remains on the slide, a highly multiplexed method. This is to say, theoretically, if tissue integrity remains high, the number of biomarkers added to one sample/slide can be limitless, leaving few constraints in the way of endless multiplexing. CyCIF is used to screen and phenotype tumor sections as well as other specimens embedded in FFPE (i.e., sections of trachea and lung tissue from human COVID-19 decedents, attenuated tuberculosis tissues etc.) through multiplexed antibody staining. Though FFPE slides are preferred, any frozen specimens can also be studied. Instead of labeling a slide with just a nuclear DNA stain (usually Hoechst), three primary antibodies concurrently, and their corresponding secondary antibodies (tagged with a fluorophore), we perform subsequent staining with sets of three additional directly conjugated antibodies thereafter, its ensuing "cycle." This process is repeated several times. A fundamental step performed between each cycle is to extinguish the fluorophores from the previous round's secondary antibodies thereby removing any residual fluorescence. CyCIF was performed on tumor tissue to provide a deep phenotyping on cell populations and to help characterize the tumor microenvironment of various patients by qualifying and quantifying abundances of cell types, assessing up and down-regulation of signaling pathways, breaking down cell-to-cell interactions, and analyzing network proximity of like and unlike cell types through staining with antibodies and clinically relevant biomarkers. Shared characteristics or trends in marker expression amongst tumor types may indicate similar tissues of origin and shed insight on particular up-or-down regulated

pathways that could expose a druggable target, an attractive prospect for drug discovery and precision medicine.

Specific CyCIF Panels Address Investigative Research Questions

With these goals in mind, we have built upon work previously described by Schapiro et al. (2021) which describes our EMIT (Exemplar Microscopy Images of Tissues and Tumors) dataset as a significantly relevant microscopy tool. Analysis of EMIT has shown that CyCIF can increase our understanding of cancer biology and improve image-post-processing tool development; here, we expand upon preliminary findings and extend the reach of its capabilities. Altogether, we stained 25 human tissue microarrays composed of over 120 1.5mm biopsy cores from 42 patients representing 34 types of cancer or non-neoplastic diseases, as well as normal tissue used as controls. Each of the TMAs was stained with particular CyCIF panels directed at answering a variety of distinct biological questions, although there were many markers overlapping between them. For example, common immune markers such as CD45, CD56, and CD68 were used to stain a majority of the TMAs as they are critical markers for staining diverse immune populations. Subsequent cycles employed additional antibodies to further subdivide these immune cell populations (CD45+ cells), such as CD4 and CD8a to differentiate helper T-cells from cytotoxic T-cells, or CD11c and CD163 to differentiate M1 and M2 macrophages that are both CD163+ (Egal et al., 2019). Another grouping seen recurrently in the TMAs provides a macro-level glance into tissue core-specific features characterized by the staining of E-cadherin, pan-Cytokeratin, and CD45 to differentiate epithelial cells from cancer/tumor cells from immune cells, respectively. These three categories gave a broad sampling of cell types within cores – allowing us to

create a more specific supplemental staining plan based on the relative abundance of cancer, immune, and epithelial cells. Here also, we have used the earlier TMAs, such as TMA1, TMA2, and TMA3, to guide our own selection of antibodies for subsequent panels through evaluating their efficacy. TMA11 and TMA22 were specifically chosen to comprise the EMIT dataset as they were stained with panels focusing on training deep learning cell segmentation algorithms and evaluating the efficiency in labeling cells undergoing the different stages of mitosis, with a secondary emphasis on targeting important sub-cellular structures. The broad objective for staining each of the TMAs can be found in Table 1. Many of the earlier TMAs were stained with traditional markers used for characterizing the tissue architecture of different cancers, such as CD31 and Vimentin. Others were stained with antibodies aimed at targeting their primary tumor-cell type composition, such as c-Kit and calponin expressed in leiomyosarcoma or p14 and p16 expressed in liposarcoma. However, in efforts to both qualify and quantify an abundance of antibodies, as well as catalyze collaborative efforts, many TMAs were stained with project-specific antibodies and biomarkers to address particular biological questions. For example, TMA5 was stained specifically to target the cancer cells within each unique cancer core through using previously established cancer-specific markers. Pax8 was stained to target cancer cells specific to ovarian cancer cores, CDX2 was used to stain tumor in the gastrointestinal (GIST) cores, p53 to stain breast cancer cores, and TTF1 for lung adenocarcinoma (AC) cores. This panel was used to directly answer whether or not the expected hallmark of cancer biomarker stained as anticipated and also if we could differentiate one tumor type from another through these biomarker expression levels. The panel was also used to determine whether or not previously established

cancer-specific biomarkers would be present in unanticipated malignancies. Further, after gauging the hallmarks of certain cancers within the TMAs, they were almost always stained with antibodies of typically common immune cell types to evaluate immune response in connection to tumor-specific antibody presence. Other instances of cancer-specific antibodies used can be found in Table 2.

With different angles to consider for staining plans, we used a selection of the TMAs to address other factors that impact tumorigenesis, tumor progression, and immune regulation among a host of other relevant biological processes. For example, it is well-established, but not well understood, how a tumor continues to exist even in the presence of a strong immune cell population: B-cells, T-cells, natural killer (NK) cells, macrophages, dendritic cells etc. By using antibodies that target different cellular contexts, we have begun to acknowledge some of the reasons tumors persist and escape the typical immune response. The underlying biology can tell us the level of immune evasion that each tumor is exhibiting and cell-checkpoint markers such as cMAF, IRF7, RunX2, and STAT5a and STAT5b can shed light on the regulation or dysregulation of the immune system as it encounters tumor. The tumor, conversely, fights back and suppresses immune-mediated tumor killing so the cancerous cells can continue to proliferate, as evident by the presence of Ki67 or PCNA nuclear staining indicative of active proliferation (Juríková et al., 2016). The relative abundance of these biomarkers aids in understanding disease state and disease progression. Other panels were stained for pro-apoptotic markers, as well as markers indicative of cell-stress, such as NOS2, cPARP, cCASP3, Cox4, NQO1, HO1, p62, and HIF1a, helping us assess proper and improper cellular processes that should be triggered when unnatural signals are received

but often not in the company of tumor. As a result, aberrant signaling can initiate tumorigenesis and tumor progression (Doheny et al., 2020), factors that we can judge vaguely when scoring expression for these particular biomarkers. Knowing which cells are undergoing the most stress will help us identify the different stages of immune response and disease progression as well as further reveal the underlying mechanism(s) that may have gone awry as a result of cancer signaling. Additionally, by staining multiple TMAs with the BCL2 protein superfamily, we can measure the levels of pro- and anti-apoptotic proteins in tumor and stromal cells that can guide therapeutic decisions in many B-cell leukemias and lymphomas. As Davids et al. found, having more cells close to their apoptotic threshold, referred to as "apoptotic priming," and therefore expressing additional pro-apoptotic markers, leads to improved clinical outcomes and reveals signaling from B-cell receptors (BCR) as druggable targets (Davids et al., 2012). In staining with BCL2 protein superfamily antibodies, we can quantify apoptotic priming, BCR signaling, and cells undergoing programmed cell death in efforts to combat the infiltrating tumor to determine whether this is normal or if these processes have been hijacked. By exploring these cellular mechanisms and related signaling pathways, we achieve a greater understanding as to what may drive disease progression in certain malignancies. Here we have provided quantifiable antibody imaging data for many signaling pathways, including the AKT and MAPK pathways, to reveal additional druggable targets as they relate to specific malignancies.

In total, we stained 25 TMAs with over 520 different antibodies that delineate tumor, immune cells, tissue architecture, signaling pathways, cycling and proliferating cells, among others in hopes of garnering a near-complete deep cellular profiling. TMA

cores were grouped in twos by diagnosis as the cores were punched and mounted sequentially. Also, almost all of the cores are located elsewhere on the TMA as biological replicates in efforts to increase sample size to inspire further confidence in our findings. Figure 1 provides a general overview of the TMAs stained with CD163 (green), CD3d (white), and CD31 (red) giving a sense of tissue composition and landscape staining macrophages, T-cells, and blood vessels, respectively. Here we can begin to assess immune cell populations and tissue morphology at a per-core basis with only three markers. We can also begin to gauge tissue integrity from a macro level as CD31 outlines vasculature which often dictates tissue integrity, which we shall discuss in greater detail later. While many of the antibodies were used to directly address specific biological questions, others were used to propagate supplementary findings as well as guide the formulation of novel questions. A marker identified within a core where it was not expected may trigger further investigation into its biological and/or clinical significance. We have begun to address these questions and have considered the limitations in the field when doing so.

Experimental Methods

As outlined by Lin and colleagues (2018), using the standard CyCIF methods, all slides were baked and de-waxed using a LEICA Bond instrument as well as underwent a programmed heat-induced epitope retrieval process using the same instrument. Pre-processing on the LEICA Bond took roughly six hours and all the TMAs were pre-processed using the same protocol throughout, in an almost entirely automated manner to reduce human handling and minimize human error. After slides were removed from the Bond, residual chemicals from the instrument were rinsed away in multiple washes of 1x

phosphate buffer saline (PBS). After slides were rinsed, they underwent an initial photobleaching step that uses a hydrogen-peroxide sodium-hydroxide (H_2O_2) solution to minimize tissue autofluorescence. As we will delve into later, tissue autofluorescence and background staining pose major challenges to downstream analyses, so performing initial bleaching step proves valuable. After two 30-minute photo-bleach incubations sandwiched between LED lights, slides were rinsed again to remove residual bleach.

At this juncture, slides were then mounted and imaged in their most raw form to capture tissue autofluorescence. Hoechst 33342 DNA stain was added in small quantities during the pre-processing steps performed by the LEICA bond, so the microscope is able to detect nuclei, thus a region of interest can be made even in the absence of antibody. After rinsing away the residual Bond chemicals, TMA cores were covered using a 70% glycerol v/v solution (this percentage parameter was optimized and selected after numerous earlier experiments). Slides were then mounted with a glass coverslip, left to dry briefly ensuring that the coverslip did not shift during image acquisition, and then imaged. By imaging tissue autofluorescence, we can get a quantitative understanding of what fluorescent properties FFPE tissues display after sectioning and pre-processing but still naïve to antibodies. These cycles are often referred to as "autofluorescence (af)-channel," for example "af-488" during imaging.

After imaging, slides were de-coverslipped, an essential step that we will dissect in greater detail, and then prepared for an additional quality control step. As with reducing tissue af, TMAs were then stained and incubated overnight (4º C) in a darkened humidified chamber with the secondary antibodies that will be bound to primary antibodies in the next round of CyCIF, as well as Hoechst (1:5000). If a rabbit primary

antibody was selected for staining in the 488 channel, an anti-rabbit 488 secondary would be used to label that antibody (frequently goat in the 555 channel and mouse in the 647 channel); thus we used species- and fluorophore-specific secondary antibodies for an initial incubation for quality control purposes. In doing so, we aimed to minimize any non-specific binding that may occur, but also quantify it if present, much like we had done with tissue autofluorescence. These cycles are often referred to as "background (bg)-antibody name," for example "bg-CD28." After overnight incubation, slides were rinsed in PBS and hidden from light as best as possible. Any fluorophore exposed to light will begin to lose intensity depending on how long the exposure lasts. Slides were then mounted and imaged using the same region of interest in which tissue af was captured from the previous day/cycle. Imaging the bg of the secondary antibodies is useful for accurate background subtraction during the post-processing of images allowing for interpretation of actual antibody stain considered "true," when subtracting non-specific binding fluorescence.

Overall, we stained various FFPE tissues with both unconjugated, species-specific primary antibodies as well as directly conjugated primary antibodies in the later "cycles." The first cycle or two of CyCIF often employs unlabeled antibodies for indirect immunofluorescence as it usually benefits from higher binding specificity as the secondary antibody binds precisely to where the primary antibody has bound, with minimal off-target binding, though others argue the difference is minimal (McMahon et al., 2020) when compared to direct IF with pre-conjugated antibodies. The fluorophores that are bound, labeled, and imaged come in two formulations: either added through the incubation of a species- and isotype-specific secondary antibody or through a fluor that

has been directly conjugated to the antibody itself (by the vendor or via in-house conjugation). The latter are referred to as direct conjugates. Regardless of the type, when excited by a light source, the fluorophores fluoresce in different wavelengths, assigning different colors to each antibody imaged. Using a RareCyte microscope (or other microscopes with similar multi-spectral imaging capabilities), we visualized three antibodies and DNA with differentially emitted and excitation filter wavelengths as follows: DNA channel excited at 390nm, emitted at 435nm; AF488/FITC channel (note: here the AF represents "Alexa Fluor" which are the most commons fluorophores used in the FITC, Cy3, and Cy5 channels; it does not mean "auto fluorescence") excited at 475/28nm, emitted at 525/48nm; AF555/Cy3 channel excited at 542/27nm, emitted at 597/45nm; AF647/Cy5 channel excited at 632/22nm, emitted at 679/34nm, respectively (Lin et al., 2018). With the three channels imaged together, as well as Hoechst, they represent a completed cycle: DNA, antibody in the FITC channel, antibody in the Cy3 channel, and antibody in the Cy5 channel. After imaging, between each cycle, we performed the same highly optimized photobleaching step that quenches the fluorophores using the aforementioned H_2O_2-based solution before staining and imaging the subsequent cycle of antibodies.

After the first couple of cycles, the importance of species is lost as direct conjugates do not require a secondary antibody, but antibody shuffling is needed to stain tissues with an antibody in each of the 488, 555, and 647 wavelength channels. Many of the more common antibodies and reagents have been well established in scientific literature, vendor websites, or from other validation efforts allowing for antibody shuffling. Markers for T- and B-cells, such as CD4, CD3d, CD8a, CD19 and CD20, are

common immune cells, which means they are usually available in many forms, either as an unlabeled version or as a direct conjugate with a number of possible fluorophore conjugations. However, less common antibodies that are more specific to particular subsets of cells or malignancy, such as MelanA (MART1), are only commercially available in the Cy5 channel. Or rather interestingly, through previous validations efforts, we have found that only the AF647 conjugate works properly given our conditions. Thus, to accommodate MART1-647, the other antibodies desired in the same cycle as MART1, perhaps HMB45 and Sox10, other markers of melanocytic differentiation, need to be in the AF488 and AF555 channels. Therefore, being able to mix and match antibodies is significant; if we run out of particular spaces for an antibody, alternative selections are a must. However, often there is no commercially available antibody to occupy the vacant channel. For this reason, we performed a rigorous initial battery of assays and context-driven validation experiments and have extended many of the preliminary findings to shape continued efforts determining which antibodies work as expected and which do not – a key feature of this work. Further, we have qualified whether the performance of antibodies is more or less effective in one particular channel than it is in another, or if a direct conjugate, as opposed to an unlabeled version of the same antibody with the same target, performs any better. While we did not expect find drastic differences in the performance of an unconjugated antibody versus conjugated one or an antibody in one channel versus another, this was not the case for several antibodies, which we will discuss in greater detail.

During imaging, a region of interest (ROI) is suggested by the RareCyte CyteFinder based on the presence of nuclear stain added during preprocessing. We either

confirm that the ROI is accurate or manually guide the microscope to scan a particular region and select desired landmarks within the tissue for focusing – focus points – which are evenly spread across the edges of the TMA with many points of focus in cellularly dense cores. By adding focus points on cellularly dense cores, we ensured a relatively consistent z-axis coordinate spanning the full TMA; if we focus on poorly adherent tissue cores where cells may be lost, the z-axis coordinate would shift too much during image acquisition to capture an in-focus image. Normally a sample ranges anywhere from 400-600 image tiles, but depending on the tissue type, more tiles may be needed to capture the full specimen. As these TMAs contained over 120 cores, they ranged anywhere from 1200-1600 tiles, meaning it took significant time to acquire each cycle's image. Further, each of the antibodies had been previously optimized with particular dilutions and exposure times to ensure the proper excitation, emission, and time captured the true signal of an antibody. These parameters were selected after evaluating consolidated data collected from many previous antibody validation experiments aimed at determining which dilutions and exposure times produced the most reliable results. Most of the exposure times used ranged from 50 milliseconds (ms) to 500 ms. Using an exposure time longer than 500 ms can photo-bleach the sample and decrease true signal intensity of adjacent tiles as they are imaged one-by-one in a snaking pattern. Without spectral overlap, these four channels can be imaged, merged, and viewed simultaneously, giving us a representative image of the whole slide, referred to as whole slide imaging (WSI).

Once the round of imaging was completed, the TMA slides were submersed in 1x PBS warmed to 42º C for a minimum of 30 minutes. The temperature of the PBS had been optimized through the same validation experiments mentioned. 42º C was the proper

temperature found to minimize shearing forces as the coverslip is removed; this process is referred to as de-coverslipping. During de-coverslipping, shearing occurs as PBS flow interacts with the glycerol mounting solution on the physical specimen often pulling tissue off the slide as the solutions interface as the coverslip begins to shift off of the slide. Tissue loss remains one of the greatest threats to CyCIF experimentation; if the de-coverslipping process is not performed properly and slides are removed prematurely from the pre-warmed PBS, one risks losing large chunks of tissue which can compromise an experiment. As we will later detail, different presentations of tissue landscape play a role in overall tissue integrity and the core's ability to remain full and adherent even after repeated rinses and de-coverslipping events.

Once de-coverslipped, slides were photobleached twice, rinsed, and then re-stained with primary antibodies, as well as Hoechst, for overnight incubation. After incubation, residual primary antibody was quickly rinsed away and the species- and isotype-specific secondary antibodies were added (to label the primary antibodies with a fluorophore) for one hour at room temperature, in the dark. The secondary antibodies were then rinsed off thoroughly and the same mounting and imaging procedure was performed. Both of these washes are critical steps in the experimental process. If primary and secondary antibody are not fully rinsed, one risks acquiring non-true antibody signal in the form of antibody aggregate, smudged signal (a literal smudge across an imaging field indicative of a poor fluorophore rinse), or saturating secondary, all of which further complicate downstream processing. Again, the same ROI is captured in successive cycles on successive days allowing for proper image registration and alignment during image post-processing through nuclear stain coordinates. Slides were then de-coverslipped,

bleached, and stained with the next round of antibodies; if another round of unconjugated primaries is used, species specificity remains a concern. Normally, rabbit, goat, and mouse antibodies are used in the first cycle, as they are the most common species of antibody. That said, if another round of indirect IF is performed, the primaries need to be a different species or isotype-specific, such as IgG1 and IgG2b, to allow for two additional mouse antibodies. Targeting IgG subclasses makes this type of double-stain possible; but the mouse antibody used in Cycle 1 must be IgG2a if an IgG1 and IgG2b secondary antibody is to be used in Cycle 2. This cyclic stain, image, bleach, stain process then repeats itself for each batch of three antibodies as many times as desired, hence cyclic immunofluorescence.

Once all cycles had been stained and imaging had been completed, WSIs were registered and stitched together through an image post-processing pipeline utilizing ASHLAR (Alignment by Simultaneous Harmonization of Layer/Adjacency Registration) (Schapiro et al., 2021). Cycles were added on top of one another to create a multiplex image stack composed of three antibodies for however many cycles are stained until tissue integrity dissipates. For example, TMA1 was stained with 24 antibodies across eight cycles whereas TMA13 was stained with 45 distinct antibodies across 15 cycles (excluding background imaging and DNA in both instances). The end-product of these post-processing steps was a stitched WSI containing each of the cycles stacked upon one another in the form of an .ome.tif file that was then uploaded into visualization software such as omero or ImageJ for image inspection. Additionally, as modules of the MCMICRO post-processing pipeline, which includes ASHLAR, probability maps, segmentation masks, quantification .csv files, and illumination profiles were also created.

One cycle of TMA imaging produces a .tif image file anywhere from 10-30GB, so the multi-cycle .ome.tif image which contains the image of each cycle individually becomes an image file of approximately 250 or more GB depending on the number of cycles. When accounting for the number of TMAs stained in total (25), massive amounts of image data was generated and leaves the experimenter and analysis team busy for weeks disentangling single cell information, neighbor analyses, and intensity values across a myriad of cancers. From this accumulation of data, we extracted the necessary information to address both our aims and some of the limitations we have encountered first-hand in the field. With such an extensive dataset, we have focused primarily on the images, cores, and antibodies that could provide the most relevant information and context towards addressing our interests and concerns regarding CyCIF multiplexed imaging and how it can contribute to a clinical setting. Though we do not believe there will be a direct translation to clinical validation, the agglomeration of underlying biology we can ascertain from multiplexed and high throughput CyCIF imaging helps research scientists, pathologists, histologists, and clinicians answer critical questions pertaining to a patient's tumor.

To answer some of the outstanding questions, we prepared aspects of these CyCIF experiments and staining plans to address our aims. One of the main aims was to assess the quality of commercially available reagents. With 25 TMAs stained with over 520 different antibodies (Table 3), we have targeted different aspects of biology that include immune cell populations and subpopulations, signaling pathways, cell states, tumor progression markers, tumor-specific markers, and many others. With so many antibodies stained under the same conditions and images processed and compiled in the same

manner, we can begin to assess the markers and determine which worked as expected, better than expected, or worse than expected to create a useful guide not only for future CyCIF experimentation but also for the clinic when exploring antibody alternatives. We have also fine-tuned the quality control parameters of these TMAs to enhance our own confidence in our staining findings; the proper controls were implemented in terms of af reduction, af capture and quantification, as well as bg subtraction steps whereby the bg of all three channels was imaged and quantified for proper quantitative background subtraction. By shedding light on poorly understood underlying biology and mechanistic underpinnings in a research setting, we are more adequately prepared to share these results with pathologists and clinicians in hopes of bettering patients' lives. If we can expose or suggest a druggable target through deep characterization of patient's tumors, we might be able to improve their prognosis as a result of enhanced personalized medicine.

Chapter III.

Results

Cell Morphology Illuminates Patterns Amongst Like and Unalike Cancers

One of the primary goals in assessing H&E and IHC images is to determine whether or not anything in the histology is unusual, typically representing the presence of disease and offering a brief glimpse into disease state. Differential growth rates, patterns, spacing, cell density, and morphology are mostly visible through evaluating IHC staining and can deliver insight as to whether abnormal growth and proliferation are occurring and sometimes the rate or extent at which these abnormalities transpire. These findings offer a unique view into a patient's specific tumor and data to consider for pathologists and clinicians to determine the next steps in treatment. Here, we show how multiplexed CyCIF imaging can be accurately mapped back to original H&E and IHC images, accomplished from pattern recognition of morphological landmarks easily detectable in both image types. To do so, in all three methods, a specific antibody or biomarker is needed to target particular cell types or cell components for visualization. In our work, including the EMIT dataset, we have profiled and deeply analyzed, written up, and published two manuscripts incorporating some of the findings from these TMAs (Schapiro et al., 2021; Yapp et al., 2021) in which we characterize a host of cell types by expression of certain antibodies. In the two particular TMAs highlighted in the EMIT dataset, both slides were stained with markers specifically designated to outline the nuclear envelope of all cells to demarcate specific classifications of cellular morphologies. These labeled images enhance deep machine learning for cellular segmentation and the downstream processes of image alignment, tile stitching and

registration, core dearray, illumination correction, and other quantitative results, all outputs of MCMICRO. But, more than for just machine learning, these TMAs can serve as a visual guide into cell morphology and the differences amongst cancer histological classifications. By first identifying and outlining the nuclear envelope of cells within a given disease, we can show and appreciate morphological differences in the same way that H&E and IHC images can. We then compare these distinct diseases and their morphologically unique nuclei side-by-side to aid pathologists in their diagnoses – especially if exemplar data is available denoting distinct features of one subtype from another – an approach that is commonly performed today in many malignancy classifications as we will discuss later.

From our data, cellular morphologies were broken down into seven distinct classes. These classes represent the most common cellular morphologies across all 25 TMAs; they are: round versus narrow, small versus large, densely packed, irregularly packed, or organized in clusters (Figure 2). To diversify the cell types that deep learning AI was trained on, a subset of cores was selected to represent a varying population of cell types and morphology; they are: lung adenocarcinoma (AC), colon AC, non-neoplastic small intestine, non-neoplastic ovary, glioblastoma, normal prostate, and tonsil. Each of these cores were composed of cells classified into one or more groups. The cores were stained with a cocktail of two different nucleoporin (NUP) antibodies and four different lamin antibodies. This cocktail was selected to stain a majority, if not all, nuclear envelopes of cells present within a given field. From these images, we can begin to visualize the different cell morphologies and classify cell types based on their appearance. As shown, the lung adenocarcinoma sample presents with two unique

cellular morphologies, large cells present as well as smaller ones. In juxtaposition, the non-neoplastic ovarian sample is composed of narrow, spindle-like cells densely packed together; two cores representing four different classifiers. While this may seem trivial, in the diagnosis of ovarian carcinomas, the classification system is almost entirely morphology-based (Cho & Shih, 2009), further emphasizing the need for our exemplar data source. A quick qualitative overview of cellular morphologies and histological classifications can help distinguish differences in disease diagnosis. Further subdividing the patterns consistent across cores can serve as a reference guide for normally unnoticed minor differences that may hold large implications: one malignancy can be diagnosed over another almost entirely by histologic classifiers.

MCMICRO and UnMICST Provide Multi-dimensional, Actionable Data

As we have discussed, the MCMICRO pipeline serves as a tool that can advance WSI data curation and analysis in multiple ways. Both Coreograph and Scimap, modules within the MCMICRO pipeline, perform image post-processing steps that prepare our data for further investigation. Coreograph de-arrays all cores within the TMA such that each can be extracted and analyzed independently and in high resolution, honing in on disease-specific differences both intra- and inter-core. Scimap clusters cells at a single-cell level, performs neighborhood analyses, and assigns a cell-type assignment based on marker expression through the generation of heat-maps that quantify expression levels across a gradient. For example, CD8 positivity is classified as cytotoxic T-cells, CD20 positivity as B-cells, and pan-Cytokeratin positivity as tumor or regions of tumor burden. By generating a variety of classes of cell types through the expression level of many antibodies, we develop a firm understanding of each cell's expression profile and how

neighborhoods of like cells interact in the presence of tumor. The more identifiers added, meaning the numbers of different antibodies a certain cell type expresses, the better we can understand the role of specific cell classes that exist, such as a CD163+ CD11c+ HLA-A+ macrophage tells us more about its role and subtype of macrophage than does a macrophage expressing only CD163.

Both MCMICRO and UnMICST serve as valuable representations as to how this data was and will continue to be used. Though this dataset has not been prepared to serve solely as a deep-learning cell segmentation training set for one specific disease, the eclectic nature of core selection serves as a vital resource to train on a variety of cancers and cell types to enhance the detection of minute differences across diseases. However, if more samples were introduced, beyond the scope of this preliminary research, it is feasible that this work could serve as a catalyst and the foundation for an atlas that can be further broken down into specific diseases, much like what Lin et al. have done for colorectal cancer (2022). Until then, both MCMICRO and UnMICST take subsets of our data to train the algorithms associated with our cell-type-calling and labeling capabilities which are sufficient in recognizing morphologic differences between cancers to reveal patterns. Both modules have been cited showcasing the strength of our WSI post-processing. Specifically, MCMIRCO and UnMICST stand relatively alone in the domain of whole-slide imaging, which has recently come to the forefront of histopathology, in that their capacities go above and beyond regions of interest being able to process large areas, an attractive prospect for data analysts in the big data era.

Further, by using exhaustive expression profiles to classify cells, we can guide machine learning to a previously unmet level with comprehensive groupings. In curating

a list of "genotypes" based on expression levels of particular antibodies, we enhance the capabilities of our AI to perform at its best. In-depth classifications of cell types can help pinpoint differences in cellular populations amongst the cores within the TMA. As a result, we create a profile for each histological classification with its associated cellular composition and the cellular neighborhood in which these groups reside, hopefully revealing patterns that exist inter-core and inter-TMA. Another way in which CyCIF serves as a powerful tool is that it generates more actionable data from the same amount of material that both H&E and IHC require. But here we have begun to uncover data revolving around cell-cell interactions and composition of the TME, neither of which are reached via histological standards – one of their major limitations. By identifying different cell populations and profiles within a core, we expand our own understanding of the underlying biology within each malignancy.

Not only do cellular morphologies matter when discussing unique phenotypes of different cancer histological classifications, but the tissue and cellular density does as well. We found that distinct cancers present differently from one another in terms of their cell populations, cell densities, and overall tissue architecture. Here, "histotype" from Lin (2022), is used when referring to a unique histological presentation or classification of different malignancies based primarily on morphology; so, subtypes within the same disease can have exclusive histotypes. Tonsil, often used as a control in many forms of antibody imaging, contains densely packed cells, both inside and around the germinal center. This histotype is starkly contrasted to that of glioblastoma and colon adenocarcinoma in which cells are more freely spaced throughout the core. Normal prostate also serves as a cancer-free control in which we are presented with a

heterogeneous mix of cellular phenotypes. Like lung AC, there are both large, rounded cells within the prostate core but also long spindly cells almost exclusively highlighted by lamin B2 staining, also seen in Figure 2. So, while there is limited clinical relevance to a normal prostate core, it can still serve as necessary training data for deep learning algorithms. Needless to say, the non-neoplastic prostate can also serve as a key comparison to a patient with a prostate malignancy as comparing cell morphologies and antibody expression levels between the two may expose investigation-worthy biology. These overall observations serve as critical material to aid diagnosis and can be used as reference material when assessing tissue morphology. While it may seem inconsequential to provide a histologic classification tool, generating disease-subtype-specific profiles based on slightly altered morphological features already serves as a critical resource in many malignancies such as lung and digestive tract cancers (Inzani et al., 2017) and we aim to expand these examples.

Histological Classifications Determined by Presence or Absence of Antibody

With 34 different tissues on the same pathology slide, it became possible to evaluate specific cores with their hallmarks of cancer. After a thorough literature search and battery of validation assays, we put together an atlas-like tool to determine which of our 500-plus antibodies can, should, and did stain the cores they were expected to stain. Table 2 provides an overview of the different cancer diagnoses, as well as benign tissues, and the particular antibodies that were expected to be expressed in each disease. For example, CD141, otherwise known as thrombomodulin, is used as a diagnostic marker to detect and classify different subtypes of mesotheliomas such as epithelioid versus sarcomatoid (Miettinen et al., 2001), yet another example whereby IHC assessment has

direct clinical translation. These findings affect how a clinician may treat a patient as one subtype of disease often requires one drug regimen versus another. As Inzani and colleagues suggest, classification tools based on morphological features have proved successful in predicting patient survival and impact both patient management and therapy establishment (Inzani et al., 2017).

One of the confounding factors we identified during the collection of this dataset are false-positives and false-negatives in staining and how to mitigate or remove them from analysis. Even though we have described a systematic and well-controlled experimental approach, there are still aspects of the process that we cannot control. While we do expect to see malignancy-specific staining of the markers listed in Table 2, such as calponin present in leiomyosarcoma and SDHA in gastrointestinal stromal tumors, these markers may also appear in other cores scattered throughout the TMA. As Figure 3 shows, the calponin is most abundant in the leiomyosarcoma core, though it is present in low quantities within breast ductal and lobular carcinoma cores as well as the seminoma core; the same goes for SDHA which is high in the GIST core as expected, but present in lower abundances in the mesothelioma, colon lymph node, and colon AC cores. Though many of these markers are highly-specific for one particular malignancy or normal cell type, there are overlaps and broad staining patterns observed throughout multiple diseases. Many markers such as pan-Cytokeratin and Ki67 appear in nearly all cores but in some IHC assessments, these markers serve as the lone critical indicators of tumor presence and tumor progression. In assessing HGSOC IHC slides, the main diagnostic markers for tumor and disease subtyping include Ki67, vimentin, E-cadherin, and CD8 – most of which are relatively common markers, thus used in many of our panels and seen

throughout many cores within the TMA. In fact, all 25 of the TMAs were stained with pan-CK, 20 of the 25 with CD8, 17 of the 25 with E-cadherin, 16 of the 25 with Ki67, and 5 of the 25 with vimentin. Therefore, it seemed imperative to add additional markers such as ER, PR, and Pax8 to better evaluate the TME within the ovarian cores. Without those markers, the histological analysis may integrate false-positives as nearly all cancers expressed some levels of Ki67, vimentin, E-cadherin, and CD8. Though Ki67+ Vimentin+ E-cadherin+ and CD8+ cells are not always false-positives, the results need to be further tuned to regard those particular groupings as cancer cells in HGSOC, but not necessarily in other cancers, recapitulating the need for advanced marker expression profiles. With HGSOC, we are more confident in qualifying cells as cancerous if they co-expresses pan-CK, Pax8, ER, or PR as opposed to pan-CK alone. Thus, our findings could not be extended without the addition of these disease-specific markers that guide our understanding of the biology and contexts that make them unique.

Nucleoporin, Lamin, and Surface Markers Outline Cellular Compartments

In staining these TMAs with lamin and nucleoporin, we afforded ourselves the ability to train deep learning AI algorithms based on the staining profiles found throughout the cancer cores, and, in turn, improve cell segmentation efforts. Automated processing tools vastly enhance the field of digital histopathology, but require rigorous training sets to guide algorithms in targeting and differentiating subtleties in images to create distinct classifications. The classifications from Figure 2 represent the basis for nuclear morphology segmenting used to train our AI. This image represents the preexisting standard as to how traditional cell segmentation occurs with a watershed approach: first identify and encapsulate the nucleus and then expand a secondary mask

around the centroid until pixel intensity values fluctuate. We then used our different nuclear masks to amend our segmentation, as seen in Figure 4, where we stained colon adenocarcinoma with lamin antibodies: lamin A/C, lamin B1, and lamin B2, to capture a large proportion of the nuclei in a desired field. If the lamin antibodies did not suffice in outlining all nuclear envelopes, the addition of NUP98 and NUP133 usually captured the remainder. We then used these markers to perform our own modification on the watershed segmentation process to create distinct classes of cell types, some of which appear in lung AC tissue. We feel as though extending these efforts to such a large number of TMAs has given us the ability to target and outline nearly all possible nuclei in a core – inspiring confidence that proper segmentation can be achieved. On top of the nuclear-envelope-cocktail, we then began to work on cytoplasmic and membranous labeling to capture the other two main components of a cell needed for cell segmentation. Other organelles and structures within the cell were also stained using a variety of antibodies that include TOMM20 to target mitochondria, catalase to target peroxisomes, and autophagosomes related to apoptosis with p62 to introduce additional classifications, however surface and cytoplasm seem to offer more intriguing and widely applicable opportunities.

Traditionally, cell segmentation has been performed solely by identifying the nucleus as the centroid position and moving outward by a fixed number of pixels, but recent advances propose using multiple membrane markers to help identify differences in the morphologies amongst tumor cells between cancers in a contour-based manner (Schüffler et al., 2015). To do this, a number of surface markers can be used to target non-nuclear components of a cell such as E-cadherin, pan-Cytokeratin, CD68, and alpha

smooth muscle actin (aSMA). These markers, seen in Figure 5, highlight some of the unique morphological presentations of the cytoplasm and cell-surface that present in different ways and abundances across unalike cancers: epithelia – a diagnostic breast cancer marker (Singhai et al., 2011) – cytoplasm and membrane, the surface of many different immune cell types, and a subset of stromal cells, fibroblasts, respectively. Again, each additional label strengthens the AI's ability to segregate cellular components. Each of kidney, lung AC, normal colon, and non-neoplastic colon show diversity in terms of surface staining abundance and intensity. Although sampling cell surfaces and cytoplasm works well with a cocktail of different antibodies, it still remains challenging to capture every distinct cell-surface or cytoplasm. Markers such as pan-Cytokeratin and E-cadherin are often used as hallmarks of these regions, but still, an outward border grown from a nuclear centroid cell makes a mask (Giotakis et al., 2021) and its accompanying drop in intensity values is what guides most cytoplasmic segmentation. Here, we have done the same but with a wide array of surface and cytoplasmic markers added ranging from N-cadherin and CD40 to Desmin and Cytokeratin 19. We hope that adding these markers will capture nearly all surfaces and cytoplasm present in cells and serve as a foundational piece in improving cytoplasmic segmentation much like the lamin and NUP antibody cocktail did for nuclei. However, this becomes only further complicated with densely populated regions of cells, such as non-neoplastic ovarian samples as it is nearly impossible to determine where one cell nuclei and/or cytoplasm begin and the next ends. With such a diverse group of surface markers across many malignancies, we have the precise dataset that can guide and enhance algorithmic nucleus and cytoplasm detection and segmentation though a scrupulous labeling session will be

essential. While it is no easy task to manually curate a large enough sample size, we find that the ground-truth of human intervention, identification, and classification is what is necessary to establish confidence in these advancing tools.

CyCIF Uncovers Disease Progression through Contextual Staining

As we have discussed, the gold standard in pathology at present remains histologic H&E and IHC staining to differentiate tumor from non-tumor and identify and quantify the presence of one particular biomarker at-a-time. To investigate and expand upon this, we probed various regions of melanoma, aiming to quantify the number of melanocytes present in a particular tissue through CyCIF. By looking at the H&E image of its serial section, it was determined that in different regions of interest there were spatially restricted regions of high melanocyte populations. These regions began superficially in the epidermis of skin and then penetrated inwards towards the dermis (seen in H&E as red and in CyCIF as green Sox10+ cells). These findings are outlined by the dotted black line seen in Figure 6, showing a differential staining pattern of melanocytes from non-cancerous tissue in the surrounding regions. That is to say that the presence of melanocytes shows a dramatically different staining pattern of densely packed pink cells, as compared to the neighboring benign tissue in dark pink and faint pink. While discernible by eye, this may be an imperfect interpretation of the data as varying shades of pink and purple may make it difficult to distinguish boundaries of similarly colored cell types and benign tissue from cancerous tissue. However, as seen on the right portion of Figure 6, after mapping the same region of interest from the H&E image to the multiplexed CyCIF image, it becomes increasingly clear that the melanocyte population(s), shown by green Sox10 staining, have sharp boundaries. These boundaries

can only be seen through the evaluation of multiplexed data and are mostly lost in a low-plex setting. The CyCIF image provides the necessary context to gauge disease status: T-cells are abundant around dense populations of melanocytes, but they also exist in regions where Sox10 expression is low. This is indicative of an immune reaction in response to the presence of melanocytes – again unseen through H&E. Seemingly, the contrast alone in CyCIF images are enough to provide contextualization and demarcate spatial restrictions as compared to white-light bright-field captured H&E stains.

When we assess the IHC image, as opposed to the H&E image, we see the Sox10 melanocyte marker (blue) appearing in high abundance, showcasing melanocytes underneath the epidermis in various fields (Figure 7) but in a more clear and quantitative fashion. The presence of dark blue is contrasted to the light blue Sox10-negative tissue and highlights where along the disease axis melanocyte populations reside, more easily distinguishable from IHC than from H&E, seen in Figure 6. Panels 1 and 2 of Figure 7 show a superficial presence of melanocytes directly below the epidermal surface and not much else. However, the CyCIF images begin to reveal a limited immune response to these melanocytes, which is not seen in the IHC image. Progressing along the x-axis both in the tissue itself and across Figure 7, the number of melanocytes increases. Panel 3 still shows superficial melanocyte presence, but interestingly a robust immune response begins to appear deeper within the skin, indicative of immune regression. Interestingly, Panel 4 highlights a large abundance of melanocytes throughout various layers within the skin with minimal spatial restriction. Not only are the melanocytes present below the epidermis, but they begin to penetrate inwards towards the dermal regions where the aforementioned immune response occurs. Strikingly, T-cells and macrophages are not

present in high numbers despite the deepening penetration of melanocytes. Panel 5 reiterates melanocytes at the superficial level, but also others that have penetrated deeper into the dermis. The accumulation of colors here highlights a tumor-infiltrating lymphocyte (TIL) response that occurs as a result of the large quantity of lymphocytes. As we review and evaluate the CyCIF images in the context of disease and disease state, we see the potential of CyCIF and how it can benefit clinical understanding of disease response through a context-driven multi-marker approach. IHC shows the various regions in which the melanocytes appear and their relative abundance, but offers nothing in the form of disease state. However, when you add immune markers for contextualization, the disease state becomes increasingly clear and can be defined into three different stages.

Taken together, we have provided a direct comparison of multiplexed CyCIF imaging to that of both H&E and IHC staining. The resolutions of the images are comparable, the magnifications, exposures, and processing of the images are also similar in scope, so therefore CyCIF should be able to directly complement the pathological standards and move beyond what is currently being performed, adding an additional layer of descriptive biology. Where CyCIF excels is in the realm of tissue context. Without the addition of markers that label cytokeratin, T-cells, macrophages, and other relevant cell types, we do not fully grasp the context in which these melanocytes live. In a broad sense, if H&E and IHC are used to diagnose and track disease, then having a more well-rounded understanding of disease can serve as an invaluable starting point. In both H&E and IHC, we are still able to answer the question “are melanocytes present in the sample,” but why would we not want to take this finding a step further and begin to evaluate the stages and progression of disease by adding specific markers to characterize

the environment in which they reside. We have shown the capabilities of CyCIF and have an extensive dataset whereby we can continue characterizing the context of many malignancies and disease states.

High-Resolution and Imaging the Z-Plane Reveals Deeper Biology

To further characterize the context of cellular environments and cell-to-cell interactions further, we subjected post-CyCIF slides to an even deeper contextualization. We imaged exemplar slides at a higher resolution (60x) to investigate our interesting findings in three-dimensional space. As our TMAs were sectioned serially, very little biological information should be lost section to section, but we wanted to explore how much, if any, was omitted. It should be noted that if missed biology remains a concern, it is possible to perform H&E on the same slide after CyCIF imaging (Lin et al., 2018) without issue, guaranteeing that the exact regions of tissue are being imaged and analyzed with nothing lost between slides. Slides imaged were sectioned at five microns and while we suspected minimal context lost from one serial section to the next, we explored how extreme some of these differences may be. Seen in Figure 8 is a high-resolution stain as well as a 3-D reconstruction and projection of a resident macrophage interfacing with an exhausted T-cell denoted by the presence of both PD1 and PDL1 on its surface. Interestingly, what is lost in lower resolution microscopy, 20x, typically the standard for multiplexed imaging, is the polarization of proteins as seen through the expressions of the corresponding antibodies. As shown in the inset, PD1, PDL1, and CD163 (the macrophage marker) are polarized towards the bottom right of the cell, which becomes more pronounced as you progress through the z-stack of an image. Here, the maximum image projection was used to emphasize the full polarization that occurs around the cell

in three-dimensional space. The right panel showcases a polarized co-stain of PDL1 atop of the CD8 T-cell marker. Not surprisingly, PD1 presents in a similar fashion as PDL1, nearby, but only on certain T-cells, the exhausted variety. While high-resolution imaging of the samples does take additional processing time and demanding pattern recognition under a more magnified microscope, the benefits are worth it. Much like how a CyCIF image piggybacks and advances histological standards, the high-resolution deconvolved and projected 60x CyCIF image perpetuates a more thorough understanding of the underlying biology that may be overlooked and lost at a lower resolution and adds considerable cell-cell biological and mechanistic information. We have performed deep-phenotyping of particular samples of interest and thus have the ability to perform similar deep-dives on cores of interest that may require a more detailed scope of biology.

The standard histological workflow employs H&E to highlight morphological disturbances indicative of disease and disease state which then guides IHC probing for certain markers specific to the suspected tumor type. Once a low-plex IHC stain has been performed, in the range of one to three antibodies, and the results have been assessed, we propose an additional arm of the workflow in which we craft a CyCIF panel addressing outstanding context-dependent questions which cannot be answered by H&E or IHC alone. Once regions of interest are found within the H&E image, they can be mapped directly onto CyCIF images. Then, the most interesting regions can be subjected to further profiling at a higher resolution to determine the exact context and interface that occurs between distinct cell populations as we have shown possible. While this process cannot be automated in entirety, the vast amount of relevant underlying biological information obtained from a deep cellular phenotyping of a patient's biopsy, can then be

used to lead further discussions in the clinic about a patient's tumor and course of treatment. There are few limitations as to how far and how much meaningful biological data and context can be extracted through CyCIF, but here we have shown four different staining modalities: H&E, IHC, CyCIF, and high-resolution CyCIF, that, when taken together, create a full mosaic of biology to be interpreted together.

De-coverslipping Dictates Duration of a CyCIF Experiment

While the markers discussed in the context of melanoma provide information associated with the immune response as it relates to the differentiation of melanocytes, the real power of CyCIF remains in its multiplex capabilities to characterize context. Cycles and antibodies can continue to be added and imaged for as long as the tissue remains intact and on the slide. That said, a central limitation of CyCIF is understanding the factors that can decrease tissue integrity. We aimed to determine whether or not there are systematic patterns emerging that dictate tissue integrity and how to account for them before beginning an experiment. Part of our efforts attempted to quantify how well tissue can hold together and recognize themes amongst the cores that hold together best. Unfortunately, many of these factors lay outside of the observable and controllable of CyCIF; the longevity of a slide may ultimately depend on storage conditions or fixation methods. However, in this work, we assess the factors that could be controlled and found that tissue integrity remains high for multiple tissue types within the TMAs for many cycles. Cores seen in Figure 9, showcase six different cancers: mesothelioma, colon AC, meningioma, glioblastoma, renal cell carcinoma, and lung small-cell cancer (from right to left) used to assess broad integrity patterns. The colon AC cores are first to succumb to tissue degradation. The reason for this degradation is likely due to three factors: 1. the

tissue is not fully sectioned on the slide itself, 2. as a result of this incomplete sectioning, there are spaces between cellularly dense regions, and 3. the overall tissue architecture of colon adenocarcinoma cores are not ideal for CyCIF as its blood vessels and associated vasculature, often defined by the presence of CD31 and/or CD34 (Qian et al., 2009), leave large gaps between cells even in dense regions, which we believe leads to systematic degradation (also seen in Figure 11b). An overview of this phenomenon in general is seen in Figure 10 where the top row of cores shows lung AC, pancreas, mesothelioma, tonsil, breast ductal carcinoma, and pulmonary lymph node with the most ideal cellular composition in three different TMAs. Conversely, the bottom row shows colon lymph node, lung non-neoplastic, colon non-neoplastic, GIST, breast lobular carcinoma, and kidney with the least ideal cellular composition as determined by the number of remaining nuclei in the last cycles from the same three TMAs. The overlap from first cycle to last cycle should appear in yellow, as evident in the top row. If red or green is seen alone, it is as a result of tissue loss. It is interesting to see in this instance that lung adenocarcinoma, which traditionally does not have the best tissue integrity, appears full and intact after twelve cycles. Typically, the cores with intrinsic large airways or gaps in the tissue, like lung AC, colon, or kidney, show the least amount of yellow overlap. While solutions interface during the de-coverslipping process, one can imagine a turbid flow of solutions that exert their strongest forces where tissue is the sparsest. Based on these findings, we can begin to establish patterns found within tissues that lead to their systematic degradation.

Intriguingly, when we further explored lung adenocarcinoma, a cancer typically associated with complex vasculature, as outlined by red CD31 stain (Figure 11b), we

found that in both TMAs 11 and 12, the tissue was able to withstand 16 cycles; and as we have already seen, twelve cycles in TMA 17. This may be coincidental that the three lung AC cores profiled here in TMA 11, 12, and 17 have relatively smaller airways as compared to the one seen in Figure 11b demonstrating that the size of the airway, indeed, correlates with integrity over time. While the cells themselves adhered to the slide for 16 cycles, Figure 11a shows other factors that impact tissue integrity over the course of the experiment, such as manual perturbations or initial sectioning success. As shown, horizontal lines begin to appear across the tissue surface in a linear fashion as we progress through cycles, leading us to believe that coverslips were dragged across the surface of the tissue, one of the only plausible ways a nearly perfect horizontal artifact appears. It seems dragging occurred during the de-coverslipping step between cycles six and seven where the coverslip did not properly shed off the slide. This artifact is most apparent in TMA 12, Cycle 13 where we can begin to see three or four nearly perfect horizontal lines emerge on the tissue – one line added for each rushed de-coverslipping event. The other main contributor seen in Figure 11a is overall tissue landscape. From initial sectioning, large regions void of cells are seen usually as a result of cross-sectioned vasculature snaking throughout the tissue. As cycles are added, spaces where original vasculature was seen grow as a result of surrounding tissue beginning to slough off. This can be seen in TMA 11 as the gaps in the 3 o'clock, 5 o'clock, and 7 o'clock positions grow from cycle to cycle. These findings support our argument that there can be systematic reasons as to why a core with one histotype lasts for fewer cycles than one of another histotype: tissue-intrinsic landscape interrupted by vasculature of varying degrees.

Though our data do not focus on improperly sectioned cores, many can be seen throughout the TMAs when referring back to Figure 1, such as multiple lung and colon tissues, skin, and hair follicle. While we would have liked each biopsy FFPE block to survive through sectioning of all 25 TMAs, sometimes this is not possible and therefore complete sectioning cannot be performed. When this happens, biological information is missing from the onset and, not surprisingly, poorly sectioned cores often fade fastest. Similarly, sometimes the FFPE block has irregularities resulting from the initial biopsy; as a result, unclean sections may be used for mounting. More examples of these improper punches from Figure 1 include the aforementioned skin and hair follicle shaft, but also mesothelioma (bottom right), two lung AC cores (middle), a tonsil section, and GI stromal tumor (right). These are just a few of the irregular cores sampled from TMA1 and do not necessarily extend through all TMAs sectioned. Sectioning may become cleaner the further into a block the histologist cuts as a result of the FFPE block shape, ergo TMA9 might have more preserved biology amongst certain cores than does TMA1 or TMA24. The overall landscape of cores is often uncontrollable from the beginning of an experiment as they extend back to initial sectioning and storage conditions. When you begin an experiment with less tissue, additional meaningful biology is omitted. If one starts at a deficit, handling slides during the CyCIF experimentation becomes even more precarious. While tissue integrity usually remains sturdy, manual perturbations can disrupt both the experiment and the downstream analysis of tissues, thus need to be controlled for as best as possible when performing CyCIF. Despite the inherent limitations of CyCIF, the potential to garner information in the 40-60 antibody range, if

not more, remains remarkable and one the most highly multiplexed assays in the field, therefore tissue integrity remains a critical aspect to achieve these thresholds.

Antibody Comparisons and Qualification Amongst Cores

In staining 25 TMAs with a wide breadth of commercially available antibodies, we have constructed both a tool and a resource to begin validating markers that can be used without concern in CyCIF experimentation. We hope that these efforts can translate clinically and be applied as much or as little as desired when selecting biomarkers specific to one's tumor or disease. Revealing the underlying biology through CyCIF in a research setting can inform clinicians of minor differences between patients that may be overlooked in a lower throughput setting. Many available markers come in a variety of formulations either as an unconjugated antibody that requires the tagging with a species-specific secondary antibody conjugated to a fluor or a directly conjugated antibody in which the fluor is already bound to the antibody itself. Even after exhaustive efforts to test and qualify antibodies, there still remain outstanding issues when performing CyCIF experiments, such as will an antibody present with signal and will it work in the desired tissue type where stain is expected (i.e., CK20 in lung cancer). Having stained 25 serial sections of TMA, which contain over 120 cores, we have over 3,000 analyzable cores to evaluate staining patterns from over 520 antibodies (Table 3). Take these 3,000 cores and stain them, conservatively, with ten cycles of CyCIF, with three markers per cycle, leads to roughly 90,000 images to evaluate. While this number of images is much too large to investigate in one work, we have begun to dig through the cores, images, and markers that provide the most insight and may be relevant in clinic, such as HER2.

Digging more deeply into TMA 22, we see different cores across six different cancer histotypes and performed a primary qualification of certain antibodies. In these cores we see various expression levels of E-cadherin, aSMA, and CD56, a marker for natural killer cells (Figure 12). Broadly, these three markers are separated into high and low expression levels. For example, looking at the lung AC core independently, CD56 expression levels are low; in a vacuum this would mean that the antibody is not working and should not be considered validated. However, taking a step back and examining other cores within the TMA, we find CD56 expression where there are expected to be high populations of natural killer cells such as non-neoplastic ovarian cancer, diverticulitis, and leiomyosarcoma. In contrast, the E-cadherin marker is barely visible in the ovarian sample, the appendix, and leiomyosarcoma and yet quite bright in the lung and small intestine. If one were to perform an IHC stain of E-cadherin in a similar ovarian core, a false conclusion may be reached; sample size and heterogeneous samples are needed to prove whether or not a stain is true. In the four ovarian cancer cores in TMA22, little, if any, E-cadherin is present (data now shown). Henceforth, we have provided the tools and resources to begin to make assessments of many antibodies that cannot be accomplished solely through IHC. Again, we find that context is crucial when qualifying these reagents, for example, cleaved caspase-3 and cleaved caspase-8 staining is not expected in cores with low levels of apoptosis (Pu et al., 2017) or tumor burden and therefore not present in many of the cores. While there are a number of reasons an antibody may not work such as a lack of signal or improper localization, we aim to further inspect if the stain is of high quality by comparing it H&E and IHC to evaluate its sensitivity, specificity, and

later, its AUC, the only way to prove its efficacy. Then we can move forward with its use in multiplexed imaging.

Taking a step further and approaching qualification specifically, we stained certain TMAs with the same antibodies, either the same clone or different, in different channels, to allow us to make direct comparisons and quantify their on-target versus off-target binding affinity; examples of like-antibody-comparisons can be found in Table 4. Various cores within TMA13 were stained with two different antibodies (with the same target) for each of Sox2, FoxP3, and CD28. We specifically selected lung small cell carcinoma (SCC) because we expected to see expression from these three antibodies. In total, we see a composite image of six total markers (Figure 13a). We have compared two unique versions of each antibody and their expected versus their actual presentation. The two Sox2 antibodies stain the same cells with strong intensity values in both; when green and red co-stain, we are presented with the nuclear yellow stain, the known localization typical of Sox2+ cells. These Sox2 antibodies were labeled with different fluorophores. For FoxP3, again, two different antibodies target the same T-regs, as evident by the localization of magenta and cyan with the expected staining pattern of bright sub-nuclear expression. These antibodies were from different vendors, were of different clones, and different fluorophores. Conversely, when lung SCC is stained with two different CD28 antibodies, typically a marker localized to the cell surface of stimulated T-cells, we see a true, albeit messy stain in dark blue and a complete failure of staining using the second CD28 marker, in orange. These antibodies were from different vendors and one was conjugated and the other was not. The one that worked as expected was the unconjugated version (from Abcam plc.), further supporting the argument that indirect IF may be more

sensitive than direct IF – though further research needs to be performed to support this generalized conclusion. The blue stains the surface of cells while the orange presents a diffuse, auto-fluorescent stain with an indiscriminate staining pattern. This pattern is comparable to what tissue autofluorescence, poorly rinsed secondary antibody, and/or non-specific binding looks like (though the contrast here has been adjusted).

When CD28 or other markers that present in the same manner have their marker intensity value distributions visualized in ImageJ, a software used to analyze multi-dimensional images, a typical bimodal distribution of marker intensity is not seen in the associated histogram. Rather, a bleb of marker intensity close to the y-axis appears, indicating that no specific on-target staining has occurred. Typically, there is a small peak around the lower end of intensity spectrum indicative of background, but also a second peak usually seen further along the x-axis indicative of real expression if an antibody has worked as expected. Figure 13b highlights this phenomenon as histograms of intensity values are representative of the signal present within a particular core. Figure 13b shows that pan-Cytokeratin has a high expression level (green), as evident by the bimodal distribution of log-transformed signal, in lung adenocarcinoma. To emphasize these findings, we plotted true signal against the signal expression of pan-CK's autofluorescence (red), which only has a left-most peak (denoted by the *). This is to say that the left-most peak is noise, whereas the peak on the right is representative of the true signal (denoted by the †). We can then gate and computationally remove the signal left of the second peak – effectively subtracting background. For comparative purposes, we then plotted CD13 (green), another typically finicky antibody, which presented similarly to CD28, in hepatocellular carcinoma, where its stain is expected. However, this time, the

histograms of true stain and autofluorescence (red) are nearly identical as the peaks overlap one another almost exactly and a second peak is not even present. That is to say, the CD13 antibody did not work in the expected tissue. In the same vein, the CD28 signal aligns closely to that of autofluorescence; thus, these particular antibodies would be categorized as a "failed reagent."

One of the more time-consuming aspects of qualifying and assessing antibodies for their proper signal and localization is flushing out false-positives, false-negatives, and to distinguish signal from noise. Figure 13b provides a quick example of this process and now needs to be extended to numerous other antibodies we have imaged. As discussed, we countered some of these difficulties by imaging background channels at the beginning of experiments which we have begun to use for quantitative background subtraction. In the process, we quantified tissue autofluorescence as well as non-specific binding, also called unspecific fluorescence background found in indirect immunofluorescence (Viegas et al., 2007), both of which pose major inconveniences in multi-channel microscopy and the downstream analyses. With the addition of photo-bleaching steps, we first diminished the tissue autofluorescence from completely naïve tissues, imaged it, and then plotted the intensity histograms for tissue autofluorescence (called "af-488). We then performed the same imaging and quantification after incubations with species-specific secondary antibodies to quantify non-specific binding and secondary antibody autofluorescence (called "bg-CD13," for example, if CD13 is our primary antibody). These secondaries will label our first cycle's primary, unconjugated antibodies in the subsequent round so it is important to quantify the non-specific binding to differentiate it from the real signal later. It is well established that the FITC channel has the highest level of tissue

autofluorescence as its peak excitation is at 500nm, but emits with a 75% relative intensity and greater from 506-532nm (Davis et al., 2014); thus, quantifying and subtracting these values are critical when it comes to assessing true marker stain, particularly in the FITC channel. After subtraction, which can be performed through ImageJ, we are left with a cleaner signal, with a bimodal distribution of intensity values which we can gate the residual non-specific binding from the real stain much like what we saw in Figure 13b. Building upon work by Du and colleagues (2019), we have created a systematic approach to qualifying these antibodies and, as a result, we have created an open-source list of antibodies that perform well in CyCIF at *https://www.cycif.org/antibodies/recommended*. This list serves as a valuable starting point for multiplexed imaging assays in many tissue and tumor types.

Size, Translation to the Clinic, and other Hindrances of CyCIF

Though many antibodies have proven to stain successfully in CyCIF experiments, it does not mean that they translate directly for clinical validation. While many of the clinically relevant antibodies, such as Ki67, HER2, and PDL1 have antibodies that can also be used in CyCIF, the opposite is not always true; that is to say we cannot claim that an antibody that worked in CyCIF experiments will work in a clinical setting. Even though we may have established some confidence in certain circumstances and under specific conditions, this does not prove sufficient for clinical standards. Therein remains the largest roadblock in the future of multiplexed imaging, be it CyCIF or some similar method: how can these assays be modified and what steps need to be taken to attain clinical validation. Regardless, we can use our dataset of hundreds of antibodies to complement the clinical standards as is and offer insight into the context of disease status

and disease progression. These advances seem inevitable and necessary in a field that is quickly headed towards digitization. One of the main limitations of this work is the overall size of the dataset and its need for automated processing and analysis of the data. Given the work we have performed, in combination with the work from Du and colleagues (2019), manually labeling, gating, and qualifying these antibodies will take an enormous amount of time, but as the field of digital histopathology grows, so too, do the tools we need to automate this workflow. Here we have presented data that can be divided and subdivided into different training sets, marker groupings, like and unlike cancer histotypes, and others to improve and complement traditional histology as well as help grow the field of digital histopathology.

Altogether, we have addressed many of the outstanding questions in the field related to high throughput multiplexed imaging: its capabilities, limitations, and areas of success as they relate to the current standing of histopathology. We have established confidence in an abundance of antibodies, be them directly conjugated or unconjugated, through their expression levels and localization(s) and have concretely mapped them back to H&E and IHC for comparative performance and evaluation. It goes without saying that once the proper landmarks and regions of interest are matched in CyCIF images and the pathology standards, we can be more confident in the staining patterns. We have provided a small glimpse of how map-back abilities between the standards and multiplexed imaging have become possible, especially as pattern recognition among cell types and cellular densities improves. Pattern recognition becomes stronger with additional antibodies that delineate tumor from stroma or benign cells, nuclei from cytoplasm, and highly dense regions from low density of specific cancers purely based on

the abundance of a marker of interest within a core. That is to say, we have shown, through various methods, that we can use this TMA resource, the EMIT dataset, and our validations efforts to move the field of histopathology forward.

Not only do we aspire to use this data to make advances in the field of histopathology, but we have shown the power and potential of automating and digitizing many of the processes still performed manually. While it remains a challenge to shift the dogma in the field, we do not propose that CyCIF multiplexed imaging, or any other multiplexed imaging modality for that matter, will wholly replace the standards, but that these tools can and should be used to improve the pre-existing methods. We have shown this is possible and will continue to make advances in our own research that can hopefully, one day, be analyzed and compared exhaustively enough with the clinical standards that sufficient confidence may be found and that these tools may be extended into a clinical setting. If for nothing else, the number of antibodies we have qualified and tested in many tissues should be used to guide future histology efforts to generate both a broader overview regarding a patient's tumor and delve into patient-specific findings. With additional information and a clearer path to follow, there should be minor advances in the field regardless of a monumental shift in the field overall.

Chapter IV.

Discussion

CyCIF Can Be Used to Complement Clinical Findings

Our findings support multiple arguments that CyCIF can be used as an atlas-like resource for clinicians, pathologists, and the field of digital histopathology as a whole in a myriad of ways. Its potential to provide a wealth of biological data through multiplexed antibody staining and imaging makes it a powerful tool. Here we have presented multiple lines of research that address the unique needs and limitations in the field of high-plex digital histology and have suggested several ways to complement and improve experimentation and analysis. High-plex tissue imaging in general, and CyCIF in particular, do not yet provide clinically validated assay technology, but propose that the results and findings obtained from high throughput multiplexed CyCIF imaging can catalyze advances in the field – and more importantly – enhance clinical outcomes for patients. In addressing our specific aims, we have outlined ways in which we can improve our understanding of a patient's tumor and its underlying biology using CyCIF. More specifically, we can begin assessing cellular morphology across cancer histotypes and use our data to improve automated cell segmentation and cell-type calling through artificial intelligence deep learning algorithms to discriminate disease-specific patterns. Thus, we can accomplish unmet needs on an individual level, but also more generally positively impact the field.

We have shown that CyCIF multiplexed data can be accurately mapped back to the pathology standards of H&E and IHC images. Through a crude analysis of tissue landmarks, we can find the same regions of interest in both modalities, demonstrating

that our findings pair well with what is currently the gold standard in diagnosis. Moreover, we frequently take use the same antibodies as in IHC slide staining while further multiplexing the number of antibodies to be visualized concurrently. In doing so, we provide the context and neighborhood in which specific cell populations reside, uncovering the unique interfaces between them. Extending this approach should not be overlooked, especially since cancer biology is not limited to a handful of immune markers. Cells in a patient's tumor can express a large diversity of antigens depending on the progression of disease and cell states, such as T-cell exhaustion, which can only be detected through the expression of a cocktail of antibodies that include, but is not limited to, CD8, PD1, PDL1, TIM3, LAG3, and TIGIT. The exact profile for what is considered an exhausted T-cell ranges across literature, but what is well-defined is that these particular cells can only be appraised through multiplexing and cannot be discriminated in single or double stain typical of H&E and IHC. The more diverse the marker expression of T-cell exhaustion antibodies, the more confident one can be in its profiling and role in immune response. This is but one example whereby a more diverse and definitive expression profile provides us with a better understanding of biological context and roles.

Improving AI's Ability to Cell-Type and Reduce Pathologist Intervention

There still remain many unresolved challenges regarding the work we have presented here. A necessary next step is firmly establishing the guidelines and parameters needed to perform antibody analysis and quality control to a level similar to that of clinical validation. While we have collaborated with pathologists and clinicians, further work with CyCIF and our antibody sets need to be run in parallel with clinical testing of

standard antibodies. As of now, no multiplexed imaging platform has reached clinical validation, but numerous efforts posit that multiplexing is nearly ready for clinical translation (McMahon et al., 2020). While other research teams have also begun to address this issue, we have created a resource that can serve as a labeling guide for deep learning AI to outperform pathologists, an essential adaptation to growing databases and atlases. With an unprecedented number of antibodies stained across many tissue types under like conditions, an automated pipeline used to differentiate and score proper antibody localization and fluorescence expression profiles is indispensable. Not only have we provided the framework to do so, we have also established morphological criterion for AI to classify histotypes based on phenotypic presentation. As discussed, manual labeling, which is considered the ground-truth of pathology, is needed to prepare an initial dataset necessary for supervised deep learning. Larger sample sizes with additional labeling will always increase the accuracy of AI, so we view this collection of TMAs, through one lens, as an expanding set of training data. Although not the main focus of this research, this work has the capability to improve our deep learning AI to perform image post-processing steps such as cell-type calling and cell segmentation through phenotypic presentation. By incorporating cellular-architecture-targeting antibodies such as NUP, lamin, and various cytoplasmic and surface markers, we are confident that our labeled training data can improve these algorithms. Certain markers emphasize the fact that many cancers have morphologically distinct cell shapes, which we broke down into seven classes and labeled them accordingly. These annotations were fed directly to our deep learning AI for training to become a fully automated process. Using AI minimizes human interaction, saves time and energy, and it will also eventually

outperform pathologists after the preliminary training sets are provided (Rawat et al., 2020) to further improve diagnosis accuracy.

It goes without saying that generating high-plex antibody-based tissue images is not an easy task using current technology. It requires meticulous adherence to protocol to generating a staining pattern that is biologically meaningful and accurate. For example, FoxP3, as it primarily serves as a transcription factor, has its expression localized to the nucleus, much like c-Myc or p-H2AX. But there are nuances of some markers, such as p27, which can stain either in the nucleus, in the cytoplasm, or both the cytoplasm and nucleus (Sawabu & Watanabe, 2005) all of which is visible from IHC. These subtleties need to be recognized and labeled by eye initially, so that our AI can also distinguish heterogeneous staining patterns of the same antibody. That is to say that some markers require a more detailed and intensive curation to guide deep learning algorithms that others, but we have the sample size needed to establish confidence in our tools once sufficient pathologist-labeled training sets are inputted. While many of the images have already been curated, there are many hundreds more regions of interest that can be annotated to provide further training modules.

Pattern Recognition Identified Through Cancer-Hallmark Antibodies

Much like we stained with particular antibodies targeting the various shapes and localizations of biomarkers, we also employed numerous cancer-specific antibodies targeting cores within the TMAs with their supposed tumor hallmark biomarker to capture and characterize as many different cancer histotypes as possible. This is not the first time this has been done, as Bagchi and colleagues have performed a similar experiment (2021), though they strictly focus on IHC scoring, with a range extending

from 0-3, a limited and relatively arbitrary scoring system based on the presence and intensity of staining (0: absent; 1: weak positive; 2: moderate positive; 3: strong positive) and only performed on so many malignancies. Like Bagchi, we have stained many cores within the TMA, most noticeably in TMA5, with their cancer-specific markers: Pax8 for ovarian, TTF1 for lung cancer, c-Met and survivin for kidney, ER for breast, CDK4 in liposarcoma to name a few. From the resulting expression levels, we are able to distinguish cancerous regions within biopsies from non-cancerous regions by the presence and localization of these tumor-specific markers. A quick evaluation of the hallmark antibody vs typical immune markers, such as CD45 or CD4 and CD8, can present striking differences between regions within the same tissue, namely boundaries between cell populations. Multiply this information by the number of cancer-specific and broad immune cell antibodies stained and we have created a phenotypic guide that directly juxtaposes tumorous tissue from benign tissue that is useful for further clinical evaluation. Once the tumor had been found, we subjected it to deeper phenotyping, thus, we are able to provide more descriptive information to the clinician about a patient's tumor and the TME in which it resides.

With these cancer hallmarks we can also begin to uncover patterns that emerge from the localization and morphology of cells within a certain malignancy. Figures 2 and 4 highlight the unique cell types and morphologies that are most abundant across cores. These classes have been deeply analyzed in this current work as well as other works that discuss the EMIT dataset (Schapiro et al., 2021), to create a visual guide that can first differentiate one cancer subtype from another, second, aid in diagnosis of particular cancers purely by the morphological presentation of certain tumor cells, and third,

provide the context in which we can truly evaluate a clinical outcome depending on disease state based on the relative abundance of certain cell types. Many cancer diagnoses and distinctions between disease subtypes are already performed in this manner, such as the expression of CK8 indicating a diagnosis of lobular carcinoma of the breast instead of ductal carcinoma (Moriya et al., 2006). We can use our work to inspire confidence in the antibodies we used as well as morphological distinction through expression gradients amongst cancers by revealing and quantifying subtle details between histotypes through morphology and context of disease state to improve a patient's prognosis by suggesting areas for therapeutic intervention. Other research groups have asserted how powerful a morphology-driven classification resource can be, but most have taken it upon themselves to create a tool specific for one disease such as lung, digestive tract, or colorectal cancers. We propose to do the same thing, but extend our reach to multiple malignancies simultaneously and our phenotyping to a newfound level.

Limitations of Our Research

Although we do not believe that this work will immediately impact how clinical pathology and histology are performed, we hope to advance some of the technology and digitization of these methods in the push towards digital histopathology. Moving forward, our resources can be used for a variety of analyses ranging forward from antibody validation through AI enrichment. One notable limitation of the current work concerns our inability to as yet fully explore all of the different staining patterns in our dataset. With 120-plus cores of tissues multiplied at least by 25-fold for the numbers of TMAs stained, there are close to 4,000 cores of analyzable data in the collection, stressing the need for a strategic, and ideally automated, approach to analysis. This number only

increases when considering the number of individual antibodies used, nuclei counted, and membranes identified, which poses a massive roadblock - but also an opportunity - that needs to be deconstructed piece by piece. Even a thorough analysis of one TMA takes exhaustive efforts, nevertheless 25 of them, further supporting our arguments for automated analytics.

While it would be conceivable to focus on a single core from each cancer and then delve into the staining patterns seen, such as the morphology of the nuclei and cytoplasm of cancerous cells versus non-cancerous, the overall goals may be lost. It is imperative to compare cores across TMAs to see if our findings reproduce and, secondly, to increase sample size allowing us to justify making broad conclusions about specific malignancies backed by our data. Many of our hypotheses have already been confirmed by the data we present and we plan on extending these findings to new experimentation and hypothesis formulation. We are able to show that there are systematic trends as to why one malignancy lasts for fewer cycles of CyCIF than another, namely due to its tissue-intrinsic characteristics such as the presence of airways or other vasculature. Typically, breast and ovarian cancers last longer in the CyCIF process (i.e., survive more cycles with tissue damage) as a result of their cell shape and densely-packed nature as compared to lung cancer which often presents with large cross-sectioned airways through the tissue. We show that many antibodies are cancer-specific, such as calponin, but others, like p53, ER, vimentin, and SDHB stain their primary malignancy, but may also be present in other tissues, just in varying degrees. Here, we need to vigorously assess true stain from background to establish further confidence in our findings, but we have laid forth the groundwork to do so. In making specific claims as they relate to numerous

processes throughout CyCIF data collection, we aim to extend these findings to make more broad and general conclusions that can positively impact scientific research as it pertains to multiplexed tumor imaging.

Though we have outlined a relatively systematic way to decipher and approach this mass of biological data, there needs to be additional automation of these tasks if the entire dataset is to be analyzed. To do so, automated post-processing needs to be performed beginning with a dearraying of the cores, for which we have a software tool called Choreograph, affording us the opportunity to examine cores one by one (Schapiro et al., 2021). Then deep learning AI needs to be run in a core-by-core independent fashion to delineate the different cell populations present in each core, or more specifically, per disease. The cell types can then be sorted and counted based on their staining profiles (i.e., CD8+LAG3+PDL1+TIM3+), giving us an overall impression of cellular communities within each disease core. From there, a marker-by-marker assessment can be performed to evaluate staining; for example, if macrophages are most heavily involved in pancreas and lung cancers (Jung et al., 2015), what are the expected counts of CD163+ cells within those cores and how do they compare to non-lung or pancreas cores? There should be an increased abundance of macrophages in the pancreatic and lung cancer cores and this trend should be consistent in the same cores across most, if not all, TMAs. Further, these counts should be compared to CD163+ cell count in other malignancies to confirm whether or not pancreatic and lung cancer do possess greater macrophage populations. Still, the need for precise positive and negative controls to assess antibody staining is needed before making any generalized conclusions. We have attempted to incorporate as many controls in this work as possible. As with

many multiplexed imaging methods, the size of the data poses a bottleneck during the analysis phase as running these images through a post-processing pipeline generates a demanding computational burden – a challenge difficult to overcome with current software tools.

Like computational burdens, there are other factors that potentially limit the applicability of CyCIF experimentation. One such limitation is understanding the biology that occurs in three-dimensional space. As we have touched upon briefly, having serial sections of these TMAs affords us different biological landscapes that alter these tumor microenvironments ever so slightly as we progress through tumor in the x- and y-axes, but we are limited in what we can interpret from the z-axis. As a general limitation of pathology, sections of tumor blocks must be cut to a certain thickness, usually five microns or less, limiting the ways in which we can decipher, or even see, three-dimensional interactions. When these sections are cut, it is likely that individual cells are sectioned straight through their nuclei, inhibiting our ability to see a complete nuclear stain. But, as we saw, many markers, such as CD163, a macrophage marker, and PD1 and PDL1, typical markers of exhaustion, specifically T-cell exhaustion, stain cells in varying polarities. That is to say that there can be a higher abundance or concentration on one side of a cell than the other. Additionally, other biologically relevant morphological processes, such as the formation of synapses, can also extend in many directions, as Figure 6 demonstrates, stressing the need for three-dimensional capabilities. These behaviors are hardly noticed through standard microscopy and are only illuminated at a greater magnification. It is difficult to anticipate the range of biology that occurs in the z-

axis, as we are limited by the five microns punched onto the slide, not offering us an opportunity to gauge this biology.

However, a serial section stained the same way as its predecessor may shed light on 3D biological structures, though it is currently not possible to obtain the precise neighboring or continued topography without losing relevant biology in the process, often in the 300–600-micron range (Merz et al., 2021) as a result of ineffective sectioning, Furthermore, microscopes traditionally cannot acquire as high resolution images in the z-plane as in the x-y plane, limiting our ability to see non-uniform staining. To address this need, assays being developed to image whole FFPE blocks aimed at preserving biology and maintaining three-dimensional image acquisition, such as light-sheet microscopy. Future studies need to be performed in order to determine the effectiveness of these methods, and the limitations of block thickness pertaining to observable biology, as they compare to other multiplexed assays, much like how multiplexed imaging needs to be fastidiously compared to pathology standards.

Another limitation – arguably the initial paramount reason for this research – is in determining what barriers remain in incorporating multiplexed imaging, namely CyCIF, into clinical work. Clinical validation of a multiplexed imaging method has not yet occurred; similarly, the clinical significance of several antibodies remains relatively limited as only a handful of biomarkers have clinically established confidence. This dilemma suggests CyCIF as possible alternative or complementary method to improve this quandary. We have evaluated hundreds of antibodies using the high throughput nature of CyCIF, including non-traditional ones, that we hope will one day achieve clinical validation. H&E and IHC stains are the clinical standards when it comes to

evaluating particular antibodies in assessing tumor type or burden. While they present useful data, the throughput of these methods is low, only a couple antibodies at a time, yet remain the gold-standard when it comes to pin-pointing an abnormality in a patient's tumor. This has remained relatively unchanged for decades. H&E presents a binary stain delineating tumor that clinicians trust, where antibody expression is either absent or present; IHC provides the same only with heightened specificity and a slightly more quantitative output. In the future, we hope to prove that CyCIF can be used as a clinical diagnostic resource by adding more antibodies intra-sample and extend findings beyond a single biomarker, in the scopes of hundreds. By doing so, we increase our understanding of a patient's specific tumor and expose possible targets for therapeutic intervention.

Given these limitations, it is important to consider this work as a catalyst for multiplexed imaging and antibody validation. As more multiplexed staining and imaging methods and manuscripts come to the forefront, many of which highlight CyCIF and its abilities, we hope to share our data and assay to exemplify deep tumor phenotyping and cell type calling an its potential in more guided therapies. This is achieved through the staining of supplemental markers that describe the context in which tumors reside as well as the composition of the TME within an individual's tumor. Characterizing a majority of cell types within a sample should be the overarching goal of many pathology trajectories regardless of whether or not they include CyCIF. To make this happen, continuous collaborations with institutions that work directly with clinicians and patients is critical for CyCIF's success showcasing its unparalleled capabilities. If we can obtain sections of tumor from pathologists to characterize cellular composition through the use of clinical-grade antibodies in both IHC and CyCIF, we can then shift our focus towards providing

precision medicine that is going to directly and positively impact patient's lives. Multiplexed imaging has the power to bolster our knowledge of tissue biology and the assessment of disease (Bodenmiller, 2016). To this point, CyCIF is on periphery of diagnosis, but in the future, with some additional optimization and clinically approved standard operating procedures (SOPs), we aspire to meet the clinical standards in some capacity.

Future Directions

Although we have suggested CyCIF as the leading multiplexed imaging to be used for complementing histopathology standards, we would be remiss not to mention other IF-based assay, such as cyclic multiplexed-immunofluorescence (cmIF), multiplexed IF (mIF), MIBI, and multiplexed IHC, which are all currently being used in energies to improve cancer therapeutic strategies and aid disease diagnoses (Eng et al., 2020; Parra, 2018). These other methods aim to perform in a similar fashion as CyCIF by complementing existing clinical standards through increased throughput, multiplexing, or automation. But, where CyCIF stands alone, is in its ability to incorporate all three of these desires in one assay. As clinical work is subjected to rigorous standards, for CyCIF to be deemed clinically validated and obstacles must be overcome. Continued collaborative efforts with pathologists will also be needed to can make clinical translation a possibility in the future. For now, we show that CyCIF remains a leading contender for clinical validation due to its multiplexed nature in which we can incorporate many forms of antibodies but also in its throughput, able to perform WSI on up to 80 slides, if not more, in a single imaging session. Further, the availability of training data has been, and will continue to be sought after for it use in improving AI labeling for image post-

processing; our data can and should contribute to these endeavors. These three distinct arms of CyCIF experimentation will continue to expand as the need for multiplexed imaging does, and it shall continue to progress in parallel with the field of digital histopathology in general, making it even more practical to integrate moving forward.

In efforts to help advance the field of digital histopathology in general, open-source data is needed as a resource for tool development in a collaborative setting both on the experimental and analytical side. In maximizing the potential of our work, we suggest that the EMIT dataset serve as an open-source catalyst for tool development and growth. The novelty of the dataset at such that much of the preliminary research has already been performed ranging from optimizing experimental conditions, which include incubation times and background controls, through imaging, which includes accurate antibody dilutions and proper exposure times. Further, the initial battery of antibody validation efforts has perpetuated this dataset forward and served as one of the main successes of this research. We have also deprioritized many antibodies that did not work in our validation efforts and incorporated those that showed relative success for future experimentation. These initial efforts, ease the burden on others in that we have already established a list of reliable antibodies that serve as a solid starting point for antibody staining and imaging before further plexing. Making this data widely available will allow the scientific community to improve tools already being used by many research groups.

As we have discussed, the CyCIF assay yields a superior amount of information as compared to H&E and IHC stains. We can explore cell-cell interactions, delve into neighborhood analyses, compare and contrast marker expression profiles of like and unalike cell types all from the same amount of biological material that H&E and IHC

require. It should be noted that more recent multiplexed histologic approaches have involved spatial studies, a hot area of scientific research that involve cellular neighborhoods and cell-to-cell interactions as they relate to proximity. We have scratched the surface of spatial interactions in our dataset by studying how certain cell populations interface with one another and what impact these relations may have. Moving beyond imaging in a traditional histologic section roughly five microns thick, newer assays have proposed using entire blocks of tissue subjecting them to three-dimensional imaging, to control for the loss of biology that may occur during sectioning. Recent studies such as those performed by Amin (Amin et al., 2017) and Lin (Lin et al., 2022), emphasize both the need and role of imaging as it is essential to synthesize patient history and physical examinations with imaging and pathological studies as they relate to patient biopsies (2017). Lin's research team has performed a similar study to ours in which they have created an atlas-like resource in which they identified cell types, cell states, and classified the underlying morphological features of diagnostic and prognostic value within colorectal cancer (2022). Their work is the genesis of the term "histotype," referring to unique tissue morphology classifications which present differently depending on the stage or subtype of a patient's colorectal cancer. In our work, we perform the same types of analyses that span across a range of diseases, many with unique histotypes that convey pertinent information regarding a patient's diagnosis and prognosis. These works, taken together, represent a shift in the field, incorporating a multi-faceted approach to interpreting and complementing histology data.

What cannot go unnoticed is that the foundation for creating disease-specific atlases is antibody validation efforts as well as the optimization of conditions with

thorough quality control to ensure clean and systematic data collection. If these steps are not taken during the creation of atlases, which consolidate large amounts of data, we may not achieve even the simplest goals, since we have seen how crucial quality control and validation efforts are. As described for the Human Tumor Atlas (Rozenblatt-Rosen et al., 2020), it is imperative to integrate all aspects of related biological data, not just H&E and IHC, to construct a potent atlas-tool to build up our knowledgebase as they pertain to cancers. The wealth of biological data includes clinical annotations, experimental, imaging, and computational data with the end goals of understanding tissue morphology amongst solid tumors, identifying common trends across tumors, and the characterization of specific tumor stage and type (Rozenblatt-Rosen et al., 2020). While these atlases should build off of one another and extend their visions towards a common goal in interpreting and reconstructing three-dimensional data, the underlying framework remains dependent on the reliability of antibodies in imaging data, a major element of these works often taken for granted. Thus, our dataset serves many purposes: as a large repertoire of well-controlled antibodies validation experiments, a preliminary assessment of cell and tumor morphology across many tissues, a diverse training set for supervised deep-learning AI, and an open-source input to improve other image-based computational processes. Therefore, we can use our data to advance tools and the like resources needed to keep up with the pace of a growing field.

Altogether, we have accomplished many of our initial aims and provided a new resource to the community that is useful in a number of ways. We have increased confidence in a large number of antibodies through numerous antibody validations efforts and rigorous quality control. This is a vital foundation which few research groups wish to

perform, especially on the scale of 500-plus antibodies. Here, we establish an extensive pre-validated grading system to serve as a spring-board for other antibody imaging efforts. We have generated a dataset in which we classified seven main types of morphologies seen across 34 tumor types and begun to assess and annotate patterns and likeness between them to serve as a reference diagnostic tool. Through iterative and repeated labeling of images, we have put forth a finely-tuned training set for supervised deep machine-learning and an AI-driven classification system for cell types and expression profiles. We have provided the scaffold for methods advancement and outlined areas in which there is a pressing need for improvement in the field of digital histopathology. CyCIF can be used as a driving force behind many of these changes and the overarching desire to create atlases through which we can quickly gauge and identify similarities across tumor types through interpretation of their morphology and biological underpinnings. We hope that the data provided here, our multi-faceted approach and resources, catalyze collaborative efforts in aiming to understand each cancer's unique and rapidly evolving properties.

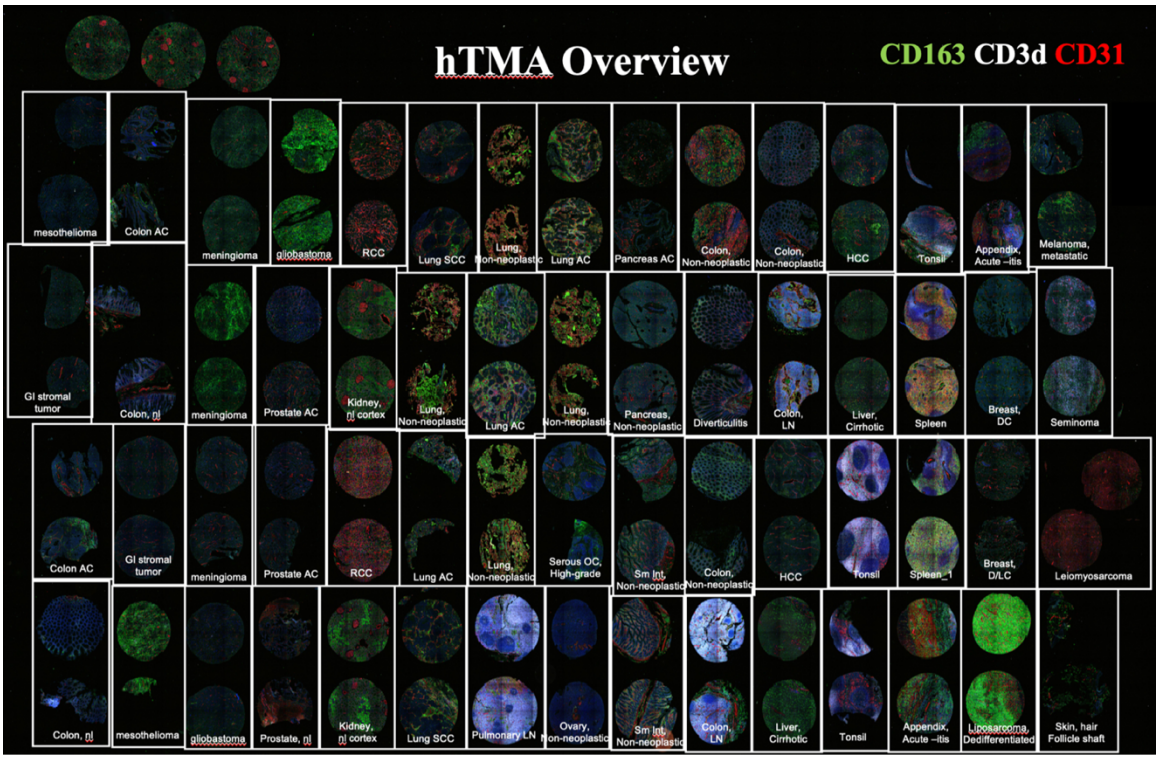

Figure 1. Tissue landscape and cellular composition of cores within HTMA 427.

Overview of the hTMA (#427) data. Here, we see staining of macrophages in green, activated T-cells in white, and blood vessels in red. Even with three markers present, it is easy to get a broad understanding of tissue characteristics and how they pertain to specific cancer types. For example, glioblastoma is chock-full of macrophages whereas leiomyosarcoma is altogether void of macrophages. Knowing these relative abundances can help guide follow-up research and the formulation of new hypotheses. We also see a brief evaluation of overall tissue integrity from initial biopsy punch. For example, the mesothelioma and lung adenocarcinoma cores do not display a full, robust punch as spleen and renal cell carcinoma.

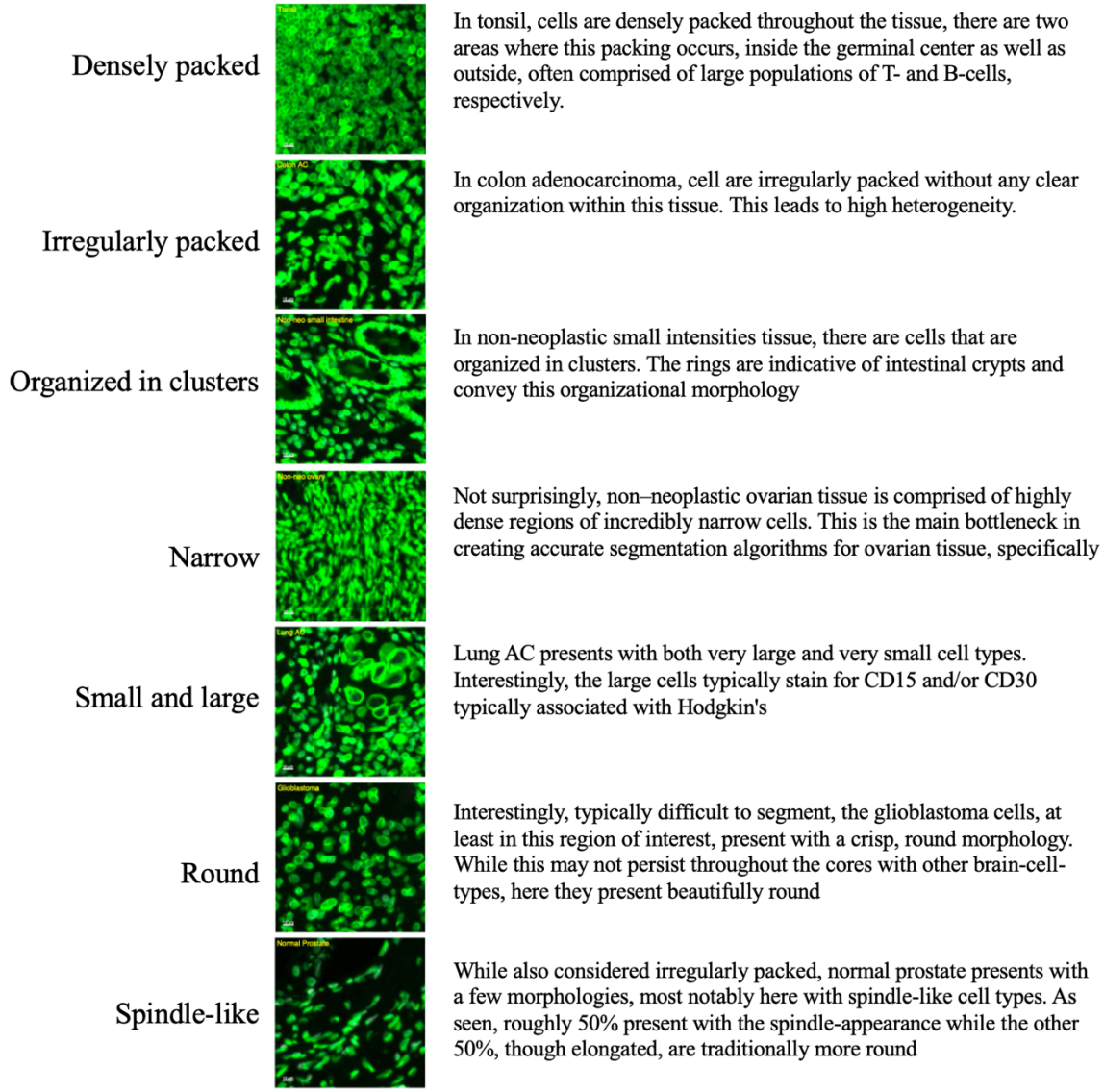

Figure 2. Cell morphology classifications as determined by NUP and lamin staining.

A cocktail of all available NUP and lamin antibodies was used to stain the maximum number of nuclear envelopes within various cancer cores. We classify specific cell shapes and densities into seven distinct classes: round versus narrow, small versus large, densely packed, irregularly packed, or organized in clusters. Using these classes, we can begin to make systematic interpretations on a core-to-core basis and make broad pattern assessments between like and unalike malignancies.

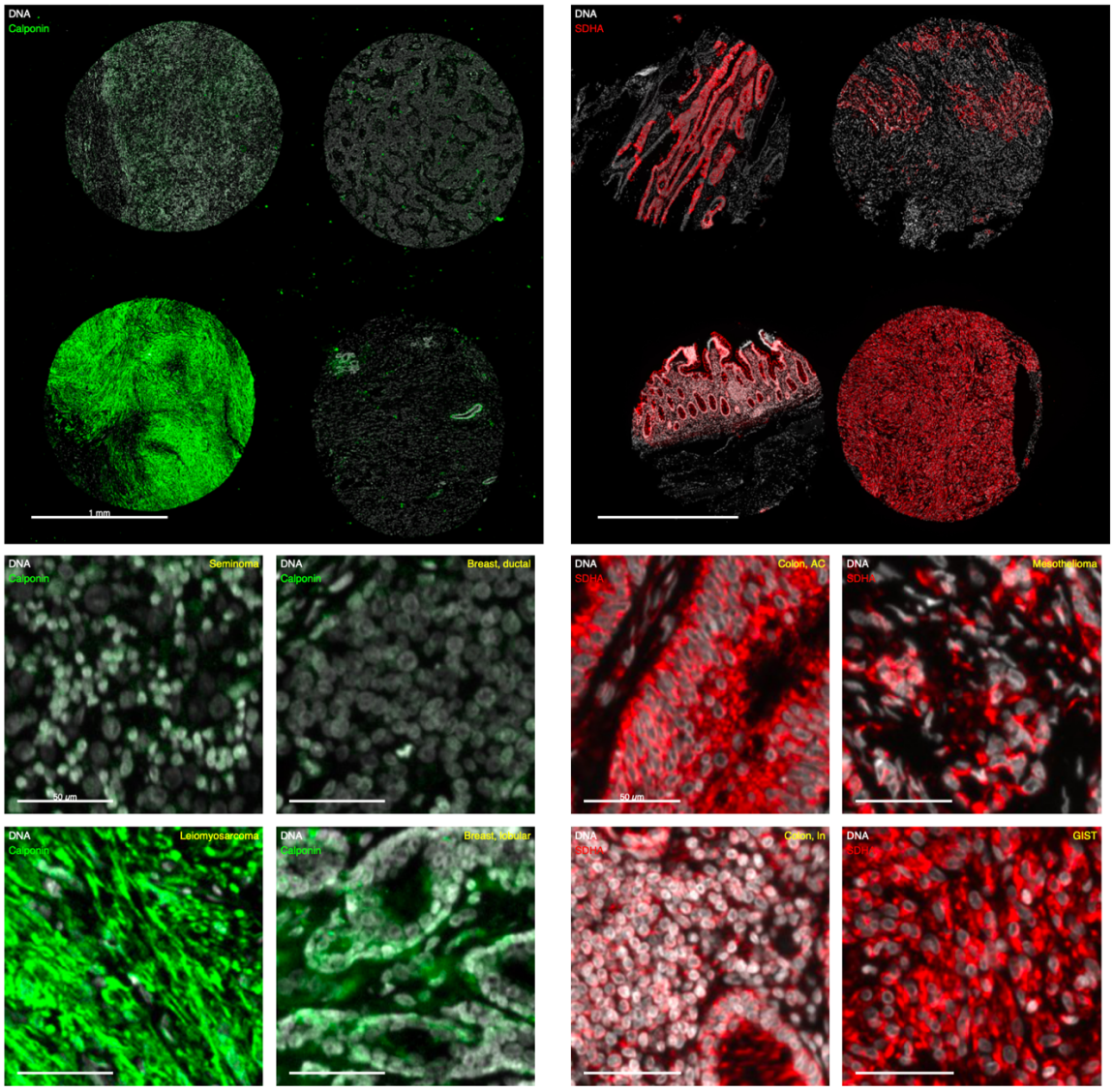

Figure 3. Variable expression of disease-specific antibodies in unexpected cores.

Calponin and SDHB, two antibodies mostly specific for leiomyosarcoma and GIST, respectively, are expressed in other cores, sometimes indistinguishable from background as seen on the left, but also in true positive staining, albeit in less abundance, as with the colon and meningioma cores. These staining patterns are gated away from true signal in terms of scoring real signal from background. Detail further in Figure 13.

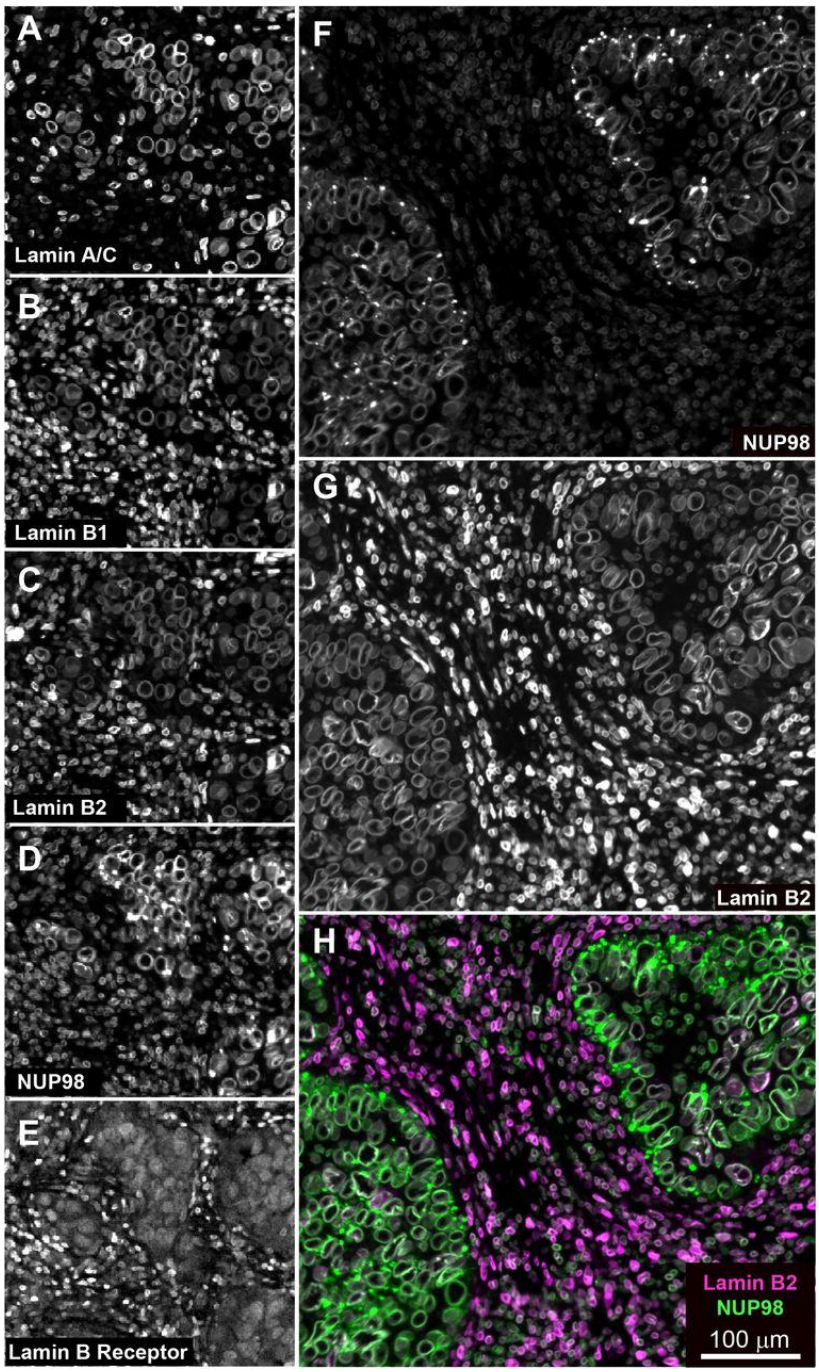

Figure 4. Cell segmentation overview targeting diverse nuclear envelope presentations.

Exemplar staining of different lamin antibodies (and NUP98) used to target phenotypically diverse nuclear envelopes. Lamin stain often juxtaposes nuclear envelope NUP98 stain (minimal overlap in merged H tile). It is important to note that the lamin subtypes come from the same family; but the A/C, B1, B2, and B receptor subtypes stain different populations of cells and in different proportions. Image credit Clarence Yapp.

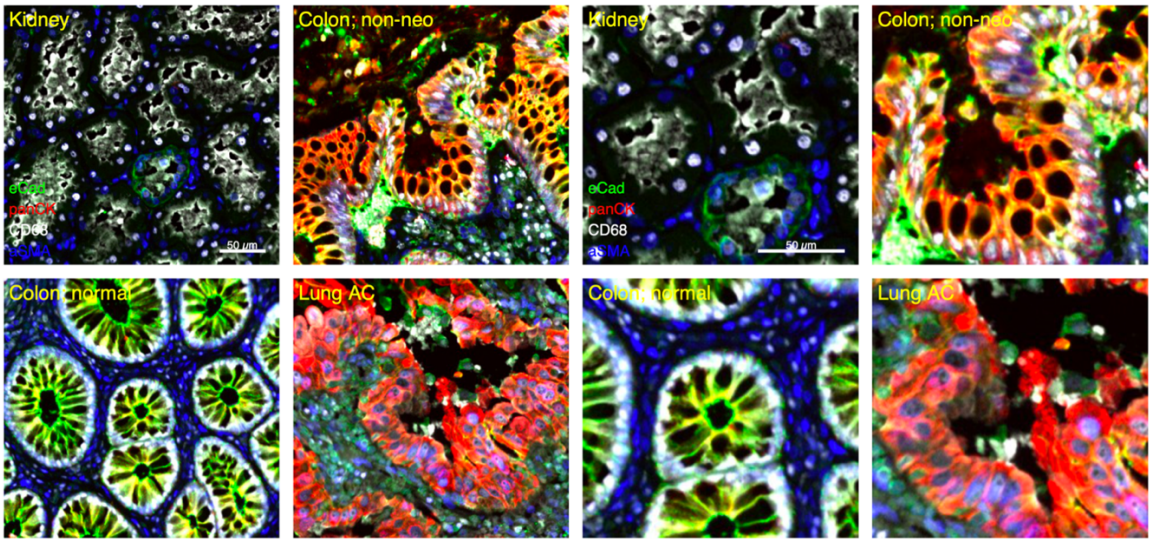

Figure 5. Cell surface markers observed in four distinct cancer histotypes.

High- and low-resolution images of four different cores within the TMA. Here, tissue from kidney, lung, and colon (two different subtypes) show varied expression of E-cadherin (green), pan-Cytokeratin (red), CD68 (white), and aSMA (blue). These markers stain epithelia, tumor, myeloid/dendritic cells, and fibroblasts, respectively. Overall cell morphology guides deep learning and cell-typing-calling of our AI. Beyond training AI, being able to identify and categorize unique histotypes affords us the ability to create a visual guide to different subtypes of disease; here the colon tissues present differently, especially in the form of differential pan-CK expression.

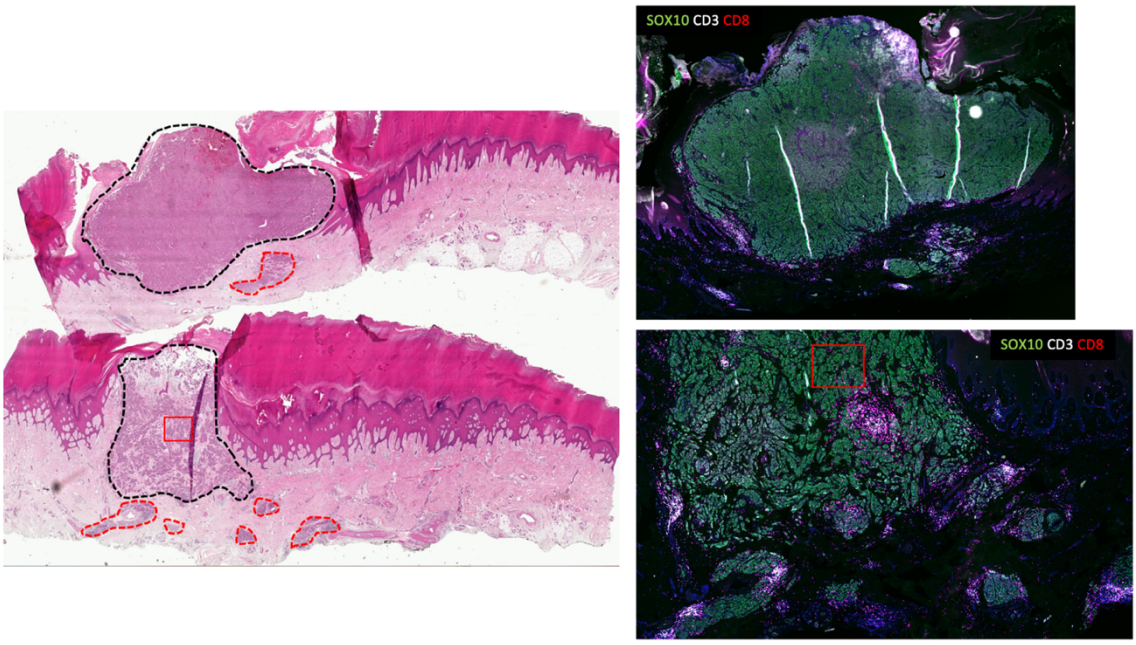

Figure 6. H&E regions mapped to multiplexed CyCIF image through tissue landmarks.

A direct comparison of traditional H&E with CyCIF. It is immediately recognizable that the serial sections map well onto one another. The dotted black lines (left) indicate regions of tumor and the same regions are seen in the CyCIF images (right) namely in the form of high Sox10 expression, the melanocyte markers (green). The strength of H&E is to delineate tumor from non-tumor regions; here we show that CyCIF, when probed with the proper markers (of tumor in melanoma i.e., Sox10), can delineate tumor equally as effectively, if not better, and provide additional context. Taken further, even metastases can be mapped directly across sections. Small populations of tumor cells (red dotted lines) in H&E are visible in the CyCIF images, again in the form of green Sox10 staining. Where CyCIF remains superior is the ability to add contextual markers, here in the form of T-cells (white and red) which provide immune reaction in response to the metastases and tumor revealing disease state. Image credit in collaboration with Tuulia Vallius and Roxanne Pelletier.

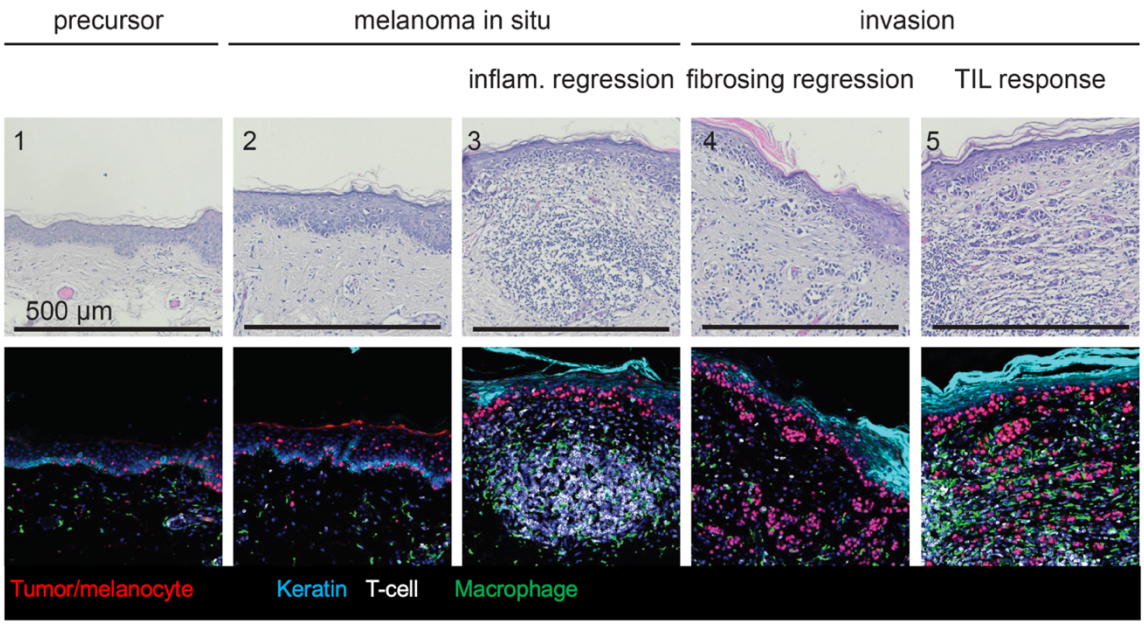

Figure 7. IHC regions mapped back to multiplexed CyCIF image outlines context.

A direct comparison of a single melanocyte IHC marker, Sox10 (dark blue), as compared to the multiplexed CyCIF image also containing Sox10 (red). While the IHC image contains pertinent information regarding melanocyte presence and abundance, it is entirely context-independent. Conversely, the CyCIF image also contains keratin, delineating epidermis from dermis, T-cells markers, and macrophages that characterize the immune response in regards to melanocytes aggregation. What is important to note is that the localized immune response heightens as the number of melanocytes increase and penetrate inwards as seen with inflammatory and fibrosing regression as well as with a localize tumor infiltrating lymphocyte response. Image credit in collaboration with Zoltan Maliga.

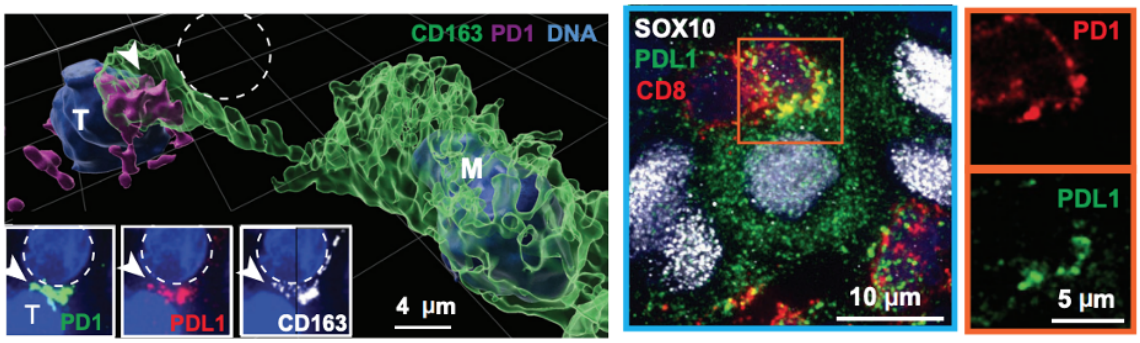

Figure 8. High-resolution image of a synapsing macrophage and antibody polarization.

***Left**: Raw data showing how biology occurs in a three-dimensional z-axis often missed during two-dimensional imaging. When computationally reconstructed, we see the synaptic projection from one resident macrophage (M) to an exhausted PD1+ T-cell (T) as it attempts to destroy it. **Inset**: Antibody localization and relative abundance of PD1, PDL1, and CD163 between the two neighboring cells comprising the synapse; PD1 most abundance in the points of contact. **Right**: high-resolution microscopy further reveals how certain antibodies aggregate on certain poles of cells and do not always present as a complete and contiguous ring usually seen in low-res microscopy. While PD1 is more widespread (red), PDL1 (green) is highly polarized to the bottom right of the cell which may require further investigation. Image credit in collaboration with Clarence Yapp and Zoltan Maliga.*

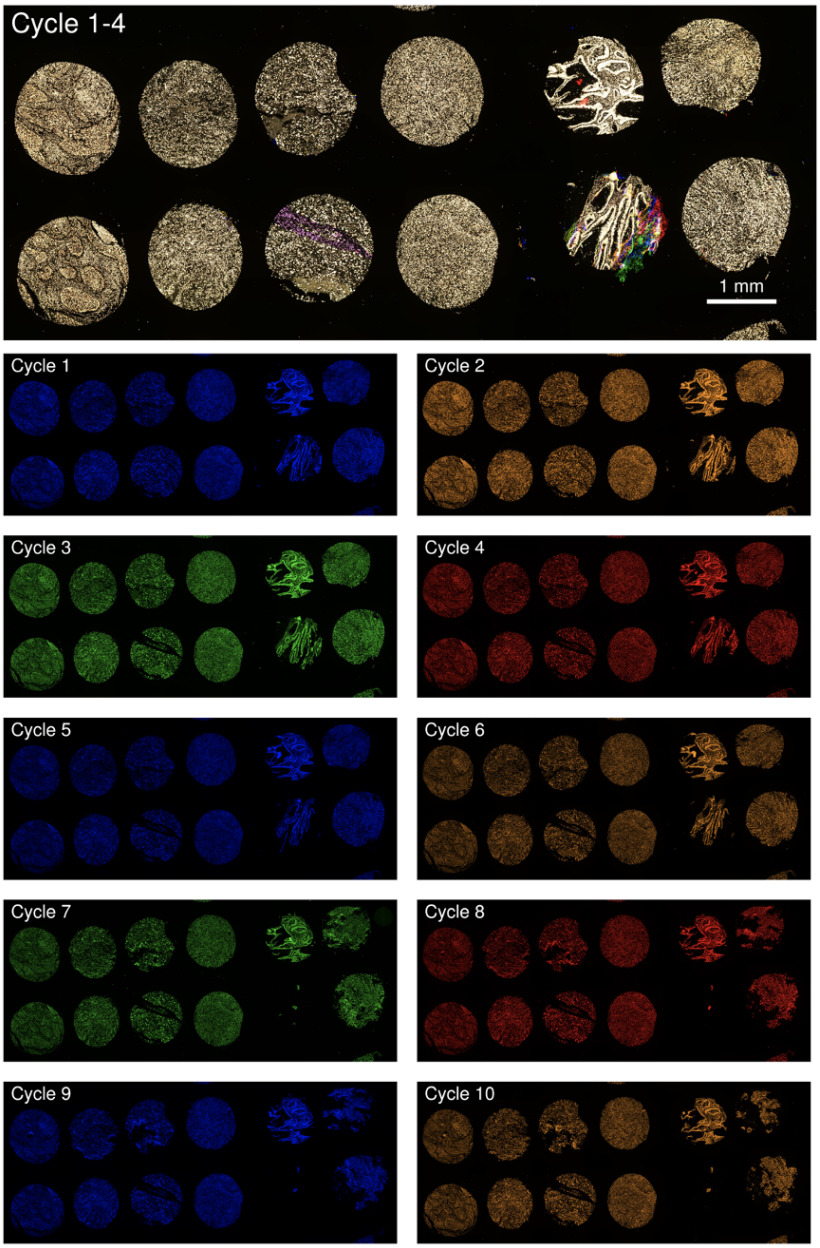

Figure 9. Systematic degradation: tissue integrity evaluated across six cancers.

***Top**: composite merged image of the first four cycles of blue, orange, green, and red DNA in TMA22. Presence of individual colors indicates tissue loss; second-from-the-right bottom (colon AC) has stripes of color whereby cells have fallen off. **Bottom**: panels show cycles independently and tissue loss across all ten cycles. Most cores remain intact apart from colon AC. The right-most cores do exhibit some tissue loss around areas where gaps appear, but there is still enough tissue to finish the experiment. From these findings, systematic conclusions can be made: gaps in colon AC tissue leads to quicker degradation as compared to more cellularly dense cores.*

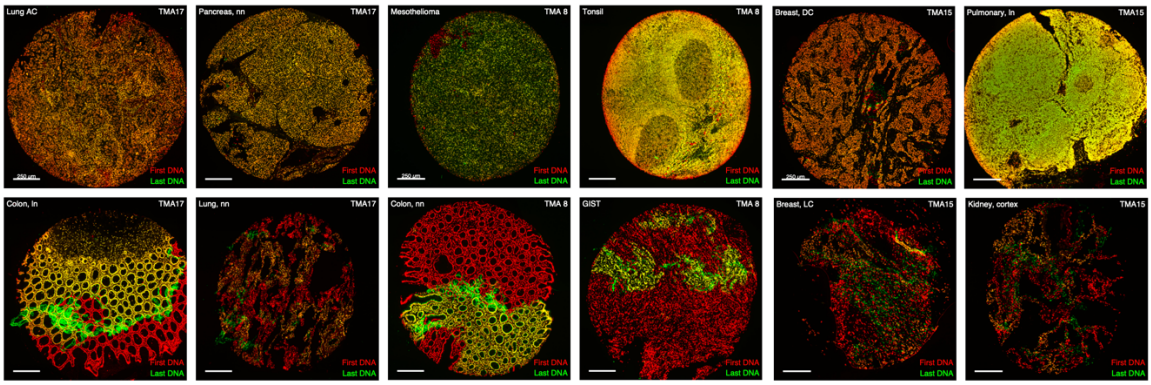

Figure 10. Best and worst cellular landscapes across a full CyCIF experiment.

***Top**: Cores with the best tissue integrity across a full CyCIF experiment from three different TMAs. Here, these cores show much yellow stain indicative of overlap of DNA from the first cycle and the last cycle, with minimal tissue loss. Not surprisingly, most of these histotypes have densely packed cells. **Bottom**: Cores with the worst tissue across the same three TMAs. In reaching conclusions regarding tissue landscape and tissue integrity, it is important to note that the cores in the bottom row almost all exhibit large gaps of space between tissue regions. As discussed, these gaps often lead to tissue sloughing off of the slide, ending an experiment prematurely.*

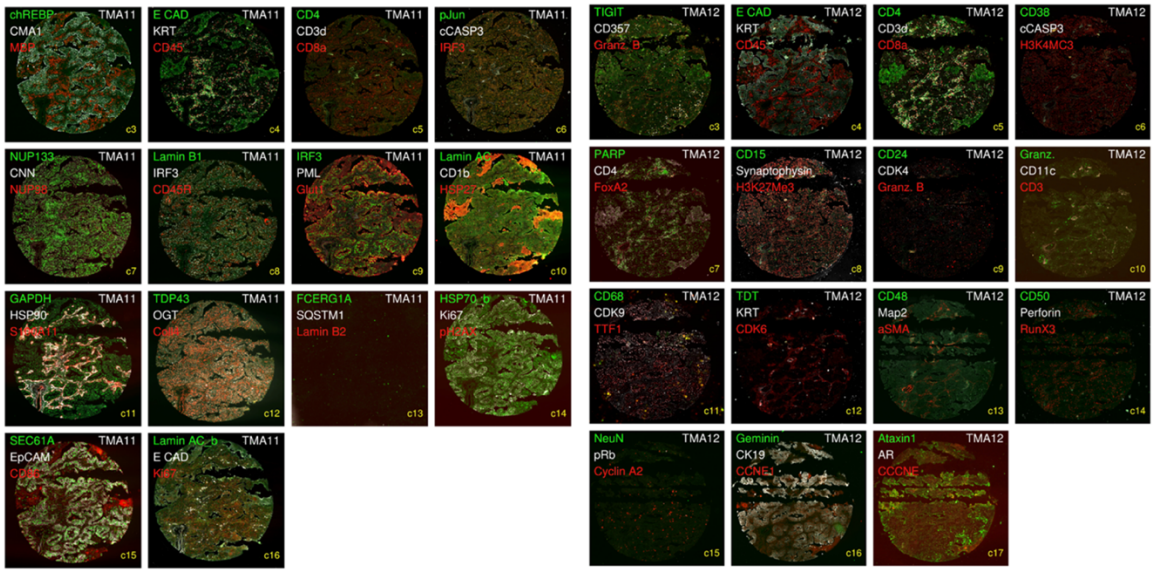

Figure 11a. Lung AC tissue integrity from TMA 11 and 12 and artifact interference.

A comparison of the same lung adenocarcinoma core across TMA11 (left) and TMA12 (right). It is important to note that 1. both cores survived ten-plus cycles 2. tissue loss was initially isolated to the right-side of the core, where a gap was first noticeable in the third cycle 3. despite certain cycles appearing to display complete tissue loss, this was only an artifact of poor staining and contrast settings (Cycle 13 left and Cycles 9, 12, and 15 right). Tissue was actually there, just not visible as a result of normalized contrasts, but it re-appeared in subsequent cycles. 4. Tissue loss in TMA12 can mainly be attributed to manual perturbations such as the initial cover-tile sliding across the tissue during de-wax or incomplete de-coverslipping as the artifact introduced is nearly linear as discussed. A thorough investigation on a core-by-core basis is needed to understand systematic degradation patterns disease-by-disease, though broad conclusions can be made from pattern recognition.

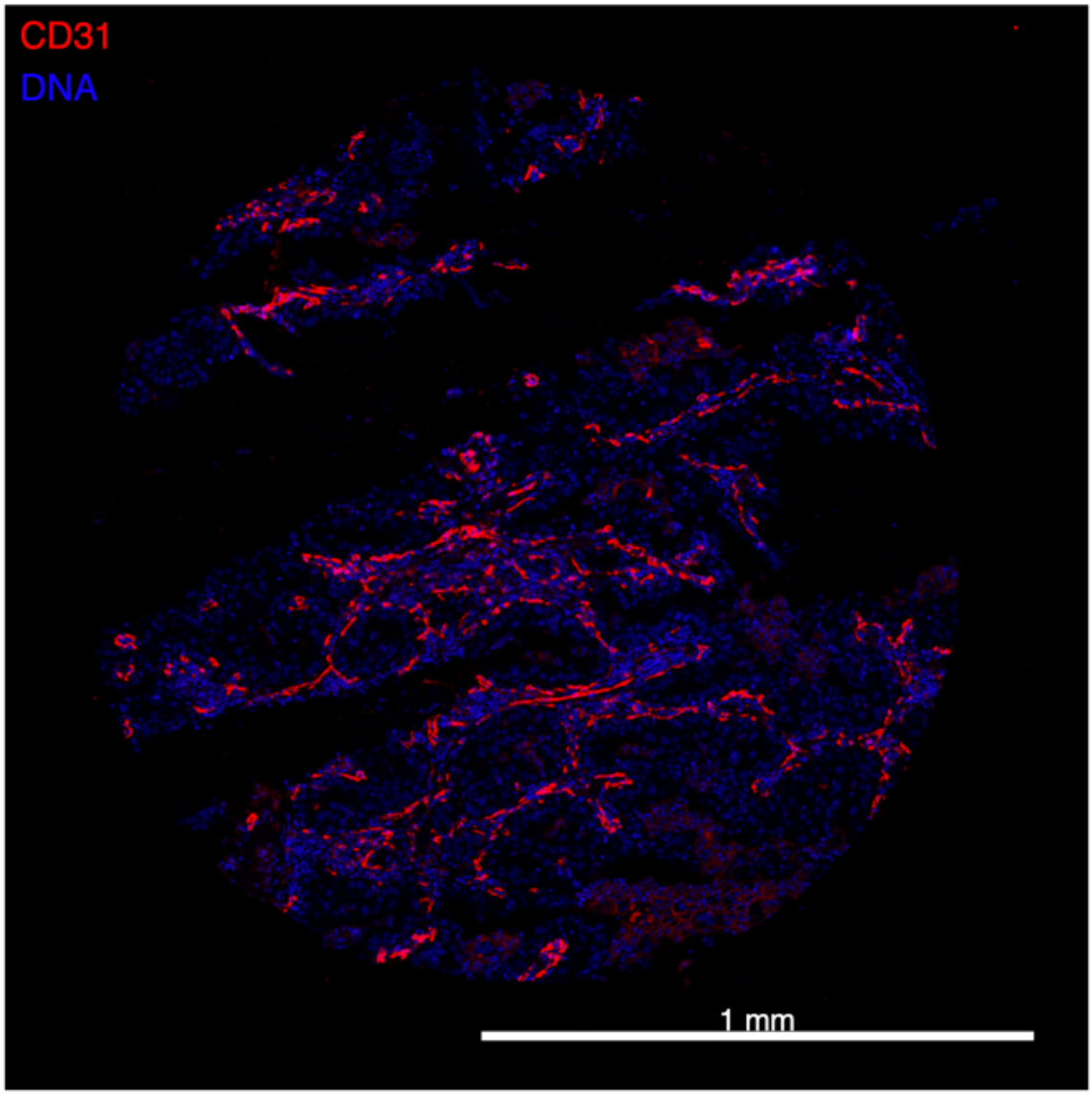

Figure 11b. Exemplary lung adenocarcinoma with CD31 outlining blood vessels.

Lung adenocarcinoma stained with CD31 (red) antibody showing the vasculature (blood vessels) that resides within these cores. By assessing CD31 staining, we can visualize the gaps in tissue and cells that have a long-term impact on overall tissue integrity. Traditionally, large gaps between cell means the tissue will degrade quickly.

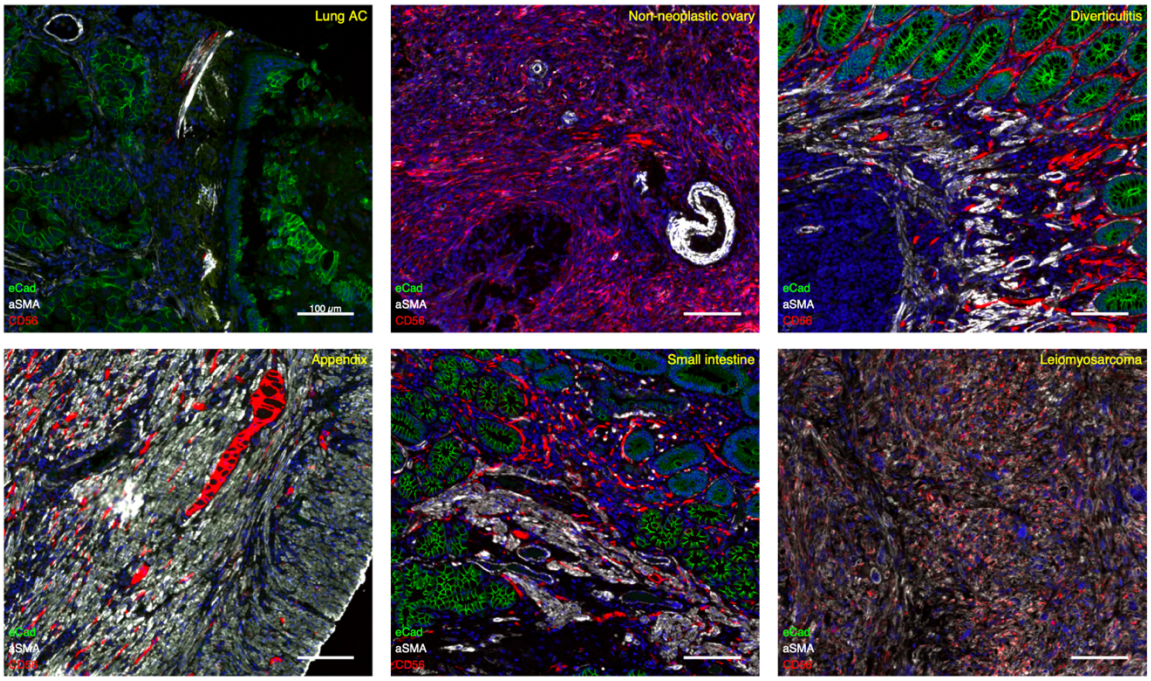

Figure 12. Cell surface marker staining across six histotypes.

A comparison of surface markers between six different cores within TMA22. Here we show varied expression of these surface markers between cores in varying degrees. Attaining the overall cell shape and discriminating between nucleus and cytoplasm/cell surface have a direct impact on improving cell segmentation. DNA (blue) shows nuclei in the cores with different shapes, which, once classified, was fed into deep learning AI for automated classification of cells across cancer indications. It is imperative for us and other research teams to make the same classification systems for surface and cytoplasmic to improve these aspects of cell segmentation in parallel.

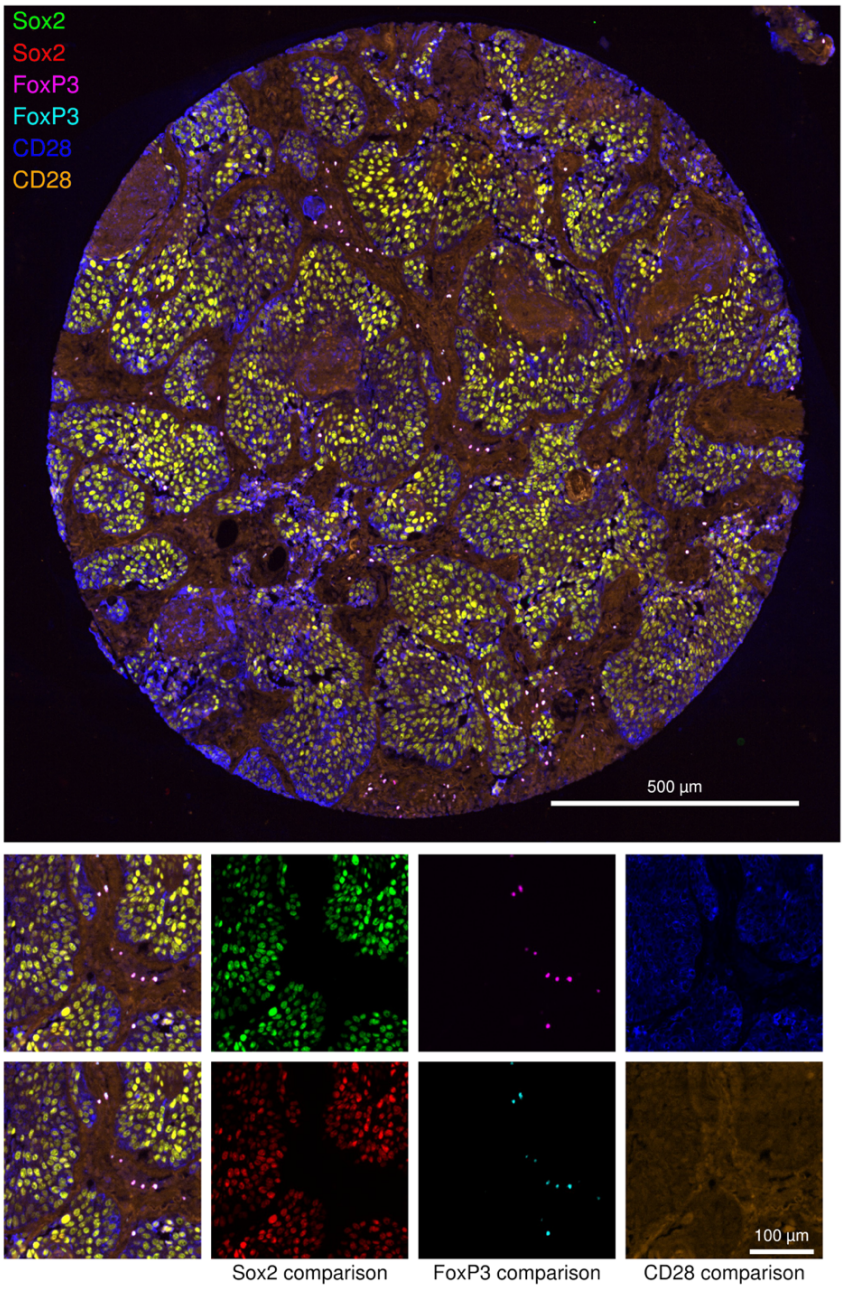

Figure 13a. Intra core comparison of antibodies for validation purposes.

Core of small-cell carcinoma used to determine the validity of like antibodies. The Sox2 antibodies (green and red), as well as the FoxP3 antibodies (purple and cyan), seem to work well, exemplify strong signal, and stain the same cells with proper colocalization. Conversely, CD28 (blue) presents with a surface stain as expected, but the bottom panel (orange) shows a diffuse, non-specific stain indicative a "failed reagent" that should not be used in future experimentation.

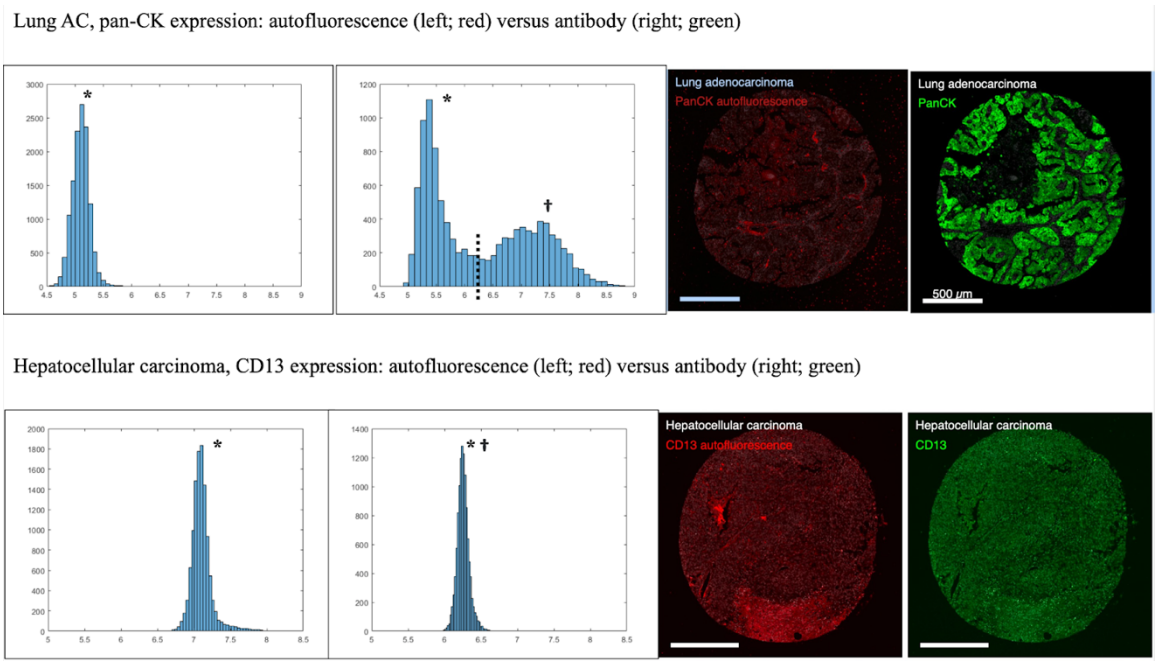

Figure 13b. Gating autofluorescence and background from true antibody signal.

As seen in Figure 13a, we see that some antibodies stain as expected with proper signal intensity and localization, however, some do not. ***Top****: pan-CK expression in a lung adenocarcinoma core. The left histogram (*) matches the red autofluorescence image with low intensity, though still visible. The right histogram shows true stain, with a bimodal distribution of intensity values indicative of true stain (†; green) versus background. When gated, we see subtract the autofluorescence values and score the true stain.* ***Bottom****: CD13 stain in hepatocellular carcinoma whereby the true stain (green) matches nearly identically to that of autofluorescence (red). When plotted together, there is no bimodal distribution (*†), therefore this signal cannot be gated, indicative of a failed reagent, like CD28 in Figure 13a.*

Table 1. Relevant TMA antibody stains according to scientific interest.

Sample	Focus/purpose of panel	Key markers for staining
TMA1	Broad characterization of tissues (architecture)	CD3d, CD11b, CD45, CD163, pan-CK, NCAM, Iba1, Elastase
TMA2	T-cell markers (version 1)	CD3d, CD4, CD8, CD25, CD26, CD27, CD28, CD138, CD207
TMA3	Natural-killer cells	CD1a, CD44, CD47, CD57, CLEC2d, NKG2c, TUJ1, IRF3, IRF5
TMA4	Myeloid cells, macrophages, and cell stress markers	CD11c, CD40, CD80, CD83, CD305, TOMM20, NQO1, iNOS
TMA5	Cancer-specific tumor markers	AXL, IDO, p53, CDX2, ZEB1, VEGFR2, CK17, HER2, Pax8, HES1
TMA6	B-cells markers	CD19, CD20, B220, CD45, CD79, Pax5, E2F1, Gata4, BCL2, CD21
TMA7	Fiborblasts, DNA-damage, and blood vessels	Podoplanin, pCHK2, pH2AX, TFEB1, SREBP1, FAP, NG2, EZH2
TMA8	BCL2-family proteins and apoptosis markers	Bok, Bid, BCL2, Bax, Bak, MCL1, Bim, Bap, p53, Puma, ACO2
TMA9	Toll-like (TLR) and innate immune receptors	TLR3, TLR4, TLR5, TLR7, TLR8, TLR10, BAP1, STING, CD13
TMA10	Receptor tyrosine kinases (RTK) and cell markers	Tyro3, MERTK, Met, ALK, pAurK, Snail1, BIRC5, TCRvd
TMA11	Nuclear and cytoplasmic markers for segementation*	NUP98, NUP133, Lamin B1, Lamin A/C, PML, S100a, EpCAM
TMA12	T-cell markers (version 2)	CD68, CD357, Gran. B, H3K4M3, FoxA2, TIGIT, CD50, CCNE1
TMA13	T-cell markers (version 3)	CD5, CD7, CD39, CD25, CD28, CD39, CD45RA, CD45RO
TMA14	Ludwig Collaboration 1	cCasp3, cParp, LC3, pSTAT1, pSTAT3, Smad1, RIP, pMKLK
TMA15	Ludwig Collab. 2: cell architecture, macrophages, B- and T-cells	4HNE, TFEB, Arg.2, GLUD1, BCL-XL, SELP, STAT3, pSTAT3
TMA16	Additional segmentation markers	CMA, MBP, Coilin, STAT6, RunX2, IRF3, STAT6
TMA17	Mast cells and myeloid populations	CD117, CMA1, MCT1, CD66b, G3BP, MPO, FUS, CEPBA, CK5
TMA18	Lymphoid, myeloid, and B- and T-cells	CD115, IRF4, IRF5, CD79a, CD2, CD35, MDM2, TIM3, ERa
TMA19	Transcription factors, immune checkpoint, and myeloid space	SPI1, CD66b, MITF, CMAF, IRF7, RunX2, STAT5A/B, IFNGR1
TMA20	Cellular metabolism and BCL2-proteins	GLUD1, TFEB, PHD3, Gata3, Bim, SMAC, Desmin, CEBP, OLFM4
TMA21	PCA1: melanoma-directed markers	5HMC, Tet2, HMB45, WT1, ICAM1, GM130, ITGAV, LDH, CD90
TMA22	PCA2: melanoma-specific unconjugated primaries*	CD73, CD107b, MART1, CDKN1A, CDKN1C, CDK2, CDKN2A
TMA23	Reagent optimization and antibody validation	Sox10 (x2), Cyclin B1, Cyclin A2, Ki67 (x2), bAmyloid, NCL, CD45RB
TMA24	Immune landscapes	H-HLA2, Nkp46, Vista, RORc, CD1d, LAG3, OX40, PD1, ICOS
TMA25	Cell segmentation advancements	
	* EMIT dataset	

Samples and antibody panels used to stain TMAs with their biological relevance. Despite common markers used in nearly all panels, such as CD3d, CD45, and Keratin, an abundance of markers was used specifically in one TMA or another to confer the most meaningful project-relevant biological data. Frequently, a number of test reagents are used to evaluate staining and determine whether or not follow-up experiments can be run using the reagent tested or if an alternative is needed, such as the B220 B-cell marker compared to CD19 and CD20. By validating antibodies in this manner, we have constructed a large list of antibodies than can be used to address many distinct biological questions and processes that extend beyond the capabilities of many other multiplexed imaging assays.

Table 2. Tumor-specific antibodies to target each malignancy within the TMA.

Histologic Classification	Tumor subtype-specfic markers
Appendix, acute -itis	TNFR2, CD38, Podoplanin
Breast D/LC	ER, PR, HER2, RORc, Tbet,
Cirrhotic liver	CD71, Smad2, MSH6, TDP43, CEPBA
Colon adenocarcinoma (AC)	CDX2, MLH1, TP53, FDX1
Colon lymph node (LN)	CPT1A, p53, VEGF, CD34
Dedifferentiated liposarcoma	p53, MDM2, CDK4, s100
Diverticulitis	s100, CD117
Ductal carcinoma, breast	GATA3, Bcl2, CK8, E-cadherin
GI stromal tumor	KIT, SDHA, SDHB, PDGFRa, PDGFRb
Glioblastoma	Hes1, p53, EGFR, GFAP
Hepatocellular carcinoma	CD13, NFATc1, CK8, CD10
High grade serous ovarian cancer	Pax8, p53, yH2AX, Ki67, CD8
Kidney LN, cortex	FDX1, pan-CK, Vimentin, WT1
Leiomyosarcoma	aSMA, Desmin, Calponin, p14, p16
Lung AC	CD1b, CD305, ALK
Lung small cell lung cancer	CD28, Sox2, NCAM, E2F1, YAP1
Meningioma	PR, STAT6, Sox10, s100
Mesothelioma	CD141, CK5, Podoplanin, BAP, CDKN2A
Metastatic melanoma	Sox10, MART1, HMGB45, PU.1, GITR,
Pancreas AC	CD47, CD63, CD166, Smad3, BclXl
Prostate AC	CDKN1b, EPCAM, FOXO1A
Prostate LN	CD1a, AR, ERG, CD10
Pulmonary LN	TTF1, CCD163, aSMA, Catenin
Renal cell carcinoma	CD27, CD86, CLEC2d, CK&, TFEB
Seminoma	p53, CD117, Podoplanin, CD30(-)
Skin, hair follicle shaft	cd34, CD207, Sox4, p27
Spleen	Nestin, CD1d, CD68, MPO
Tonsil	CD3, CD4, CD19, CD20
Non-neoplastic colon	
Non-neoplastic lung	
Non-neoplastic ovary	
Non-neoplastic pancreas	
Non-neoplastic small intestine	Nrf2

Antibodies that were used in efforts to identify the "hallmark" of specific cancers. Though we expect antibodies to be most specific for their suspected cancer type, they often stain other cores, thus follow-up investigation must be performed. Note: this is not the completed list.

Table 3. Overall antibodies used to stain each of the 24 TMAs

TMA1	TMA2	TMA3	TMA4	TMA5	TMA6	TMA7	TMA8	TMA9	TMA10	TMA11	TMA12	TMA13	TMA14	TMA15	TMA16	TMA17	TMA18	TMA19	TMA20	TMA21	TMA22	TMA23	TMA24	TMA25
FDX1	CD25	CLEC2d	CD40	CD11C	CD19	SREBP1	BOK	TLR7	ARG2	chREBP	TIGIT	CTLA4	pMKLK	4HNE	IRF3	CD117	CD115	CD86	GLUD1	5HMC	CD73	SOX10	HHLA2	**
GITR	CD207	CLEC2d_2	GLUT2	AXL	MERTK	TFEB1	BID	TLR10	MERTK	CMA1	CD357	CD28	AXL	TFEB	CMA	CMA1	CD207	TIA1	TFEB1	TET2	CD107B	CMA1	NKp46	
CD1d	RORc	CD1a	CD83	IDO	CD10	FAP	BCL2	TLR4	TYRO3	MBP	GZMB	CD25	RIP	ARG2	MBP	MCT1	IRF4	SPI1	PHD3	HMB45	MART1	SOX10_b	CD25	
CD163	*ECad*	*ECad*	*ECad*	*ECad*	*ECad*	*ECad*	*ECad*	*ECad*	*ECad*	*ECad*	*ECad*	*ECad*	*KI67*	*KI67*	*KI67*	*KI67*	*KI67*	*KI67*	*KI67*	*KI67*	*KI67*	CD209	RORC	
CD3d	*Keratin*	*Keratin*	*Keratin*	*Keratin*	*Keratin*	*Keratin*	*Keratin*	*Keratin*	*Keratin*	*Keratin*	*Keratin*	*Keratin*	*Keratin*	*Keratin*	*Keratin*	*Keratin*	*Keratin*	*Keratin*	*Keratin*	*Keratin*	*Keratin*	Keratin	Keratin	
CD31	*CD45*	*CD45*	*CD45*	*CD45*	*CD45*	*CD45*	*CD45*	*CD45*	*CD45*	*CD45*	*CD45*	*CD45*	*CD45*	*CD45*	*CD45*	*CD45*	*CD45*	*CD45*	*CD45*	*CD45*	*CD45*	CD123	CD1D	
LDH	CD4	CD11b	pTBK1	EPCAM	CD19_b	CD90	BAX	TLR9	MET	CD4	CD4	CD4	CD163	CD163	CD163	MPO	CD11B	CD206	ECad	ECad	ECad	KI67	KI67	
CD66b	CD3d	CD57	LC3	AXL_b	CD3D	CD29	CD3D	CD3D	CD3D	CD3D	CD3D	CD3D	CD3D	CD3D	CD3D	CD66B	CD11C	CD68	aSMA	aSMA	aSMA	CD3D	CD3D	
VDAC	CD8a	NKG2c	HIF1A	CTNNB1	CD20	PDPN	MCL1	TLR4_b	CD7	CD8A	CD8A	CD8A	CD20	CD20	CD20	CD16	IRF5	VISTA	CD56	CD56	CD56	CD45	CD45	
Elastase	CD28	CD57_2	IBA1	PCNA	CD11B	CD26	TCRb	CD11B	CD4	pJUN	CD38	CD28_b	cCASP3	cCASP3	cCASP3	CD163	CD163	CD163	GLUD1_b	pS6	CD13	MET	CD8A	
CD57	CD25_2	Smad3	CD83_b	bg3f	MYC	NG2	BAK	TLR3	AXL	cCASP3	cCASP8	cPARP	pSTAT1	pSTAT1	pSTAT1	CD3D	CD3D	CD3D	GATA3	NOS2	CD63	CD90	LAG3	
CD45	Tbet	NCAM	CD305	CD3D	BCL6	pSTAT3	pS6_235	CD20	CD8A	IRF3	H3K4M3	MDM2	cPARP	cPARP	cPARP	CD14	CD14	CD14	DESMIN	GM130	CD32	CDKN2A	PD1	
CD11b	Gata3	CD1a_2	cCASP3	P53	JUN	CD90_b	PUMA	CAT	CCND1	NUP133	PARP	CD103	STAT3	STAT3	STAT3	CD79A	SPI1	SPI1_b	GATA3_b	LDH	CDKN1A	MITF	CD163	
aSMA	CTLA4	IRF5	CD80	PDGFRb	CD34	CD146	CD33	pSTAT1_S727	ALK	CALP	CD4	ACTB	LC3	LC3	LC3	FOXO3A	IRF5_b	CD66B	VIM	CD90	CCNA2	BIM	FOXP3	
CD16	STAT5a	CD44	NQO1	CTNNB1_b	HLADPB1	CD31	BCLXL	MYD88	CDKN1B	NUP98	FOXA2	FOXP3	pSTAT3	pSTAT3	pSTAT3	CD66B_b	CD115_b	IRF7	CD3D	pMTOR	CDKN1C	cPARP	HLADPB1	
ECad	STAT6	CD47	NRF2	EGFR	CD43	CD33	CD8A	CD11B_b	CD30	LMNB1	CD15	CTLA4_b	bg2h	GLUD1	COIL	MITF	MITF	MITF	ANXA2	GAPDH	PCNA	CCND1	KIT	
FoxP3	CD27	CD44_2	TOMM20	CK7	FOXO1A	pChk2	BIM	TLR8	pAURK	IRF3_b	SYP	FOXP3_b	CCNB1	SELP	STAT6	FOXO1A	IRF7	IRF7_b	CD11C	pERK	pAUR	pRb	CD40	
NCAM	PD1	Smad2	CD853	CDX2	BCL2	MSH6	pMTOR	CD103	PD1	CD45R	H3K27M3	HLAA	SMAD1	BCLXL	RUNX2	IRF8	CD5	cMAF	cPARP	MTOR	CDKN1B	CD31	OX40	
CD4	CD161	Smad5	CD163	CD4	CD45RA	STAT3	BIM_b	MPO	SHP1	IRF3_c	CD24	HES1				CD30	CD8A	CD27	SMAC	WT1	CCND1	SNAIL1	IBA1	
Keratin	Gata3_2	IRF7	iNOS	aSMA	GATA3	pH2AX	pSRC	TLR5	pRB	PML	CDK4	SOX2				CD66B_c	CD4	CD4	BIM	aSMA_b	cPARP	CCNB1	CD68	
CD14	PDL1	CD33	CD86	CD8A	MCL1	MLH1	BCL2_b	STING	CDKN1A	GLUT1	GZMB_b	pTyr				FOXO3A_b	CD79A	LAG3	LYSC	NQO1	p27	CCNA2	CD56	
Iba1	STAT5b	STAT6	HO1	EGFR_b	CD34_b	RAD51	BAP1	pS6_240	SNAIL1	LMNAC	GzB	CD7				CD16_b	TIM3	IFNGR1	ICAM1	CD146	pCREB	S100A	MPO	
CD1b	STAT4	TNFR2	CD68	VIM	ESR2	aSMA	CD33_b	TLR2	MLH1	CD1B	CD11C	ALDH1A1				G3BP	CD19	PDL1	CEBP	CD90	CCNB1	AXL	NOS2	
CD8a	CD26	IRF5_2	HIF1A_b	ZEB1	CD21	FANCD2	ACO2	AHR	BIRC5	HSP27	CD3	SOX2				pJNK	CD11B_b	RUNX2	none	ITGAV	CCNE	pATM	GZMB	
	CD166	PU1	MAC387	CK8	CD45RO	KI67	pERK	pNDRG1	CD43	GAPDH	CD68	CD7				TOMM40	ER alpha	CD43	CD141	ICAM1	PCNA	CD73	NKp46_b	
	Lag3	CD133	P62	VEGFR2	BAK	pH3	PKM2	TLR1	KI67	HSP90	CDK9	S6				pIKBA	POUF51	CD86_b	CD90	CD11B	CDK2	DCP1A	LAG3_b	
	Vista	NGFR	CD64	YAP1	PR	BRCA1	MTOR	VIM	CD5	S100A11	TTF1	IRF1				FOXO3A_c	TIM3_b	STAT5A	ITGAV	CYSC	CDKN2A	aSMA	VISTA	
	CPT1A	CD71	CD206	CK17	PR_b	cCASP3	PDL1	CD10	TCRvd	TDP43	TDT	SMAD5				CD45RA	TLR9	STAT5B	Z_CD36	Z_CD73	zCD48	CD45RB	NRP1	
	NFATc1	IRF3	RELA	VCL	FosB	PMS2	PDGFRa	PKM1	none_3	OGT	Keratin_b	HER3				CD31	CK19	TNFR2	Z_OLFM4	Z_CD117	zCD40	NCL	ICOS	
	CD134	TUJ1	cPARP	SMO	CD61	MCM2	COX4	RELA	none_4	COLL4	CDK6	KI67				MCSF	PAX5	MHCII	Z_ICOS	Z_CD40L	zCD137	BAmyloid	CD209	
	PU1	ERG	PRLR	NFIL	BRD4	CD90_c	pP38	CD13	TCF7	FCERG1A	CD48	CD5				CK5	CD2	IRF3						
	Lag3_b	PU1_2	CD49F	SYK	HER2	bg3m	pJNK	pERK	AURKA	SQSTM1	MAP2	CD133				CEBPA	CD35	CD86_c						
	TIM3	CD31	CD206_b	HER2	ESR1	bg4m	pSTAT6	CD80	TCRgd	LMNB2	aSMA	SOX4				FUS	MDM2	VIM						
	STAT3	Cox4	LAMP1	SYK_b	NOXA2	cCASP3_b	CD19	CD138	ARG1	HSP70	CD50	TMEM173												
	STAT1	CYCS?	COX4	HER2_b	GATA4	CD90_d	CCNA	cPARP	cCASP8	KI67	PRF1	HMGB1												
	Sox2	LAMP2	NANOG	HES1	AR	EZH2	SDHB	IRF1	pH2AX	pH2AX	RUNX3	pBTK												
				cCASP3	MITF	EZH2_b	BIRC5	NCAD	ARG1_b	SEC61A	NEUN	CD45RA												
				TRKA	E2F1	CDK2	S6	pSTAT1_Y701	MAD2L2	EPCAM	pRb	SMAD3												
				PAX8	GATA4	NQO1	MDM2	CD138_b	CDKN2A	CD86	CCNA2	CD45RO												
							TP53	CD10_b	pCDK1	LMNAC_b	GMNN	CD39												
							POU5F1	GFAP	CDKN1A_b	ECad_b	CK19	VIM												
							SDHA	EMD	BANF1	KI67_b	CCNE1	pAKT												
							FN	NES	ARG1_c	LMNB	SCA1	pS6												
							CK19	MAP2	CCNA2	VEGFR2	AR	LC												
							CYCS	NECTIN1	ACO2	TUBG	CCCNE	AKT												

Here we show the list of antibodies that were used to stain each of the TMAs. We can begin to see, by comparing this list to Table 1, how some overarching questions begin to appear. For example, TMA7 was stained in part to gauge DNA damage, thus we stained with NQO1, cCASP3, pH2AX among others. Our goal was to allow for ease of collaborations; if a collaborator wants to target particular biological mechanisms, we have antibodies tested, and ideally validated, for those processes. Note: this does not show the unique antibodies (i.e., vendor, fluor etc.); some can be seen in Table 4.

Table 4. Segment of antibodies used to stain TMAs per cycle per channel.

TMA	Image	Channel	Antigen	Vendor	Cat No	Dilution
TMA1	8	3	FOXP3	eBioscience	41-4777-82	200
TMA1	9	3	pan-CK	Thermo-Fisher	41-9003-82	1000
TMA1	7	3	SMA	Abcam	ab202509	1000
TMA1	5	4	VDAC	abcam	ab179840	200
TMA1	7	2	CD11B	Abcam	ab204271	300
TMA1	4	2	CD163	abcam	ab218293	500
TMA1	9	2	CD4	R&D	FAB8165G	300
TMA1	8	2	ECAD	CST	3199S	300
TMA1	6	2	ELANE1	Santa-Cruz	sc-55549	100
TMA1	3	2	FDX1	Abcam	ab108257	50
TMA1	10	2	IBA1	Abcam	ab195031	500
TMA1	5	2	LDH	abcam	ab202652	500
TMA10	17	2	ARG1	CST	66297S	100
TMA10	14	2	ARG1	LSBio	LS-C447908	100
TMA10	15	2	ARG1	LSBio	LS-C447914	100
TMA10	3	2	ARG2	Cell Signaling	55003S	300
TMA10	17	4	ACO2	Abcam	ab198050	300
TMA10	7	3	ALK	CST	8868S	200
TMA10	13	3	AURKA	CST	50235S	200
TMA10	6	3	AXL	CST	78909S	300
TMA10	16	4	BANF1	Abcam	ab208621	200
TMA10	14	3	cCASP8	CST	12602S	100
TMA10	12	3	CCNA	SC	sc-271682	100
TMA10	17	3	CCNA2	abcam	ab297731	200
TMA10	12	4	CD11c	Santa-Cruz	sc-19601 AF647	100
TMA10	5	3	CD3D	abcam	ab208514	150
TMA10	4	4	CD45	BioLegend	304056	300
TMA10	11	4	CD5	Santa-Cruz	sc-53204 AF647	200
TMA10	5	4	CD7	abcam	ab199023	200
TMA10	6	4	CD8A	eBioscience	50-0008-80	300
TMA10	15	4	CDKN2A	Abcam	ab192054	
TMA10	11	3	Ki67	eBioscience	41-5699-80	100
TMA10	15	3	Mad2L2	Abcam	ab210653	200
TMA10	3	3	MERTK	abcam	ab110108	100
TMA10	10	3	MLH1	abcam	ab215303	200
TMA10	8	3	p-AUR	CST	13464S	200
TMA10	14	4	p-H2A.X	CST	9720S	100
TMA10	9	3	p-Rb	CST	8957S	300
TMA10	16	3	p21 CIP/WAF	CST	8493S	100
TMA10	9	4	p21 CIP/WAF	CST	8587S	200
TMA10	7	4	p27	Abcam	AB194234	300
TMA10	4	3	pan-CK	Thermo-Fisher	41-9003-82	1000
TMA10	8	4	PD1	abcam	ab201825	300
TMA10	10	4	Survivin	CST	2866S	200
TMA10	7	2	CCND1	Abcam	AB190194	200
TMA10	13	4	TCRgd	Santa-Cruz	sc-19601 AF647	100
TMA10	3	4	TYRO3	R&D	MAB859-SP	100
TMA10	8	2	CD30	Santa-Cruz	sc-19658 AF488	200
TMA18	10	4	TIM3	CST	78226S	300
TMA18	10	2	ER alpha	Abcam	ab194150	100
TMA18	3	2	KI67	CST	11882S	200
TMA18	7	2	MITF	Abcam	ab201675	200
TMA18	6	2	PU.1	Santa-Cruz	sc-390405 AF488	100
TMA18	9	2	TIM3	CST	54669S	100
TMA18	11	2	TLR9	Abcam	ab58864	200
TMA19	5	2	CD163	Abcam	ab218293	400
TMA19	4	2	CD206	Santa-Cruz	sc-376108 AF488	100
TMA19	8	2	CD27	Santa-Cruz	sc-25289 AF488	100
TMA19	10	2	CD43	Santa-Cruz	sc-6256 AF488	100
TMA19	2	2	CD86	Abcam	ab53004	100
TMA19	5	4	CD14	Abcam	ab196169	1000
TMA19	5	3	CD3D	Abcam	ab208514	150
TMA19	8	3	CD4	eBioscience	41-2444-82	100
TMA19	3	4	CD45	BioLegend	304056	300
TMA19	6	3	CD66B	BioLegend	392903	100
TMA19	4	3	CD68	CST	79594S	300
TMA19	12	3	CD86	BioLegend	305405	100
TMA19	10	3	CD86	Abcam	ab77226	100
TMA19	7	4	cMAF	abcam	ab225416	100
TMA19	11	4	HLADPB1	abcam	ab201347	200
TMA19	7	3	IRF7	Abcam	ab210435	300
TMA19	6	4	IRF7	Santa-Cruz	sc-74472 AF488	200
TMA19	8	4	LAG3	LS Bio	LS-C344749	100
TMA19	3	3	pan-CK	Thermo-Fisher	41-9003-82	1000
TMA19	9	3	PDL1	Abcam	AB213358	150
TMA19	2	4	PU.1	BD	554268	100
TMA19	9	4	RUNX2	abcam	ab215955	200
TMA19	10	4	STAT5A	Abcam	ab194309	300
TMA19	2	3	TIA1	Santa-Cruz	SC-1751	300
TMA19	11	3	TNFR2	abcam	ab209582	200
TMA19	12	4	VIM	CST	9856S	300
TMA19	4	4	VISTA	CST	92734S	100
TMA19	9	2	IFNGR1	Abcam	ab200327	300
TMA19	12	2	IRF3	abcam	ab204647	200
TMA19	3	2	KI67	CST	11882S	200
TMA19	7	2	MITF	Abcam	ab201675	200
TMA19	6	2	PU.1	Santa-Cruz	sc-390405 AF488	100
TMA19	11	2	STAT5B	abcam	ab199767	300
TMA2	9	2	CD161	Abcam	ab210285	200
TMA2	11	2	CD166	abcam	ab197543	200
TMA2	3	2	CD25	Abcam	ab128955	200
TMA2	6	2	CD28	BioLegend	302916	200
TMA2	5	2	CD4	R&D Systems	FAB8165G	200
TMA2	12	2	CPT1A	abcam	ab171449	150
TMA2	12	4	CD134	BioLegend	350018	200
TMA2	3	3	CD207	R&D	AF2088-SP	500
TMA5	11	4	YAP1	CST	38707S	300
TMA5	10	4	ZEB1	abcam	ab216121	300
TMA5	6	2	PCNA	CST	8580S	1000
TMA5	14	2	Syk	abcam	ab198938	200
TMA5	7	2	TP53	CST	5429S	300
TMA6	13	2	BRD4	abcam	ab197606	200
TMA6	6	2	CD11b	Abcam	ab204271	300
TMA6	3	2	CD19	CST	90176S	500
TMA6	5	2	CD19	abcam	ab196468	200
TMA6	10	2	CD34	Santa Cruz	sc-74499 AF488	200
TMA6	8	2	CD43	Santa Cruz	sc-6256 AF488	300
TMA6	9	2	CD45RA	BioLegend	304114	300
TMA6	11	2	CD45RO	BioLegend	304212	300
TMA6	7	2	cJun	abcam	ab193780	300
TMA6	4	2	ECAD	CST	3199S	300
TMA6	15	2	MITF	abcam	ab201675	200
TMA6	14	2	Noxa2	abcam	ab206256	200
TMA6	14	4	AR	abcam	ab194195	200
TMA6	11	3	BAK	Cell Signaling	14155S	200
TMA6	8	4	BCL2	BioLegend	658705	200
TMA6	6	4	BCL6	Santa-Cruz	sc-7388AF647	300
TMA6	3	4	CD10	Abcam	ab951	200
TMA6	5	4	CD20	eBioscience	50-0202-80	200
TMA6	10	4	CD21	abcam	ab202693	300
TMA6	7	3	CD34	Abcam	ab30377	200
TMA6	5	3	CD3D	abcam	ab208514	200
TMA6	4	4	CD45	BioLegend	304056	300
TMA6	12	4	CD61	Biolegend	336408	100
TMA6	6	3	cMyc	abcam	ab201780	200
TMA6	15	3	E2F1	abcam	ab208078	300
TMA6	12	2	PR	abcam	ab199224	300
TMA6	13	4	ER alpha	abcam	ab205851	200
TMA6	10	3	ER beta	abcam	ab205541	200
TMA6	12	3	FOSB	abcam	ab211854	200
TMA6	8	3	FOXO1A	abcam	ab207244	200
TMA6	9	3	GATA3	abcam	ab210672	300
TMA6	15	4	GATA4	abcam	ab194072	200
TMA6	14	3	GATA4	SC	sc-25310 PE	300
TMA6	13	3	HER2	CST	98710S	200
TMA6	7	4	HLADPB1	abcam	ab201347	300
TMA6	9	4	MCL1	abcam	ab197035	300
TMA6	3	3	MERTK	Abcam	ab110108	100
TMA6	4	3	pan-CK	Thermo-Fisher	41-9003-82	1000
TMA6	11	4	PR	eBioscience	50-9764-80	200
TMA7	12	2	cCasp3	CST	9669S	100
TMA7	14	2	cCASP3	R&D	IC835G	200
TMA7	6	2	CD26-FITC	BioLegend	302704	200
TMA7	8	2	CD33	abcam	ab187838	300

A portion of the overall antibodies used to stain the full dataset. Antibodies are organized by the TMA they stained as seen in Table 3, but here we also show the channel and the dilution used as well as the vendor. This information is critical for antibody validation as clones, fluorophores, and vendors may show different staining presentations, as seen in Figure 13a. Note: this is not the complete list, but rather a portion from various TMAs.

References

Aeffner, F., Wilson, K., Martin, N. T., Black, J. C., Hendriks, C. L. L., Bolon, B., Rudmann, D. G., Gianani, R., Koegler, S. R., Krueger, J., & Young, G. D. (2017). The Gold Standard Paradox in Digital Image Analysis: Manual Versus Automated Scoring as Ground Truth. *Archives of Pathology & Laboratory Medicine*, *141*(9), 1267–1275. https://doi.org/10.5858/ARPA.2016-0386-RA

Amin, M. B., Greene, F. L., Edge, S. B., Compton, C. C., Gershenwald, J. E., Brookland, R. K., Meyer, L., Gress, D. M., Byrd, D. R., & Winchester, P. (2017). The Eighth Edition AJCC Cancer Staging Manual: Continuing to build a bridge from a population-based to a more "personalized" approach to cancer staging. *CA: A Cancer Journal for Clinicians*, *67*(2), 93–99. https://doi.org/10.3322/CAAC.21388

Andreou, C., Weissleder, R., & Kircher, M. F. (2022). Multiplexed imaging in oncology. *Nature Biomedical Engineering 2022 6:5*, *6*(5), 527–540. https://doi.org/10.1038/s41551-022-00891-5

Angelo, M., Bendall, S. C., Finck, R., Hale, M. B., Hitzman, C., Borowsky, A. D., Levenson, R. M., Lowe, J. B., Liu, S. D., Zhao, S., Natkunam, Y., & Nolan, G. P. (2014). Multiplexed ion beam imaging of human breast tumors. *Nature Medicine 2014 20:4*, *20*(4), 436–442. https://doi.org/10.1038/nm.3488

Arneth, B. (2019). Tumor Microenvironment. *Medicina (Kaunas, Lithuania)*, *56*(1). https://doi.org/10.3390/MEDICINA56010015

Bagchi, A., Madaj, Z., Engel, K. B., Guan, P., Rohrer, D. C., Valley, D. R., Wolfrum, E., Feenstra, K., Roche, N., Hostetter, G., Moore, H. M., & Jewell, S. D. (2021). Impact of Preanalytical Factors on the Measurement of Tumor Tissue Biomarkers Using Immunohistochemistry. *The Journal of Histochemistry and Cytochemistry : Official Journal of the Histochemistry Society*, *69*(5), 297–320. https://doi.org/10.1369/0022155421995600

Bellizzi, A. M. (2020). An Algorithmic Immunohistochemical Approach to Define Tumor Type and Assign Site of Origin. *Advances in Anatomic Pathology*, *27*(3), 114–163. https://doi.org/10.1097/PAP.0000000000000256

Bodenmiller, B. (2016). Multiplexed Epitope-Based Tissue Imaging for Discovery and Healthcare Applications. *Cell Systems*, *2*(4), 225–238. https://doi.org/10.1016/J.CELS.2016.03.008

Chen, M., Zhang, B., Topatana, W., Cao, J., Zhu, H., Juengpanich, S., Mao, Q., Yu, H., & Cai, X. (2020). Classification and mutation prediction based on histopathology

H&E images in liver cancer using deep learning. *Npj Precision Oncology 2020 4:1*, *4*(1), 1–7. https://doi.org/10.1038/s41698-020-0120-3

Chen, X., Cho, D.-B., & Yang, P.-C. (2010). Double staining immunohistochemistry. *North American Journal of Medical Sciences*, *2*(5), 241. https://doi.org/10.4297/NAJMS.2010.2241

Cho, K. R., & Shih, I. M. (2009). OVARIAN CANCER. *Annual Review of Pathology*, *4*, 287. https://doi.org/10.1146/ANNUREV.PATHOL.4.110807.092246

Cosatto, E., Laquerre, P.-F., Malon, C., Graf, H.-P., Saito, A., Kiyuna, T., Marugame, A., & Kamijo, K. (2013). Automated gastric cancer diagnosis on H&E-stained sections; ltraining a classifier on a large scale with multiple instance machine learning. *SPIE*, *8676*, 867605. https://doi.org/10.1117/12.2007047

Davids, M. S., Deng, J., Wiestner, A., Lannutti, B. J., Wang, L., Wu, C. J., Wilson, W. H., Brown, J. R., & Letai, A. (2012). Decreased mitochondrial apoptotic priming underlies stroma-mediated treatment resistance in chronic lymphocytic leukemia. *Blood*, *120*(17), 3501–3509. https://doi.org/10.1182/BLOOD-2012-02-414060

Davis, A. S., Richter, A., Becker, S., Moyer, J. E., Sandouk, A., Skinner, J., & Taubenberger, J. K. (2014). Characterizing and Diminishing Autofluorescence in Formalin-fixed Paraffin-embedded Human Respiratory Tissue. *Journal of Histochemistry and Cytochemistry*, *62*(6), 405. https://doi.org/10.1369/0022155414531549

Dixon, A. R., Bathany, C., Tsuei, M., White, J., Barald, K. F., & Takayama, S. (2015). Recent developments in multiplexing techniques for immunohistochemistry. *Expert Review of Molecular Diagnostics*, *15*(9), 1171–1186. https://doi.org/10.1586/14737159.2015.1069182

Djuric, U., Zadeh, G., Aldape, K., & Diamandis, P. (2017). Precision histology: how deep learning is poised to revitalize histomorphology for personalized cancer care. *Npj Precision Oncology 2017 1:1*, *1*(1), 1–5. https://doi.org/10.1038/s41698-017-0022-1

Doheny, D., Manore, S. G., Wong, G. L., & Lo, H. W. (2020). Hedgehog Signaling and Truncated GLI1 in Cancer. *Cells*, *9*(9). https://doi.org/10.3390/CELLS9092114

Drake, C. G., Jaffee, E., & Pardoll, D. M. (2006). Mechanisms of immune evasion by tumors. *Advances in Immunology*, *90*, 51–81. https://doi.org/10.1016/S0065-2776(06)90002-9

Du, Z., Lin, J. R., Rashid, R., Maliga, Z., Wang, S., Aster, J. C., Izar, B., Sorger, P. K., & Santagata, S. (2019). Qualifying antibodies for image-based immune profiling and multiplexed tissue imaging. *Nature Protocols 2019 14:10*, *14*(10), 2900–2930. https://doi.org/10.1038/s41596-019-0206-y

Duffy, M. J., Synnott, N. C., O'Grady, S., & Crown, J. (2022). Targeting p53 for the treatment of cancer. *Seminars in Cancer Biology*, *79*, 58–67. https://doi.org/10.1016/J.SEMCANCER.2020.07.005

Egal, E., Rodrigues, N. de M., Mariano, F., Souza, R., Scarini, J., Sabino, W., Aguiar, L., Montalli, V., Gondak, R., Soares, C., Morais, T., & Altemani, A. (2019). Immunohistochemical Study of M1 and M2 Macrophages Population in Chronic Villitis of the Placenta. *American Journal of Clinical Pathology*, *152*(Supplement_1), S102–S102. https://doi.org/10.1093/AJCP/AQZ120.001

Eng, J., Thibault, G., Luoh, S. W., Gray, J. W., Chang, Y. H., & Chin, K. (2020). Cyclic Multiplexed-Immunofluorescence (cmIF), a Highly Multiplexed Method for Single-Cell Analysis. *Methods in Molecular Biology (Clifton, N.J.)*, *2055*, 521–562. https://doi.org/10.1007/978-1-4939-9773-2_24

Figueroa, G., Parira, T., Laverde, A., Casteleiro, G., El-Mabhouh, A., Nair, M., & Agudelo, M. (2016). Characterization of human Monocyte-derived Dendritic cells by imaging flow Cytometry: a comparison between two Monocyte isolation protocols. *JoVE (Journal of Visualized Experiments)*, (116), e54296. https://doi.org/10.3791/54296

Fischer, A. H., Jacobson, K. A., Rose, J., & Zeller, R. (2008). Hematoxylin and eosin staining of tissue and cell sections. *CSH Protocols*, *2008*(5). https://doi.org/10.1101/PDB.PROT4986

Galarraga, M., Campión, J., Munõz-Barrutia, A., Boqué, N., Moreno, H., Martínez, J. A., Milagro, F., & Ortiz-de-Solórzano, C. (2012). Adiposoft: Automated software for the analysis of white adipose tissue cellularity in histological sections. *Journal of Lipid Research*, *53*(12), 2791–2796. https://doi.org/10.1194/JLR.D023788

Giotakis, A. I., Dudas, J., Glueckert, R., Dejaco, D., Ingruber, J., Fleischer, F., Innerhofer, V., Pinggera, L., Bektic-Tadic, L., Gabriel, S. A. M., & Riechelmann, H. (2021). Characterization of epithelial cells, connective tissue cells and immune cells in human upper airway mucosa by immunofluorescence multichannel image cytometry: a pilot study. *Histochemistry and Cell Biology*, *155*(3), 405–421. https://doi.org/10.1007/S00418-020-01945-Y

Gorczyca, W., Sun, Z. Y., Cronin, W., Li, X., Mau, S., & Tugulea, S. (2011). Immunophenotypic Pattern of Myeloid Populations by Flow Cytometry Analysis. *Methods in Cell Biology*, *103*, 221–266. https://doi.org/10.1016/B978-0-12-385493-3.00010-3

Huss, R., & Coupland, S. E. (2020). Software-assisted decision support in digital histopathology. *The Journal of Pathology*, *250*(5), 685–692. https://doi.org/10.1002/PATH.5388

Inzani, F., Petrone, G., Fadda, G., & Rindi, G. (2017). Cyto-histology in NET: what is necessary today and what is the future? *Reviews in Endocrine and Metabolic Disorders*, *18*(4), 381–391. https://doi.org/10.1007/S11154-017-9428-X/TABLES/3

Jager, E. A., Willems, S. M., Schakel, T., Kooij, N., Slootweg, P. J., Philippens, M. E. P., Caldas-Magalhaes, J., Terhard, C. H. J., & Raaijmakers, C. P. J. (2016). Interobserver variation among pathologists for delineation of tumor on H&E-

sections of laryngeal and hypopharyngeal carcinoma. How good is the gold standard? *Acta Oncologica (Stockholm, Sweden)*, *55*(3), 391–395. https://doi.org/10.3109/0284186X.2015.1049661

Jung, K. Y., Cho, S. W., Kim, Y. A., Kim, D., Oh, B. C., Park, D. J., & Park, Y. J. (2015). Cancers with Higher Density of Tumor-Associated Macrophages Were Associated with Poor Survival Rates. *Journal of Pathology and Translational Medicine*, *49*(4), 318. https://doi.org/10.4132/JPTM.2015.06.01

Juríková, M., Danihel, Ľ., Polák, Š., & Varga, I. (2016). Ki67, PCNA, and MCM proteins: Markers of proliferation in the diagnosis of breast cancer. *Acta Histochemica*, *118*(5), 544–552. https://doi.org/10.1016/J.ACTHIS.2016.05.002

Li, L. T., Jiang, G., Chen, Q., & Zheng, J. N. (2015). Ki67 is a promising molecular target in the diagnosis of cancer. Molecular medicine reports, 11(3), 1566-1572. https://doi.org/10.3892/mmr.2014.2914

Lin, J. R., Fallahi-Sichani, M., & Sorger, P. K. (2015). Highly multiplexed imaging of single cells using a high-throughput cyclic immunofluorescence method. *Nature Communications 2015 6:1*, *6*(1), 1–7. https://doi.org/10.1038/ncomms9390

Lin, J. R., Izar, B., Wang, S., Yapp, C., Mei, S., Shah, P. M., Santagata, S., & Sorger, P. K. (2018). Highly multiplexed immunofluorescence imaging of human tissues and tumors using t-CyCIF and conventional optical microscopes. *ELife*, *7*. https://doi.org/10.7554/ELIFE.31657

Lin, J.-R., Wang, S., Coy, S., Chen, Y.-A., Yapp, C., Tyler, M., Nariya, M. K., Heiser, C. N., Lau, K. S., Santagata, S., & Sorger, P. K. (2022). Multiplexed 3D atlas of state transitions and immune interactions in colorectal cancer. *BioRxiv*, 2021.03.31.437984. https://doi.org/10.1101/2021.03.31.437984

Litjens, G., Bandi, P., Bejnordi, B. E., Geessink, O., Balkenhol, M., Bult, P., Halilovic, A., Hermsen, M., van de Loo, R., Vogels, R., Manson, Q. F., Stathonikos, N., Baidoshvili, A., van Diest, P., Wauters, C., van Dijk, M., & van der Laak, J. (2018). 1399 H&E-stained sentinel lymph node sections of breast cancer patients: the CAMELYON dataset. *GigaScience*, *7*(6), 1–8. https://doi.org/10.1093/GIGASCIENCE/GIY065

Lu, S., Stein, J. E., Rimm, D. L., Wang, D. W., Bell, J. M., Johnson, D. B., Sosman, J. A., Schalper, K. A., Anders, R. A., Wang, H., Hoyt, C., Pardoll, D. M., Danilova, L., & Taube, J. M. (2019). Comparison of Biomarker Modalities for Predicting Response to PD-1/PD-L1 Checkpoint Blockade: A Systematic Review and Meta-analysis. *JAMA Oncology*, *5*(8), 1195–1204. https://doi.org/10.1001/JAMAONCOL.2019.1549

McMahon, N. P., Jones, J. A., Kwon, S., Chin, K., Nederlof, M. A., Gray, J. W., & Gibbs, S. L. (2020). Oligonucleotide conjugated antibodies permit highly multiplexed immunofluorescence for future use in clinical histopathology. *Journal of Biomedical Optics*, *25*(5), 1. https://doi.org/10.1117/1.JBO.25.5.056004

Merz, S. F., Jansen, P., Ulankiewicz, R., Bornemann, L., Schimming, T., Griewank, K., Cibir, Z., Kraus, A., Stoffels, I., Aspelmeier, T., Brandau, S., Schadendorf, D., Hadaschik, E., Ebel, G., Gunzer, M., & Klode, J. (2021). High-resolution three-dimensional imaging for precise staging in melanoma. *European Journal of Cancer*, *159*, 182–193. https://doi.org/10.1016/J.EJCA.2021.09.026

Miettinen, M., Limon, J., Niezabitowski, A., & Lasota, J. (2001). Calretinin and other mesothelioma markers in synovial sarcoma: analysis of antigenic similarities and differences with malignant mesothelioma. *The American Journal of Surgical Pathology*, *25*(5), 610–617. https://doi.org/10.1097/00000478-200105000-00007

Moriya, T., Kasajima, A., Ishida, K., Kariya, Y., Akahira, J. I., Endoh, M., Watanabe, M., & Sasano, H. (2006). New trends of immunohistochemistry for making differential diagnosis of breast lesions. *Medical Molecular Morphology*, *39*(1), 8–13. https://doi.org/10.1007/S00795-006-0309-8

Nadarajan, G., Hope, T., Wang, D., Cheung, A., Ginty, F., Yaffe, M. J., & Doyle, S. (2019). Automated multi-class ground-truth labeling of H&E images for deep learning using multiplexed fluorescence microscopy. *Https://Doi.Org/10.1117/12.2512991*, *10956*, 102–111. https://doi.org/10.1117/12.2512991

Nguyen, D. (2013). *Quantifying chromogen intensity in immunohistochemistry via reciprocal intensity*. https://doi.org/10.1038/protex.2013.097

Parise, C. A., & Caggiano, V. (2014). Breast Cancer Survival Defined by the ER/PR/HER2 Subtypes and a Surrogate Classification according to Tumor Grade and Immunohistochemical Biomarkers. *Journal of Cancer Epidemiology*, *2014*. https://doi.org/10.1155/2014/469251

Parra, E. R. (2018). Novel Platforms of Multiplexed Immunofluorescence for Study of Paraffin Tumor Tissues. *Journal of Cancer Treatment and Diagnosis*, *2*(1), 43–53. https://doi.org/10.29245/2578-2967/2018/1.1122

Patel, S. P., & Kurzrock, R. (2015). PD-L1 Expression as a Predictive Biomarker in Cancer Immunotherapy. *Molecular Cancer Therapeutics*, *14*(4), 847–856. https://doi.org/10.1158/1535-7163.MCT-14-0983

Peters, N., Schubert, M., Metzler, G., Geppert, J. P., & Moehrle, M. (2019). Diagnostic accuracy of a new ex vivo confocal laser scanning microscope compared to H&E-stained paraffin slides for micrographic surgery of basal cell carcinoma. *Journal of the European Academy of Dermatology and Venereology : JEADV*, *33*(2), 298–304. https://doi.org/10.1111/JDV.15243

Pu, X., Storr, S. J., Zhang, Y., Rakha, E. A., Green, A. R., Ellis, I. O., & Martin, S. G. (2017). Caspase-3 and caspase-8 expression in breast cancer: caspase-3 is associated with survival. *Apoptosis*, *22*(3), 357–368. https://doi.org/10.1007/S10495-016-1323-5/TABLES/5

Qian, C. N., Huang, D., Wondergem, B., & Teh, B. T. (2009). Complexity of tumor vasculature in clear cell renal cell carcinoma. *Cancer*, *115*(10 Suppl), 2282–2289. https://doi.org/10.1002/CNCR.24238

Rawat, R. R., Ortega, I., Roy, P., Sha, F., Shibata, D., Ruderman, D., & Agus, D. B. (2020). Deep learned tissue "fingerprints" classify breast cancers by ER/PR/Her2 status from H&E images. *Scientific Reports 2020 10:1*, *10*(1), 1–13. https://doi.org/10.1038/s41598-020-64156-4

Rimm, D. L. (2014). Next-gen immunohistochemistry. *Nature Methods*, *11*(4), 381–383. https://doi.org/10.1038/NMETH.2896

Rozenblatt-Rosen, O., Regev, A., Oberdoerffer, P., Nawy, T., Hupalowska, A., Rood, J. E., Ashenberg, O., Cerami, E., Coffey, R. J., Demir, E., Ding, L., Esplin, E. D., Ford, J. M., Goecks, J., Ghosh, S., Gray, J. W., Guinney, J., Hanlon, S. E., Hughes, S. K., … Zhuang, X. (2020). The Human Tumor Atlas Network: Charting Tumor Transitions across Space and Time at Single-Cell Resolution. *Cell*, *181*(2), 236–249. https://doi.org/10.1016/J.CELL.2020.03.053

Rüschoff, J., Dietel, M., Baretton, G., Arbogast, S., Walch, A., Monges, G., Chenard, M. P., Penault-Llorca, F., Nagelmeier, I., Schlake, W., Höfler, H., & Kreipe, H. H. (2010). HER2 diagnostics in gastric cancer-guideline validation and development of standardized immunohistochemical testing. *Virchows Archiv : An International Journal of Pathology*, *457*(3), 299–307. https://doi.org/10.1007/S00428-010-0952-2

Sadanandan, S. K., Ranefall, P., le Guyader, S., & Wählby, C. (2017). Automated Training of Deep Convolutional Neural Networks for Cell Segmentation. *Scientific Reports 2017 7:1*, *7*(1), 1–7. https://doi.org/10.1038/s41598-017-07599-6

Sawabu, N., & Watanabe, H. (2005). Altered Expression of p27 Protein in Pancreatic Carcinoma. *Handbook of Immunohistochemistry and in Situ Hybridization of Human Carcinomas*, *3*, 331–333. https://doi.org/10.1016/S1874-5784(05)80037-6

Schapiro, D., Sokolov, A., Yapp, C., Chen, Y. A., Muhlich, J. L., Hess, J., Creason, A. L., Nirmal, A. J., Baker, G. J., Nariya, M. K., Lin, J. R., Maliga, Z., Jacobson, C. A., Hodgman, M. W., Ruokonen, J., Farhi, S. L., Abbondanza, D., McKinley, E. T., Persson, D., … Sorger, P. K. (2021). MCMICRO: a scalable, modular image-processing pipeline for multiplexed tissue imaging. *Nature Methods 2021 19:3*, *19*(3), 311–315. https://doi.org/10.1038/s41592-021-01308-y

Schüffler, P. J., Schapiro, D., Giesen, C., Wang, H. A. O., Bodenmiller, B., & Buhmann, J. M. (2015). Automatic single cell segmentation on highly multiplexed tissue images. *Cytometry. Part A : The Journal of the International Society for Analytical Cytology*, *87*(10), 936–942. https://doi.org/10.1002/CYTO.A.22702

Singhai, R., Patil, V. W., Jaiswal, S. R., Patil, S. D., Tayade, M. B., & Patil, A. v. (2011). E-Cadherin as a diagnostic biomarker in breast cancer. *North American Journal of Medical Sciences*, *3*(5), 227. https://doi.org/10.4297/NAJMS.2011.3227

Tan, W. C. C., Nerurkar, S. N., Cai, H. Y., Ng, H. H. M., Wu, D., Wee, Y. T. F., Lim, J. C. T., Yeong, J., & Lim, T. K. H. (2020). Overview of multiplex immunohistochemistry/immunofluorescence techniques in the era of cancer immunotherapy. *Cancer Communications (London, England)*, *40*(4), 135–153. https://doi.org/10.1002/CAC2.12023

Taube, J. M., Akturk, G., Angelo, M., Engle, E. L., Gnjatic, S., Greenbaum, S., Greenwald, N. F., Hedvat, C. v., Hollmann, T. J., Juco, J., Parra, E. R., Rebelatto, M. C., Rimm, D. L., Rodriguez-Canales, J., Schalper, K. A., Stack, E. C., Ferreira, C. S., Korski, K., Lako, A., … Bifulco, C. B. (2020). The Society for Immunotherapy in Cancer statement on best practices for multiplex immunohistochemistry (IHC) and immunofluorescence (IF) staining and validation. *Journal for Immunotherapy of Cancer*, *8*(1), 155. https://doi.org/10.1136/JITC-2019-000155

Tellez, D., Balkenhol, M., Otte-Höller, I., van de Loo, R., Vogels, R., Bult, P., Wauters, C., Vreuls, W., Mol, S., Karssemeijer, N., Litjens, G., van der Laak, J., & Ciompi, F. (2018). Whole-Slide Mitosis Detection in H&E Breast Histology Using PHH3 as a Reference to Train Distilled Stain-Invariant Convolutional Networks. *IEEE Transactions on Medical Imaging*, *37*(9), 2126–2136. https://doi.org/10.1109/TMI.2018.2820199

van der Wal, D., Jhun, I., Laklouk, I., Nirschl, J., Richer, L., Rojansky, R., Theparee, T., Wheeler, J., Sander, J., Feng, F., Mohamad, O., Savarese, S., Socher, R., & Esteva, A. (2021). Biological data annotation via a human-augmenting AI-based labeling system. *Npj Digital Medicine 2021 4:1*, *4*(1), 1–7. https://doi.org/10.1038/s41746-021-00520-6

Viegas, M., Martins, T. C., Seco, F., & do Carmo, A. (2007). An improved and cost-effective methodology for the reduction of autofluorescence in direct immunofluorescence studies on formalin-fixed paraffin-embedded tissues. *European Journal of Histochemistry : EJH*, *51*(1), 59–66. https://pubmed.ncbi.nlm.nih.gov/17548270/

Wisell, J. A., & Sams, S. B. (2013, February). Influence of External Factors on Frozen Section Performance. In *LABORATORY INVESTIGATION* (Vol. 93, pp. 489–504 (2013). https://doi-org.ezp-prod1.hul.harvard.edu/10.1038/labinvest.2013.37

Yamashita, R., Long, J., Longacre, T., Peng, L., Berry, G., Martin, B., Higgins, J., Rubin, D. L., & Shen, J. (2021). Deep learning model for the prediction of microsatellite instability in colorectal cancer: a diagnostic study. *The Lancet Oncology*, *22*(1), 132–141. https://doi.org/10.1016/S1470-2045(20)30535-0

Yapp, C., Novikov, E., Jang, W.-D., Chen, Y.-A., Cicconet, M., Maliga, Z., Jacobson, C. A., Wei, D., Santagata, S., Pfister, H., & Sorger, P. K. (2021). UnMICST: Deep learning with real augmentation for robust segmentation of highly multiplexed images of human tissues. *BioRxiv*, 2021.04.02.438285. https://doi.org/10.1101/2021.04.02.438285

Zhao, J., Xu, W., Zhang, Z., Song, R., Zeng, S., Sun, Y., & Xu, C. (2015). Prognostic role of HER2 expression in bladder cancer: a systematic review and meta-analysis. *International Urology and Nephrology*, *47*(1), 87–94. https://doi.org/10.1007/S11255-014-0866-Z